UNIVERSITY OF SOUTHAMPTON

OPTOELECTRONICS RESEARCH CENTRE

Power Scaling of Novel Frequency Doubled Continuous-Wave Fibre Lasers

by

Stanislav Krassimirov Vassilev

Thesis for the degree of Doctor of Philosophy

December 2017

UNIVERSITY OF SOUTHAMPTON

ABSTRACT

OPTOELECTRONICS RESEARCH CENTRE

Thesis for the degree of Doctor of Philosophy

Power Scaling of Novel Frequency Doubled Continuous-Wave Fibre Lasers

Stanislav Krassimirov Vassilev

A novel method for power scaling continuous-wave (CW) rare-earth (RE) doped frequency doubled fibre lasers is investigated. The limiting effects on output power are discussed. A fibre ring cavity is proposed to improve feedback into the laser oscillator. Second harmonic generation is implemented in an internal resonant enhancement cavity that allows for a high power build up. Results from the design and development of a ring fibre laser are presented along with the physical and mechanical limitations. Techniques to overcome fibre end reflections such as angle cleaving and fusing of bulk end caps succeed in reducing feedback to below 0.1%. The ring fibre laser is used in frequency doubling experiments in multiple cavity configurations. A maximum second harmonic output power of 17.4W is achieved with a maximum conversion efficiency of the useful infra-red signal to green output of 47% and pump power to green output of 18%. The output signal operated with an excellent beam quality of $M^2 \approx 1.09$ and power stability less than 1% rms. The main limitation in the power scaling ability of the system is identified as the spatial mode matching overlap between the signal and second harmonic with potential solutions discussed.

Table of Contents

Academic Thesis: Declaration Of Authorship

I, ... [please print name]

declare that this thesis and the work presented in it are my own and has been generated by me as the result of my own original research.

[title of thesis] .....

.....

I confirm that:

1. This work was done wholly or mainly while in candidature for a research degree at this University;
2. Where any part of this thesis has previously been submitted for a degree or any other qualification at this University or any other institution, this has been clearly stated;
3. Where I have consulted the published work of others, this is always clearly attributed;
4. Where I have quoted from the work of others, the source is always given. With the exception of such quotations, this thesis is entirely my own work;
5. I have acknowledged all main sources of help;
6. Where the thesis is based on work done by myself jointly with others, I have made clear exactly what was done by others and what I have contributed myself;
7. [Delete as appropriate] None of this work has been published before submission [or] Parts of this work have been published as: [please list references below]:

Signed: .....

Date: .....

What your hands do,
It is your own eyes that have seen,
So won't you judge your actions,
To make sure the results are clean,
It's your own conscience,
That is going to remind you,
That it's your heart and nobody else's,
That is going to judge.

Be not selfish in your doings,
Pass it on,
Help your brothers in their needs,
Pass it on,
Live for yourself and you will live in vain,
Live for others, you will live again,
In the kingdom of Jah men shall reign,
Pass it on.

Bob Marley & The Wailers

Acknowledgements

First and foremost my thanks goes to my supervisor, Prof. Andrew Clarkson. His support has been ever present from my first day in the lab, through the difficulties that I encountered right up to the days spent writing this thesis. Always able to offer potential solutions to problems and providing continuing encouragement and support, for all of that I am very thankful.

Members, past and present, of the Advanced Solid State Sources group also deserve a special mention. Dr Peter Shardlow and Dr Alex Butler, always finding the time in between their work to help with the smallest and most trivial problems. My fellow students, Dr Jae Daniel, Dr Matt Eckold, Dr Antonin Billoud, Dr Callum Smith, Robin Uren and Florian Leroi, helping out in various ways both in and out of the lab, whether it involved splicing fibres or drinking beer.

A very special mention to my colleagues and fellow founding members of the PKF Society, Dr Jiannis Katis, Dr Aabid Patel, Dr Kyle Bottrill and Dr Peter Baksh. Friendships formed by chance that will no doubt last a lifetime.

My last and most sincere appreciation is reserved for my parents, Anjela and Krassimir, without who this would not have been possible. Not only over the last five years, with never ending encouragement, support and reassurance but over my whole life. Undoubtedly the opportunity for me to achieve so much began with their decision to leave their home, their family and their friends, and for that I am in their debt today and always.

CHAPTER 1

1. Introduction

1.1 Motivation

The impact of the laser is ever present in today's world. Over 50 years after its invention [1.1] the laser is commonplace in the modern world with a continuing fascination in further developing this well-established technology. At first described as "a solution looking for a problem" laser applications include high capacity communication systems that power the World Wide Web, home entertainment electronics, as tools in the medical world, in manufacturing, defence and in numerous research laboratories across the globe.

Ever more advanced applications require ever more advanced lasers with tailored specifications. This places tough requirements for new lasers in terms of high power, high brightness, operating wavelength, linewidth, and beam quality; all the while ensuring an efficient laser system in terms of electrical-to-optical conversion efficiency and cost. All these challenges drive the research in power scaling of laser technologies.

Bulk solid state lasers operating on rare-earth doped media were the frontrunners in the chase for ever increasing laser powers, but the thermal issues induced at increasing pump power levels limited the output powers achievable. Rare-earth (RE) solid-state lasers in a fibre geometry allow for generation of high power and high brightness whilst alleviating the thermal issues that are encountered in bulk solid-state lasers. Generating wavelengths from the visible part of spectrum at higher powers proves difficult as the best performing gain media emit radiation in the near infra-red. The most common way to generate frequencies outside the natural emission of laser media requires the implementation of nonlinear frequency conversion techniques using a non-linear medium. Naturally these nonlinear conversion schemes are limited in efficiency, hence why new and unique laser geometries are needed to achieve high powers whilst also maintaining good efficiencies.

This thesis will present a novel concept for a visible fibre laser geometry to enable power-scaling and outline the subtleties in constructing this device, the limits of its performance and potential for further development. This work will focus on lasers operating in the continuous wave (CW) regime.

1.2 Research area

1.2.1 Evolution of Fibre Lasers

Theoretically, the foundations of laser emission were described in terms of the probability coefficients for absorption, spontaneous emission and most importantly stimulated emission by A. Einstein [1.2] decades before the first working laser was invented by T.H. Maiman [1.1]. Maiman built a working solid-state laser based on a Ruby gain medium with gas lasers like Helium-Neon [1.3], diode lasers [1.4] and the first fibre laser [1.5] following soon after. Optical pumping of the laser medium was first done using flash lamps as the power and brightness of early diode lasers was not good enough. Once these issues were resolved and the lifetimes of diodes could compete they soon became the common pumping method of choice for solid state lasers, both bulk and fibre.

The first fibre lasers and amplifiers were constructed using a fibre with a single cladding and would couple the pump light into the doped core to propagate together with the signal. This imposed a limit on the maximum output power due to the limit in power of single mode diode lasers. The invention of double-clad fibre lasers was able to get around this problem by having the pump light propagating inside an inner cladding, bigger than the core, lifting the restrictions on diode beam quality and increasing the pump power to reach very high output powers [1.6]. The double clad geometry proved to be a winning formula and in subsequent years, thanks to improvements in pump diodes and the double clad structure, the output power of fibre lasers grew dramatically, as shown in Figure 1.1.

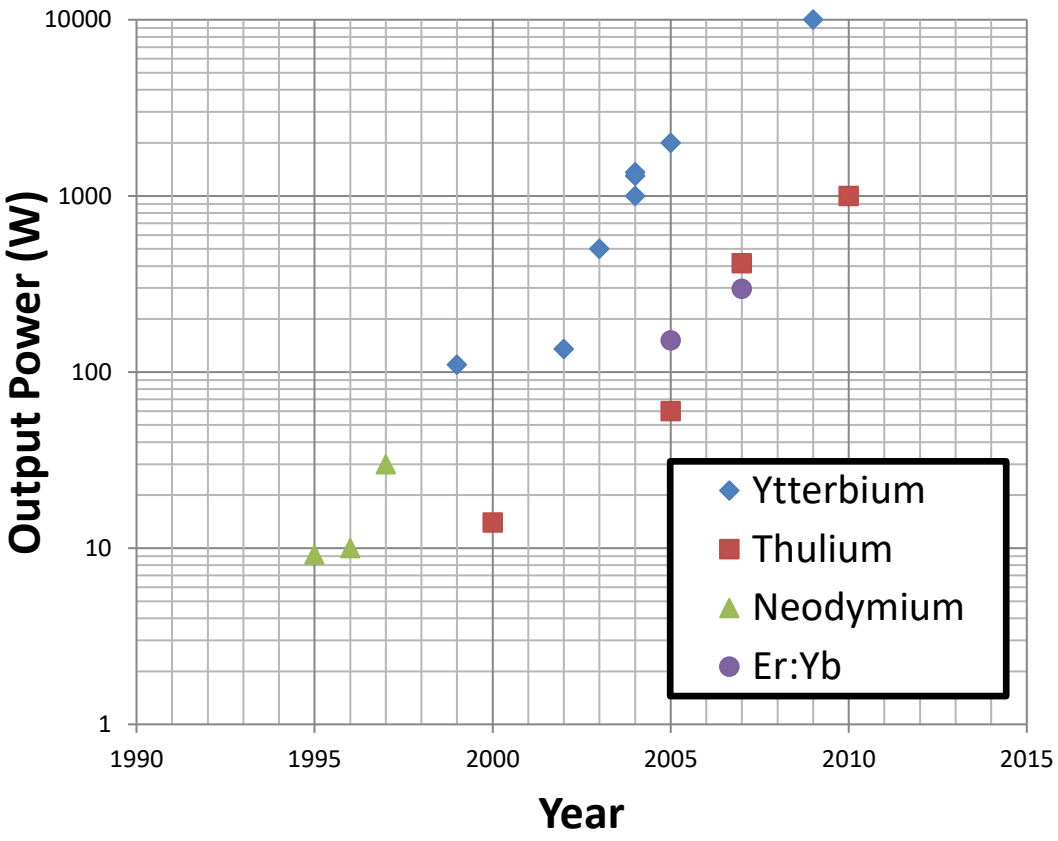

Figure 1.1 Plot showing evolution of output power from double clad fibre lasers over time. Output is close to diffraction limit and across several spectral regions using different RE dopants, Neodymium [1.6-9], Thulium [1.10-13], Erbium:Ytterbium [1.14, 15] and Ytterbium [1.16-23].

As with bulk solid state lasers the emission wavelength is determined by the active ion chosen for the gain medium, this being the doped into the core of the active fibre. Early fibre lasers continued with the trend of using Neodymium for emission at 1064nm [1.6-9]. Subsequent work utilised other lanthanides depending on the required emission wavelength. Erbium, and erbium co-doped with ytterbium, was the weapon of choice for improving the optical telecoms network due to its low loss at 1.5μm [1.14, 15]. Erbium serves as the active ion in erbium-doped fibre amplifiers, EDFA, which revolutionised the optical fibre telecoms world. Over the past decades ytterbium has proven to be a great choice for power scaling strategies due to numerous factors, one being its small quantum defect and output powers well above 1kW have been reported with commercial systems reaching 10kW [1.16-23]. Thulium doped fibres have seen much research as they allow access to the 2μm region which has medical and military applications [1.10-13].

1.2.2 High Power Visible Sources

Fibre lasers achieve impressive output powers in the near-IR spectral band and further beyond, however the output power in the visible region is far less spectacular. Direct emission in the visible region is difficult as there are not that many laser media with transitions emitting visible wavelength photons. However, the high powers generated in the near-IR region can be harnessed through nonlinear frequency conversion, namely second harmonic generation (SHG), to realise high power visible fibre lasers. One approach to yield high powers in the visible region is to use an external enhancement cavity [1.24]. This method suffers from cavity stabilisation problems which make the system very sensitive. By incorporating the enhancement cavity within the main fibre resonator the stabilisation issues are resolved and the system can yield good efficiency [1.25]. This report will explore the power scaling ability of the internal enhancement cavity approach further. One issue is the feedback in the current approach which is based on a linear resonator. Arranging the main fibre cavity in a ring formation will improve feedback. This thesis will focus on the development of a ring fibre laser designed for intracavity second harmonic generation.

Using fibres in a ring arrangement has been investigated previously; however the main research looked at creating very narrowband output in the 1.5μm region usually using an EDFA [1.26, 27]. Widely tunable fibre ring sources have been demonstrated with tuning ranges close to 60nm [1.28] and with output powers of 10W using a double clad ytterbium fibre [1.29]. The majority of the approaches use a combination of circulator and fibre Bragg gratings as the wavelength selection element [1.30]. Recently a ring laser using an ytterbium rod-type fibre was demonstrated with output powers of 41W, widely tunable across the Ytterbium emission spectrum [1.31].

1.3 Thesis Structure

This thesis will present the work undertaken to prototype an internal resonantly enhanced frequency doubled CW fibre ring laser.

Chapter 1 will serve as an introduction to the topic and overall field of high power fibre lasers. It will look at the progression of the highest attainable power levels for fibres doped with the most commonly used rare earth elements like Neodymium, Ytterbium and Erbium and how the developments of fibres themselves helped push on the

maximum powers of solid state lasers beyond what was achievable in traditional bulk rod lasers.

Chapter 2 continues with a more specific look at the science of fibre lasers and the theoretical concepts applied in the design and realisation of the device that this work is based on. The basics of solid state lasers will be discussed and in particular those lasers based on a fibre geometry, discussing how fibres overcome the problems that bulk media suffer from and where their limits lie currently. The theory of second harmonic generation will be outlined as the tight tolerances and requirements for efficient conversion are what set the specifications for the ring fibre laser. A look at the standard techniques of SHG will be discussed with a discussion of the different intra and extra cavity approaches demonstrated over time. More specifically the theory behind internal enhancement cavities will be introduced and championed as the best solution for power scaling of IR fibre lasers into the visible wavelength regime.

Chapter 3 will present the fibre ring laser and discuss the engineering and physical challenges that were overcome to build a device suitable for nonlinear frequency conversion via the use of an internal resonant cavity. A detailed description of the laser geometry and specifically the alignment techniques that were tried and tested. As this ring laser design is a hybrid of fibre and free space optics, the feedback suppression at the fibre ends became very important, why this is an issue and the attempts to overcome it are presented in this chapter. The different methods of feedback suppression are discussed and their performance analysed.

Chapter 4 presents results of the first experiments with nonlinear frequency conversion and discussed the problems that needed to be overcome whilst also detailing the alignment technique. Building up on the fibre ring laser design from chapter 3 and introducing the enhancement cavity and how it is incorporated into the laser. Different enhancement cavity designs are implemented and their performance discussed highlighting the main limiting factors in output power and the potential for further power scaling.

Chapter 5 will be a summary of the work carried out and highlight the key results and future developments that should be possible for this laser design.

1.4 References

1.1. Maiman, T.H., *Stimulated optical radiation in ruby.* Nature, 1960. **187**: p. 493-494.

1.2. Einstein, A., *On the quantum theory of radiation.* Physikalische Zeitschrift, 1917. **18**: p. 121-128.

1.3. Javan, A., W.R. Bennett Jr, and D.R. Herriott, *Population inversion and continuous optical maser oscillation in a gas discharge containing a He-Ne mixture.* Physical Review, 1961. **6**(3): p. 106-110.

1.4. Hall, R.N., et al., *Coherent light emission from GaAs junctions.* Physical Review, 1962. **9**(9): p. 366-368.

1.5. Koester, C. and E. Snitzer, *Amplification in a fibre laser.* Applied Optics, 1964. **3**(1): p. 1182-1186.

1.6. Snitzer, E., et al., *Double clad, offset core Nd fiber laser*, in *Optical Fibre Sensors*1988, Optical Society of America. p. PD5.

1.7. Zekkner, H., et al., *Double-clad fiber laser with 30 W output power.* Optical Amplifiers and Their Applications. Topical Meeting. OSA Trends in Optics and Photonics Series. Vol.16, 1997: p. 137-40.

1.8. Zellmer, H., et al., *HIGH-POWER CW NEODYMIUM-DOPED FIBER LASER OPERATING AT 9.2 W WITH HIGH BEAM QUALITY.* Optics Letters, 1995. **20**(6): p. 578-580.

1.9. Tunnermann, A., *High-power Nd double-clad fiber lasers.* CLEO '96. Summaries of Papers Presented at the Conference on Lasers and Electro-Optics. Vol.9. 1996 Technical Digest Series. Conference Edition (IEEE Cat. No.96CH35899), 1996: p. 528-528.

1.10. Meleshkevich, M., et al., *415W single-mode CW thulium fiber laser in all-fiber format.* CLEO/Europe - IQEC 2007. European Conference on Lasers and Electro-Optics and the International Quantum Electronics Conference, 2007: p. 725-725.

1.11. Hayward, A., et al., *Efficient cladding-pumped Tm-doped silica fibre laser with high power singlemode output at 2µm.* Electronics Letters, 2000. **36**(8): p. 711-712.

1.12. Barannikov, Y.A., et al., *Linear-polarization, CW generation of 60W power in a single-mode, Tm fibre laser*. 2005 Conference on Lasers & Electro-Optics. 2005. 811-812.

1.13. Ehrenreich, T., et al. *1 kW All-Glass Tm:fiber laser*. in *SPIE Photonics West*. 2010.

1.14. Jeong, Y., et al., *High-power tunable single-frequency single-mode erbium:ytterbium codoped large-core fibre master-oscillator power amplifier source.* Optics Letters, 2005. **30**(22): p. 2997-2999.

1.15. Jeong, Y., et al., *Erbium:Ytterbium codoped large-core fiber laser with 297W continuous-wave output power.* J. Sel. Quant. Electron., 2007. **13**: p. 573-579.

1.16. Dominic, V., et al., *110W fibre laser.* Electronics Letters, 1999. **35**(14): p. 1158-1160.

1.17. Platonov, N.S., et al., *135W CW fibre laser with perfect single mode output*, in *Conference on Lasers and Electro-Optics*2002. p. CPCD3-1.

1.18. Limpert, J., et al., *500W continuous-wave fibre laser with excellent beam quality.* Electronics Letters, 2003. **39**(8): p. 645-647.

1.19. Jeong, Y., et al., *Ytterbium-doped large core fiber laser with 1kW continuous-wave output power*, in *Advanced Solid-State Photonics*2004, Optical Society of America: Santa Fe, New Mexico, USA.

1.20. Liem, A., et al. *1.3kW Yb-doped fiber laser with excellenmt beam quality*. in *Conference on Lasers and Electro-Optics*. 2004. San Francisco, California.

1.21. Jeong, Y., et al., *Ytterbium-doped large-core fiber laser with 1.36 kW continuous-wave output power.* Optics Express, 2004. **12**(25): p. 6088-6092.

1.22. Gapontsev, V., et al., *2 kW CW ytterbium fiber laser with record diffraction-limited brightness.* 2005 Conference on Lasers and Electro-Optics Europe (IEEE Cat. No. 05TH8795), 2005: p. 508-508.

1.23. Stiles, E. *New developments in IPG fiber laser technology*. in *Proceedings of the 5th International Workshop on Fibre Lasers*. 2009.

1.24. Suedmeyer, T., et al., *Efficient 2(nd) and 4(th) harmonic generation of a single-frequency, continuous-wave fiber amplifier.* Optics Express, 2008. **16**(3): p. 1546-1551.

1.25. Cieslak, R. and W.A. Clarkson, *Internal resonantly enhanced frequency doubling of continuous-wave fiber lasers.* Optics Letters, 2011. **36**(10): p. 1896-1898.

1.26. J.L., Z. and e. al., *Electrically tunable, diode-pumped erbium-doped fibre ring laser with fibre Fabry-Perot etalon.* Electronics Letters, 1991. **27**(21): p. 1950-1951.

1.27. M.J., G., T. J.R., and K. R., *Single-frequency erbium fibre ring laser with intracavity phase-shifted fibre Bragg grating narrowband filter.* Electronics Letters, 1995. **31**(22): p. 1924-1925.

1.28. Feifei, Y., et al., *60-nm-Wide Tunable Single-Longitudinal-Mode Ytterbium Fiber Laser With Passive Multiple-Ring Cavity.* IEEE Photonics Technology Letters, 2011. **23**(22): p. 1658-60.

1.29. Auerbach, M., et al., *10W Widely tunable narrow linewidth double-clad fiber ring laser*, in *Conference on Lasers and Electro-Optics*2002.

1.30. al., P.A.e., *Single-frequency fiber ring laser with 1W output power at 1.5μm.* Optics Express, 2005. **13**(8): p. 3179-3184.

1.31. Royon, R., et al., *High power, continous-wave ytterbium-doped fiber laser tunable from 976nm to 1120nm.* Optics Express, 2013. **21**(11): p. 13818-13823.

CHAPTER 2

2. Background

2.1 Background

Scaling the output power from solid state lasers has seen vast amount of research due to the many applications already mentioned. However it is important to note that it is not raw output power alone that is required. Other parameters like beam quality, single mode operation, power stability and overall laser efficiency are important factors for a useful high power laser and need to be considered. Bulk solid state laser crystals suffer from thermal management issues that impact greatly on the beam quality and limit the output power achievable. One way of improving the output power and maintaining other beam parameters is the use of optical fibre with a doped active core as opposed to bulk laser crystals. Thermal management in optical fibres is far easier to accomplish as will be explained later. Due to the limits of fibre lasers in generating light in the visible region, nonlinear frequency conversion has to be utilised.

2.2 Theory of Laser Performance

2.2.1 Ytterbium Spectroscopy

Ytterbium is one of the rare earth (RE) elements from the lanthanide group. When used as a dopant within a host material like silica glass, as used in fibres, ytterbium atoms are triply ionized, Yb^{3+}. A comprehensive study of the performance of ytterbium as the active ion in fibre lasers was carried out by Pask, et al. [2.2.1]. The energy level structure, as seen in Figure 2.1, is relatively simple in comparison to other lanthanide ions with just two manifolds: a ground state manifold $^2F_{5/2}$ (consisting of four Stark levels, (a)-(d)) and the excited state manifold $^2F_{7/2}$ (consisting of three Stark levels, (e)-(g)). This results in no excited state absorption at the pump or laser wavelengths. The large energy gap between the manifolds prevents non-radiative decay from the upper manifold along with reduced concentration quenching. The subsequent highly efficient operation of lasers based on ytterbium has caused them to be the prime candidate for new laser devices seeking ever higher powers. The typical cross sections for an Ytterbium doped germano-sillicate glass is shown in Figure 2.2 [2.1].

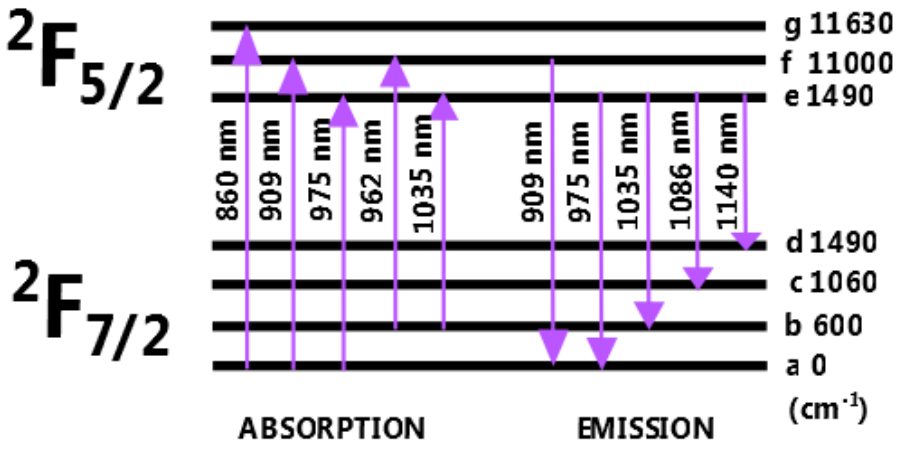

Figure 2.1 The energy level structure of Yb^{3+} with some absorption and emission transitions [2.1]

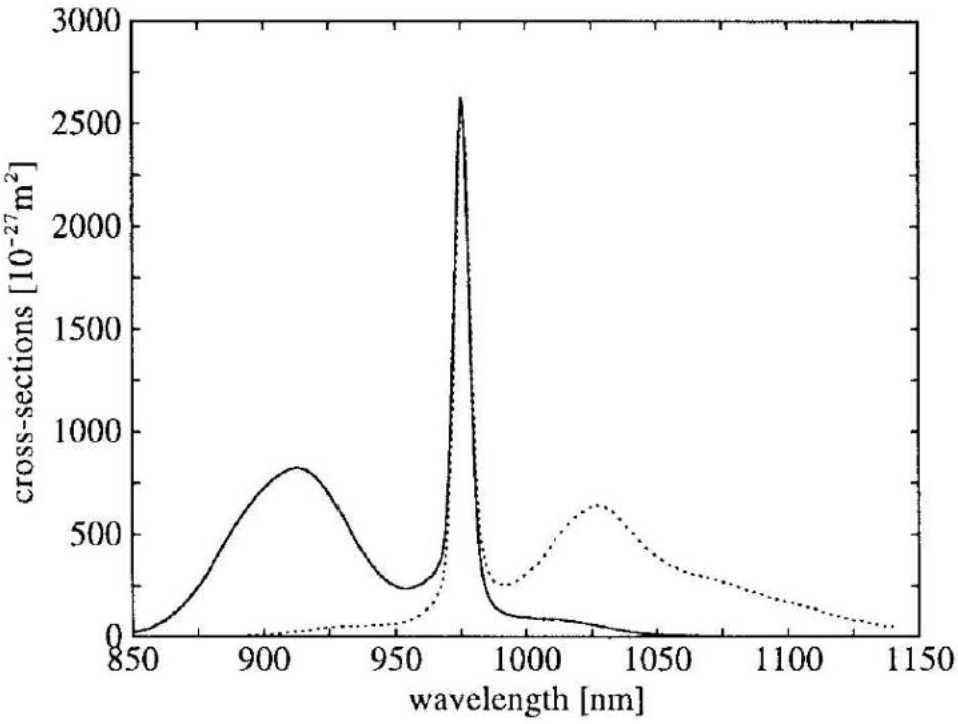

Figure 2.2 Absorption (solid line) and emission (dotted line) cross sections of Yb^{3+} [2.1]

2.2.2 Power and Efficiency

The output power, $P_{OUT,}$ emitted form a solid state laser can be expressed using the following approximation [2.2]:

$$P_{OUT} \approx (P_P - P_{PTH})\eta_s \tag{2.1}$$

where P_P is the pump power, P_{PTH} is the threshold pump power required for the laser to begin lasing and η_s is the slope efficiency of the laser. The slope efficiency is a measure of how much of the pump power is converted into useful output power. It is obvious from Eq. (2.1) that to maximise output power one can increase the pump power, lower the pump threshold or increase the slope efficiency of the laser. Since the pump power is dependent on the pump source chosen this cannot be altered through the design of the laser. To see how the laser architecture influences pump threshold and slope efficiency it is useful to understand a little more about them. The two can be expressed by the following equations:

$$P_{PTH} \approx \frac{\pi h \nu_p (L+T)(w_p^2 + w_l^2)}{4\sigma_e \tau_f \eta_p \eta_{abs}} \tag{2.2}$$

$$\eta_s \approx \left(\frac{T}{L+T}\right)\left(\frac{\nu_l}{\nu_p}\right)\eta_p \eta_{abs} \eta_{PL} \tag{2.3}$$

where h is Planck's constant, L is the round trip loss in the cavity, T is the output coupler transmission, w_p is the pump beam waist or fibre core radius, w_l is the laser mode radius, τ_f is the fluorescence lifetime of the upper laser level, η_p is the pumping quantum efficiency, η_{abs} is the fraction of pump light absorbed, ν_p and ν_l are the pump and laser frequency, respectively, and η_{PL} is the pump-laser mode overlap factor. The threshold for fibre lasers can be much lower than for bulk due to smaller core (pump beam size). Also, due to the small core size, it is easier for stimulated emission to dominate in a fibre laser resulting in improved slope efficiency. A smaller quantum defect, discussed later, can improve the efficiency. Laser materials with large emission cross-sections and long fluorescence lifetimes contribute to lower thresholds.

2.3 Modelling Fibre Lasers

The equations in the previous sections take into account a number of assumptions to show the advantages of RE doped fibre lasers compared to bulk solid state lasers. The

equations above are valid for conventional four level lasers, like Nd:YAG, but the case for fibre lasers based on Ytterbium is different. Ytterbium behaves as a quasi-three level laser due to the small quantum defect. This results in a higher threshold condition compared with four-level lasers as a population inversion occurs only when more than half of the ions are pumped into the upper laser level.

Taking into consideration the two active energy levels, ground state and excited state, we can derive equations for the threshold pump power and slope efficiency for an Ytterbium fibre laser. Under steady state conditions the population densities for the lower (N_1) and upper (N_2) manifolds can be described by the following rate equations:

$$\frac{dN_2}{dt} = (R_{12} + W_{12})N_1 - (R_{21} + W_{21} + A_{21})N_2 = 0 \tag{2.4}$$

$$\frac{dN_1}{dt} = -(R_{12} + W_{12})N_1 + (R_{21} + W_{21} + A_{21})N_2 = 0 \tag{2.5}$$

with the transmission rates, pump absorption rate R_{12}, stimulated emission rate at the pump wavelength R_{21}, signal absorption rate W_{12}, stimulated emission rate at laser wavelength W_{21}, spontaneous emission rate A_{21}, given by:

$$R_{12} = \frac{\sigma_a(\lambda_p)I_p}{h\nu_p},\ R_{21} = \frac{\sigma_e(\lambda_p)I_p}{h\nu_p},\ W_{12} = \frac{\sigma_a(\lambda_l)I_l}{h\nu_l},$$

$$W_{12} = \frac{\sigma_e(\lambda_l)I_l}{h\nu_l},\ A_{21} = \frac{1}{\tau_f}$$

σ_a and σ_e are the absorption and emission cross sections respectively, λ_l and λ_p are the laser and pump wavelengths respectively, ν_l and ν_p are the laser and pump frequencies respectively, h is Planck's constant, τ_f is the upper state lifetime and I_l and I_p are the laser and pump intensities respectively.

The total ion concentration $N = N_1+N_2$, hence:

$$N_2 = \frac{N(R_{12} + W_{12})}{R_{12} + R_{21} + W_{12} + W_{21} + A_{21}} \tag{2.6}$$

The pump power loss, P_p, and laser power growth along the fiber, P_l, (+) denoting co-propagation with pump and (–) denoting counter propagation in respect to the pump, along the z direction are given by:

$$\frac{dP_p}{dz} = \eta_p[\sigma_e(\lambda_p)N_2 - \sigma_a(\lambda_p)N_1]P_p \tag{2.7}$$

$$\frac{dP_l^+}{dz} = \eta_l[\sigma_e(\lambda_l)N_2 - \sigma_a(\lambda_l)N_1]P_l^+ \tag{2.8}$$

$$\frac{dP_l^-}{dz} = -\eta_l[\sigma_e(\lambda_l)N_2 - \sigma_a(\lambda_l)N_1]P_l^- \tag{2.9}$$

with η_p and η_l are the pump and laser overlap factors with the doped core. For a double clad fibre $\eta_p \approx A_{core}/A_{clad}$, with A_{core} is the area of the doped core and A_{clad} is the inner cladding area, $\eta_l \approx 1$. In general equations (2.7-2.9) have to be solved numerically to give the amplifier gain and laser output power. However by making some simplifying assumption then expressions for amplifier small signal gain and laser threshold can be obtained in the following way. In the absence of laser power and assuming that the amplified spontaneous emission (ASE) power is negligible:

$$\frac{dP_p(z)}{dz} = -\frac{A_{core}h\nu_p N_2(z)}{\eta_q \tau_f} \tag{2.10}$$

Where η_q is the pumping quantum efficiency. And from equations (2.7) and (2.10):

$$\ln\left[\frac{P_p(z)}{P_p(0)}\right] + \frac{P_p(z) - P_p(0)}{P_{psat}} = -\eta_p\sigma_a(\lambda_p)Nz \tag{2.11}$$

With the pump saturation power given by:

$$P_{psat} = \frac{h\nu_p}{[\sigma_a(\lambda_p) + \sigma_e(\lambda_p)]\eta_q\tau_f}\left(\frac{A_{core}}{\eta_p}\right) \tag{2.12}$$

Equation (2.11) would usually need to be solved numerically to calculate the pump power that is absorbed in a given length of fibre. For low pump power $P_p(0) << P_{psat}$ equation (2.11) is simplified to:

$$P_p(z) = P_p(0)\exp[-\eta_p\sigma_a(\lambda_p)Nz] \tag{2.13}$$

The single pass gain for a fibre of length l is given by:

$$G = \exp\left(\int_0^l g(z)dz - \alpha_L l\right) \tag{2.14}$$

Where

$$g(z) = \sigma_e(\lambda_l)N_2(z) - \sigma_a(\lambda_l)N_1(z) \tag{2.15}$$

Where α_L is the attenuation coefficient for the laser light. Combining with equation (2.10) results in a simplified expression for small signal gain

$$G = \exp\left(\frac{[\sigma_e(\lambda_l) - \sigma_a(\lambda_l)]\eta_q\tau_f P_{pabs}}{A_{core}h\nu_p} - \sigma_a(\lambda_l)Nl - \alpha_L l\right) \tag{2.16}$$

With P_{pabs} being the absorbed pump power.

If we consider a standing wave fibre laser with a output coupler transmission T and cavity loss L then the round trip gain at threshold and pump power absorbed at threshold are:

$$\mathrm{G} = \left[\exp\left(\frac{[\sigma_e(\lambda_l) - \sigma_a(\lambda_l)]\eta_q\tau_f P_{pabs}}{A_{core}h\nu_p} - \sigma_a(\lambda_l)Nl - \alpha_L l\right)\right]^2 (1-T)(1-L) = 1 \tag{2.17}$$

$$P_{pabs,th} = \frac{A_{core}h\nu_p}{2[\sigma_e(\lambda_l) - \sigma_a(\lambda_l)]\eta_q\tau_f}\left[-\ln(1-T) - \ln(1-l) + 2\sigma_a(\lambda_l)Nl + 2\alpha_L l\right] \tag{2.18}$$

One has to be careful when considering a ring laser in which the round trip includes only one passage through the gain medium resulting in a higher threshold pump power.

When the laser is operating at power levels well above threshold and core propagation loss is assumed to be negligible and the slope efficiency is approximated as:

$$\eta_s = \frac{dP_{Lout}}{dP_p} \approx \frac{T\sqrt{1-L}}{T\sqrt{1-L} + L\sqrt{1-T}} \cdot \left(\frac{\lambda_p}{\lambda_l}\right) \cdot \eta_q\eta_{abs} \tag{2.19}$$

Where η_{abs} is the absorption efficiency which for the correctly chosen length of fibre can be close to unity.

2.3.1 Beam Quality

The most popular way to define beam quality is using the beam parameter product, (BPP) and the invariant parameter known as the beam propagation factor, or "M-

squared factor" written as M^2. The BPP is the product of the beam radius w_0 and the beam divergence half angle θ, in the far field; the higher the BPP the poorer the beam quality. A diffraction limited Gaussian beam would give the smallest possible BPP of λ/π, with λ being the mean laser wavelength. M^2 is defined as the ratio of the BPP of a real beam to that of an ideal diffraction-limited Gaussian beam. It can be expressed as:

$$M^2 = \frac{\theta \pi w_o}{\lambda} \tag{2.20}$$

A beam with M^2 equal to 1 is diffraction limited. The M^2 defines a minimum possible waist that can be obtained when focusing a laser beam. From Gaussian optics we can determine the Rayleigh range z_0. A long Rayleigh range means a long depth of focus and large depth of field.

2.3.2 Thermal Effects

The efficiency of solid state lasers is always limited by the quantum defect. For a standard 4 level laser the transition from the pump level to the upper laser level and from the lower laser level to the ground state generate heat which is deposited in to the laser medium. This fraction of heat energy of the pump photon energy is called the quantum defect. In simple terms it is the energy difference between the pump photon and the laser photon. Another source of heat deposition is fluorescence quenching which reduces the lifetime of laser-active electronic levels. If the upper state lifetime is reduced this can increase the pump threshold and reduce gain. Quenching can be a result of many things such as multi-phonon transitions, energy transfer to other ions from impurities or to other laser-active ions when high concentrations are present.

The deposited heat means that the laser material has to be actively cooled. Without it this can lead to changes in the properties of the medium altering the spectroscopy amongst other things and in some cases resulting in damage such as melting or burning. Removing the heat prevents the extreme cases but leads to temperature gradients forming in the laser medium. In a bulk laser crystal this can create a thermal lens or thermal guiding in a rod fibre laser. Another effect is thermally induced stress leading to added birefringence or even physical damage. These thermal effects become ever more pronounced at higher pump powers and their management is key in generating high output powers.

2.4 Cladding Pumped Fibre Geometry

One of the best methods for generating high output power whilst maintaining good beam quality and controlling the thermal load in the laser medium is using cladding pumping. Reducing thermal effects can be done by increasing the ratio of the cooled surface area. Bulk solid state laser solutions looked at using slabs, disks and rods of active laser material. An alternative that easily increases the cooling surface is to use optical fibre.

Originally RE doped fibre was pumped directly by coupling the pump light into the core. This can prove difficult; if the core is of dimensions for single mode operation then the pump light will nearly always also need be single mode to propagate. Diode pump sources have limited power in single mode operation. By applying the cladding pumping strategy, the higher power multimode pump source can be coupled into a larger multimode inner cladding and propagate around the active doped core. The basic principle is shown in Figure 2.3. This allows for higher powers to be generated and the fibre architecture provides excellent thermal management. Again if the core supports only the fundamental laser mode then the output will be close to diffraction limited. The standard optical fibres used in power scaling consist of a RE-doped silica core typically a few percent, surrounded by an inner silica cladding of slightly lower refractive index and an outer cladding again with a lower refractive index. The resulting refractive index profile is what leads to total internal reflection which is essential for light to be guided along the fibre.

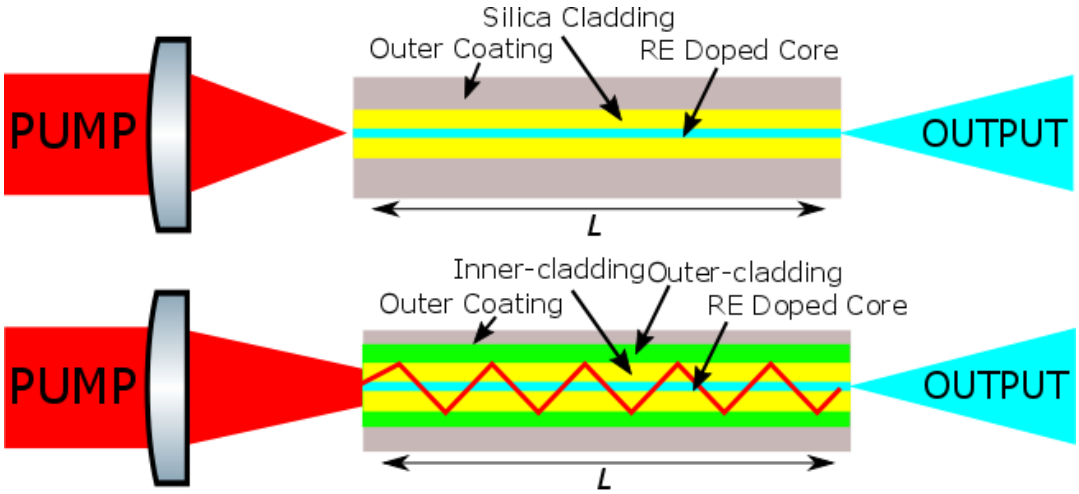

Figure 2.3 Diagram demonstrating differences between core and cladding pumping. While core pumping couples the pump light into the core, cladding pumping couples the light into the bigger inner cladding allowing for higher power multimode pump diodes.

An advantage of cladding pumping is the brightness enhancement that results from the geometry. Brightness is defined as:

$$B = \frac{Power}{Area \times Solid\ Angle} \approx \frac{P}{\pi^2 w_0^2 \theta^2} \qquad (2.21)$$

The brightness enhancement for a typical Yb-doped fibre laser B_{laser}/B_{pump} can exceed 5000.

A conventional inner cladding geometry, having a symmetrical arrangement of core and inner cladding, leads to only partial overlap of the pump light and active core increasing the required device length compared to core pumped designs. The symmetrical core/cladding also leads to helical trajectories being traced out by the pump light and is unwanted. Bending of the fibre can counter this but breaking the core/cladding geometry is preferred for longer fibres and higher NA's. Some types of non-symmetrical inner-cladding geometries are shown in Figure 2.4. The large offset of the core (B) required can cause difficulty in manufacture and splicing of such types of fibre. Breaking the symmetry can also be done by changing the shape of the inner cladding (C and D). Some types of fibre also allow for polarised light to propagate and maintain their polarisation state. This can be done by inducing birefringence into the inner cladding. An example of this is the "Panda" (E) or "Bow-tie" (F) inner cladding which has added stress rods to introduce stress birefringence and also break the radial geometry. This improves the pump power absorption, as they are of higher refractive index the scenario seen in [A] is avoided. Throughout all of the experimental work the 'Panda' type [E] is used.

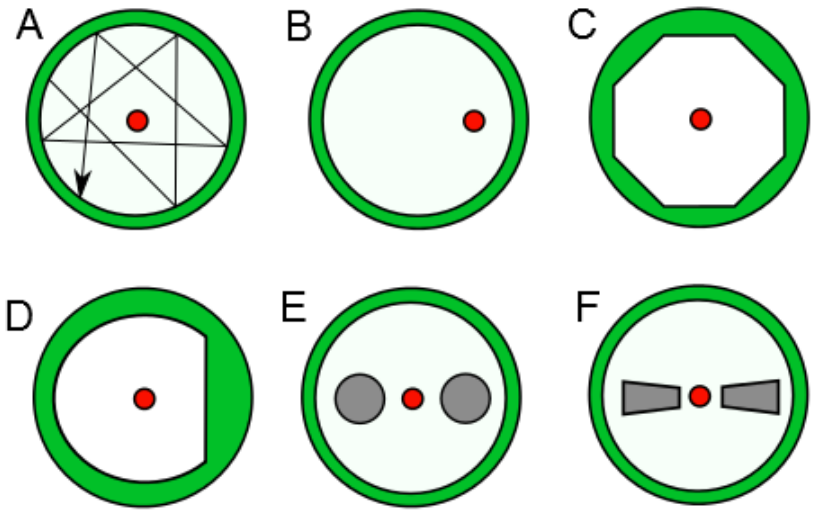

Figure 2.4 Common inner-cladding geometries to allow for more efficient pump absorption by breaking symmetries (B-D) and polarisation maintaining (PM) fibres incorporating birefringent stress rods.

2.4.1 Effects Limiting Output Power in Fibres

Cladding pumped fibre lasers allow for high output powers but even they have their limits. Many factors can contribute, either individually or combined. The detailed analysis by J.W. Dawson et al. [2.3] covered many factors that limit the output power possible, giving a maximum output peak power of 36.6kW. Once again thermal effects come into play; consequences of high heat generation include thermal fracture and lensing, in rod fibres, and even melting of the core. Away from heat other limiting factors include the onset nonlinearities at high intensities such as Stimulated Brillouin Scattering (SBS) in the case of narrowband emission and Stimulated Raman Scattering (SRS) for the broadband emission case. Optical damage mainly to the end faces of the fibre can be a barrier and ultimately again the available pump power (brightness) will limit performance. Figure 2.5 and Figure 2.6 and show which factors limit the output power for various fibre core diameters and fibre lengths.

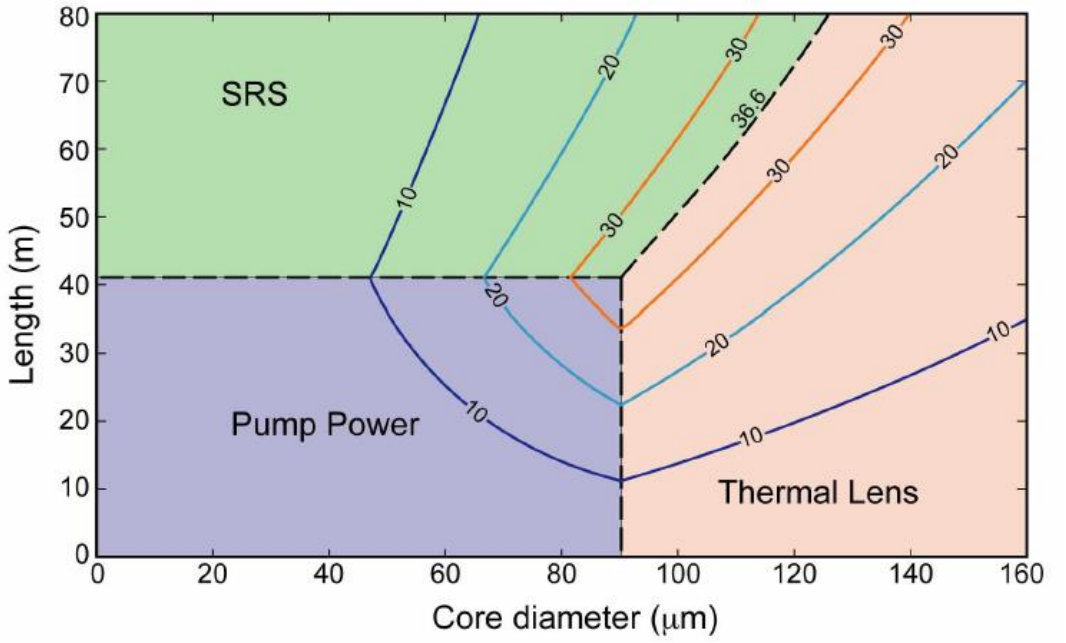

Figure 2.5. Contour plot taken from [2.3] taking into account several limiting factors and displaying the three limiting factors in this case for different fibre core diameters and fibre lengths. SBS has been ignored.

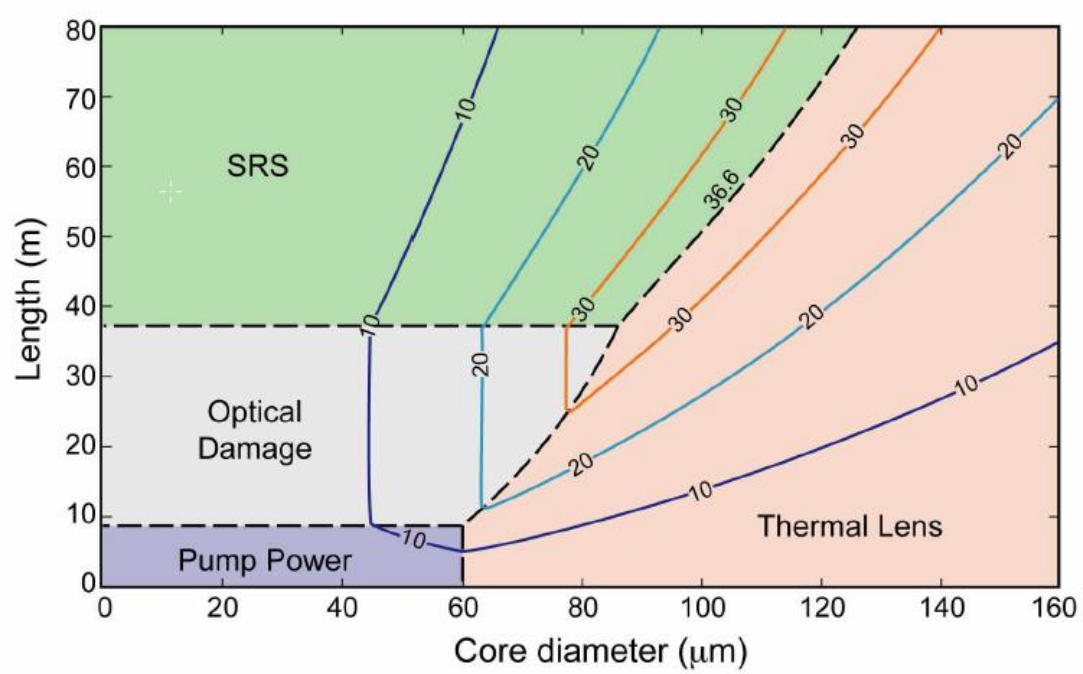

Figure 2.6 Contour plot taken from [2.3] taking into account several limiting factors and displaying the three limiting factors in this case for different fibre core diameters and fibre lengths this time accounting for an improvement in pump brightness. This introduces another limiting factor due to optical damage. SBS has been ignored.

Both figures ignore the effects of SBS which is more relevant to sources emitting in a narrowband. Dawson et al. consider the other 6 factors, thermal fracture, melting of the core, thermal lens, SRS, damage and pump power. Assuming that the diode pump brightness will continue to increase Figure 2.5 can be re-plotted with increased pump brightness of 5 times that of before, giving Figure 2.6. A new region emerges which limits the output power, resulting from optical damage. The maximum power is still 36.6kW. The other 3 limiting factors remain the same with the pump power region decreasing as a result of the improved brightness.

2.5 Nonlinear Frequency Conversion

2.5.1 Second Harmonic Generation

When high intensity light is incident on dielectric media, bound charges become separated and rapidly oscillating dipole moments become present. This results in a nonlinear polarisation P being created by the total electric field E, commonly expressed as [2.4]:

$$P = \varepsilon_0 \chi^{(1)} E + \varepsilon_0 \chi^{(2)} EE + \varepsilon_0 \chi^{(3)} EEE + \cdots \quad (2.22)$$

where ε_0 is the permittivity of free space, $\chi^{(1)}$ is the linear electric susceptibility, $\chi^{(2)}$ and $\chi^{(3)}$ being the second and third order nonlinear susceptibilities respectively. Certain nonlinear crystals exhibit a strong $\chi^{(2)}$ and can be used to generate the second harmonic of the incident signal photon. The nonlinear polarisation represented in its Fourier components consists of many components oscillating at different frequencies; hence generating new wavelengths of light if the right conditions are met. SHG is the process of taking an incoming photons of frequency ω and generating photons at frequency 2ω on passage through the nonlinear crystal.

The two waves are coupled due to the nonlinear polarisation of the medium with their amplitude changing along the interaction length. First solved by Armstrong et al. [2.5] they can be described by the coupled wave equations:

$$\frac{dE_{2\omega}}{dz} = \frac{i\omega}{n_{2\omega}} d_{eff} E_{\omega}^2 \exp(i\Delta k z) \quad (2.23)$$

$$\frac{dE_{\omega}}{dz} = \frac{i2\omega}{n_{\omega}} d_{eff} E_{\omega}^* E_{\omega} \exp(-i\Delta k z) \quad (2.24)$$

With $i=\sqrt{-1}$, E_ω and $E_{2\omega}$ are the fundamental and second harmonic wave amplitudes respectively, n_ω and $n_{2\omega}$ are the refractive index values of the medium for the respective waves, d_{eff} is the effective nonlinear coefficient of the medium and Δk represents the phase velocity mismatch between the two waves, which is given by:

$$\Delta k = (2\boldsymbol{k}_w - \boldsymbol{k}_{2w}) \,.\, \hat{z} \quad (2.25)$$

Where $\mathbf{k}_\omega$ and $\mathbf{k}_{2\omega}$ ar the wave vectors for the fundamental and second harmonic waves respectively and $\hat{z}$ is the unit vector in the propagation direction. The intensity of the optical wave at frequency ω is:

$$I_\omega = 2\varepsilon_0 n_\omega c|E_\omega|^2 \tag{2.26}$$

With c being the speed of light in a vacuum. If we consider the total optical power within a Gaussian beam of spot size w_0, with a central intensity I_0, by integrating the intensity over the beam with area A:

$$P = \int_A IdA = \frac{1}{2}\pi w_0^2 I_0 \tag{2.27}$$

This allows us to express the total conversion efficiency for SHG as in [2.6];

$$\eta_{SHG} = \frac{P_{2\omega}}{P_\omega} = tanh^2\left(\sqrt{\epsilon P_\omega}\right) sinc^2\left(\frac{\Delta kL}{2}\right) \tag{2.28}$$

With P_ω being the fundamental power incident on the crystal of length L and ϵ containing a lot of the other constants:

$$\epsilon = \frac{16\pi d_{eff}^2 L^2}{w^2 \varepsilon_0 n_\omega^2 c \lambda_\omega^2} \tag{2.29}$$

where w is the average spot size within the nonlinear crystal and λ_ω is the fundamental wavelength. These equations show that due to the $sinc^2(\Delta kL/2)$ term even small values of Δk lead to a very small conversion efficiencies being realised. If the phase matching condition is met, Δk=0, and the fundamental wave power is not significantly depleted then equation (2.28) will simplify to:

$$\eta_{SHG} = \epsilon P_\omega \tag{2.30}$$

2.5.2 Phase Matching

A number of techniques exist for phase matching the interacting waves. These include angular phase matching of the two **k** vectors, known as critical phase matching, tuning the refractive index values for the fundamental and second harmonic by changing the temperature of the crystal, known as non-critical phase matching along with quasi-phase matching in periodic media or making use of wave-guiding media.

It is useful to note that there are two types of SHG possible depending on the polarisation of the fundamental and second harmonic waves with respect to the crystal axis. In Type I phase-matching the pump wave is an o-wave polarized along one of the crystal axis and the second harmonic is an e-wave with polarised in the orthogonal direction.

$$o_\omega + e_\omega = e_{2\omega} \tag{2.31}$$

Type II phase matching concerns a pump wave that comprises a superposition of o- and e- waves and the second harmonic is again an e-wave. In the photon picture two photons at frequency ω from the o-wave are annihilated to produce one photon at frequency 2ω adding to the e-wave.

$$o_\omega + o_\omega = e_{2\omega} \tag{2.32}$$

2.5.2.1 Non-critical Phase Matching

Non-critical phase matching (NCPM) refers to a scenario in which the fundamental and second harmonic waves propagate along one of the principle axes of the crystal with the phase matching condition satisfied by temperature tuning the refractive index of the two waves. The general condition for NCPM is expressed by:

$$n_{2\omega}(T_{pm}) = \frac{1}{2}[n_w(T_{pm}) + n'_\omega(T_{pm}) \tag{2.33}$$

which can be simplified for the case of Type I SHG (ooe):

$$n^e_{2\omega}(T_{pm}) = n^o_\omega(T_{pm}) \tag{2.34}$$

with the refractive indices n_w and n'_ω for orthogonal pump polarisation components are different and 'o' and 'e' refer to the refractive index values along the ordinary and extraordinary axes respectively. If the refractive index is expanded into a Taylor series around the room temperature T_0:

$$n^k_j(T_{pm}) = n^k_j(T_0) + \left.\frac{\partial n^k_j}{\partial T}\right|_{T=T_0} (T_{pm} - T_0) \tag{2.35}$$

And following from (2.34) the phase matching temperature is

$$T_{pm} = T_0 + \frac{n^e_{2\omega}(T_0) - n^o_{\omega}(T_0)}{\left[\frac{\partial n^o_{\omega}}{\partial T} - \frac{\partial n^e_{2\omega}}{\partial T}\right]_{T=T_0}} \tag{2.36}$$

To determine the temperature bandwidth, the phase velocity mismatch is expanded in a Taylor series about the phase matching temperature [2.6]:

$$\Delta k(T) = \left.\frac{\partial(\Delta k)}{\partial T}\right|_{T=T_0} \Delta T \equiv \gamma_T \Delta T \tag{2.37}$$

The $sinc^2(\Delta kL/2)$ factor in (2.28) drops to 0.5 when

$$\Delta kL \approx 2.784 \tag{2.38}$$

Then results in the temperature bandwidth to be:

$$\Delta T_{BW} = |2.784/(\gamma_T L)| \tag{2.39}$$

where in the case for Type-I SHG (ooe):

$$\gamma_T = \frac{4\pi}{\lambda_\omega}\left[\frac{\partial n^o_{\omega}}{\partial T} - \frac{\partial n^e_{2\omega}}{\partial T}\right]_{T=T_{pm}} \tag{2.40}$$

2.5.2.2 Critical Phase Matching

Critical phase matching refers to a configuration on which the interacting waves are aligned to some angle relative to the principle axis of the crystal. An advantage of critical phase matching is that no temperature tuning is required allowing for the efficient conversion at room temperature. Hence the term 'critical' comes from the fact that very careful alignment has to be ensured for efficient phase matching to occur.

In uniaxial crystals, there is a single axis of symmetry, usually denoted as the Z-axis, which coincides with the principle optic axis. The principle refractive indices are therefore labelled as $n_x = n_y = n^o$ and $n_z = n^e$. When $n^o < n^e$ the crystal is referred to as a positive uniaxial crystal, when the opposite is true the crystal is called a negative uniaxial crystal. When propagating at an angle θ with respect to the Z-axis, the extraordinary wave has a refractive index given by:

$$\frac{1}{[n^e(\theta)]^2} = \frac{cos^2(\theta)}{[n^o]^2} + \frac{sin^2(\theta)}{[n^e]^2} \tag{2.41}$$

This relation is used to calculate the phase matching angle for SHG processes.

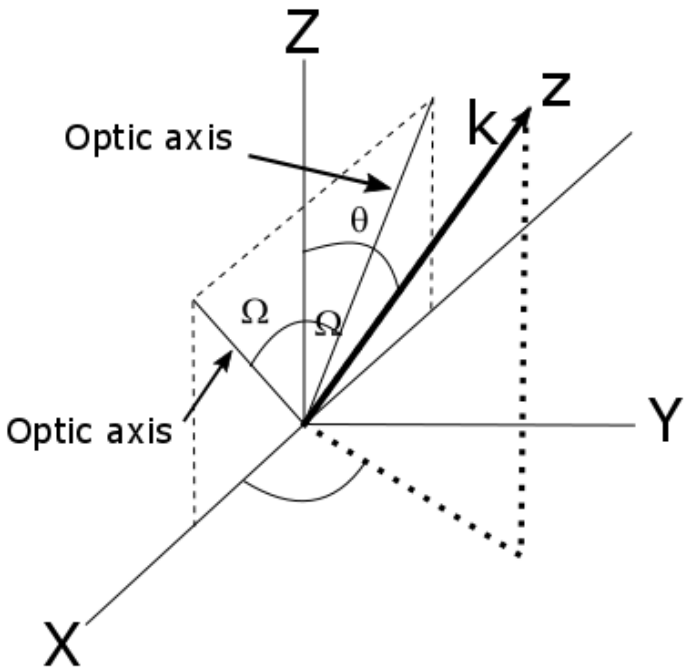

Figure 2.7 Schematic of wave propagation in the crystal coordinate system for a biaxial crystal. Adapted from [2.6].

In this experiment we will be using a biaxial crystal, where there are two optic axes which both lie in the XZ plane, shown in Figure 2.7. Convention states that $n_Z > n_Y > n_X$ Both of these optic axis make an angle Ω with respect to the Z-axis given by:

$$\sin\Omega = \frac{n_Z}{n_Y}\left(\frac{n_Y^2}{n_Z^2} - \frac{n_X^2}{n_X^2}\right)^{1/2} \tag{2.42}$$

They are situated symmetrically about the Z-axis and can propagate at an angle ϕ with respect to the X-axis and angle θ with respect to the Z-axis. The two allowed modes of propagation have refractive indices that can be calculated from the Fresnel equation as in [2.6]:

$$\frac{sin^2\theta cos^2\phi}{(n)^{-2} - (n_X)^2} + \frac{sin^2\theta cos^2\phi}{(n)^{-2} - (n_Y)^2} + \frac{cos^2\theta}{(n)^{-2} - (n_Z)^2} = 0 \tag{2.43}$$

This is used to calculate the phase matching angles for SHG. For Type-I (ooe) SHG the phase matching direction is given by angles ϕ_{pm} and θ_{pm} in the XY and XZ planes respectively, again taken from [2.6]

$$tan^2\phi_{pm} = \frac{1 - \left(\frac{n_\omega^Z}{n_{2\omega}^Y}\right)^2}{\left(\frac{n_\omega^Z}{n_{2\omega}^X}\right)^2 - 1} \tag{2.44}$$

$$tan^2\theta_{pm} = \frac{1 - \left(\frac{n_\omega^Y}{n_{2\omega}^X}\right)^2}{\left(\frac{n_\omega^Y}{n_{2\omega}^Z}\right)^2 - 1} \tag{2.45}$$

The sensitivity in angular alignment for this phase matching technic result in the term 'critical'. For small deviations $\Delta\theta = \theta - \theta_{pm}$ about the pahse matching direction the efficiency will decrease. The phase velocity mismatch due to an angular deviation $\Delta\theta$ can be computed by expanding Δk in a Taylor series [2.6]

$$\begin{aligned}\Delta k(\theta - \theta_{pm}) &= \left.\frac{\partial(\Delta k)}{\partial\theta}\right|_{\theta=\theta_{pm}} \Delta\theta + \frac{1}{2}\left.\frac{\partial^2(\Delta k)}{\partial\theta^2}\right|_{\theta=\theta_{pm}} (\Delta\theta)^2 \\ &\equiv \gamma_{CPM}\Delta\theta + \gamma_{NCPM}(\Delta\theta)^2\end{aligned} \tag{2.46}$$

Where CPM and NCPM stand for critical phase matching and non-critical phase matching. For CPM only the first term should be retained. Substituting for the phase matching bandwidth (2.38) results in the angular phase matching bandwidth for Type-I CPM SHG (ooe):

$$\Delta\theta_{BW} = |2.784/(\gamma_{CPM}L)| \tag{2.47}$$

Where:

$$\gamma_{CPM} = \frac{2\pi}{\lambda_\omega}(n_\omega^o)^3\left[\frac{(n_{2\omega}^o)^2 - (n_{2\omega}^e)^2}{(n_{2\omega}^o)^2 + (n_{2\omega}^e)^2}\right] sin2\theta_{pm} \tag{2.48}$$

and for Type-I NCPM SHG (ooe):

$$\Delta\theta_{BW} = |2.784/(\gamma_{NCPM}L)|^{1/2} \tag{2.49}$$

Where:

$$\gamma_{NCPM} = \frac{2\pi}{\lambda_\omega} n_{2\omega}^e\left[\frac{(n_{2\omega}^e)^2}{(n_{2\omega}^o)^2} - 1\right] sin2\theta_{pm} \tag{2.50}$$

Beam divergence must be limited in the case of CPM to work due to the small range of beam angles, implying that a larger beam waist than that for NCPM should be used.

2.5.2.3 Quasi-phase Matching

In the case of the quasi phase matching scheme for SHG a plane wave at the signal frequency ω_1 and with wavevector $k_1 = n1 \ \ \omega_1/c$ passes through a medium with nonlinear susceptibility d generating a nonlinear polarisation wave proportional to the input wave amplitude at a frequency $\omega_2 = 2\omega_1$ and wavevector $2k_1$. The free and forced wave accumulate a phase shift of π over a specific distance known as the coherence length [2.7]:

$$l_c = \frac{\pi}{(k_2 - 2k_1)} = \frac{\lambda_\omega}{4(n_2 - n_1)} = \frac{\pi}{\Delta k} \tag{2.51}$$

where λ_ω is the wavelength of the fundamental wave in vacuum.

The direction in which the power flows between the signal wave and the harmonic will change every coherence length as it depends on the relative phases of each wave. Changing the sign of the nonlinear susceptibility every coherence length will induce a phase shift of π for the polarisation wave. This re-phases the interaction and leads to monotonic power flow into the harmonic wave, shown in Figure 2.8, adapted from [2.7]. It is evident from Figure 2.8 that the QPM second harmonic intensity will be lower than that for a perfectly phase matched wave in the same medium, however QPM does have its advantages. QPM does not rely on birefringence meaning that any polarisations can be used. All waves can be polarised along the same plane allowing them to couple to the strongest nonlinear susceptibility tensor of the material used and can even be used in isotropic media such as GaAs where birefringent phase matching is not possible. Problems can arise from parasitic higher-order nonlinear processes that generate light at non-desired wavelengths affecting efficiency. Fabricating the periodically poled material to use for QPM is difficult and limited to specific crystal materials. The periodic polling always changes for different nonlinear processes requiring separate crystals to be made which are expensive to manufacture to the high material quality that is required for highly efficient frequency conversion. The limit in size of the crystal that can be manufactured puts an upper limit on the power levels that can be used.

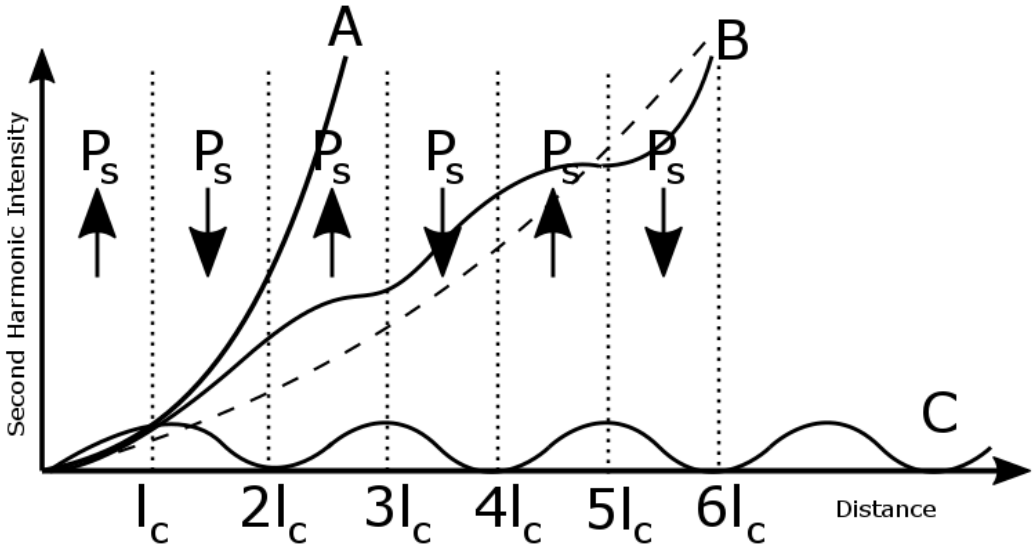

Figure 2.8 The effect of phase matching on the growth of second harmonic intensity with distance in a nonlinear crystal. A: perfect phase matching in a uniformly poled crystal. C: non phase matched interaction.
B: first order QPM by flipping the sign of the spontaneous polarisation(P_s) every coherence length(l_c) of the interaction curve C.

One of the popular crystals used for frequency doubling is Lithium Triborate (LiB_3O_5) referred to as LBO. LBO is a biaxial crystal with a wide transparency window (0.16 – 2μm), high damage threshold, good birefringence for phase matching visible and UV interactions along with a wide acceptance angle. LBO has been used for second and third harmonic generation of 1.06μm radiation and can be temperature tuned for noncritical phase matching.

2.5.3 Nonlinear Crystals

This thesis will focus on one crystal from the borate family: Lithium Triborate (LiB_3O_5) or LBO. This is a biaxial crystal which has a high transparency window (0.16-2μm), a high damage threshold (18.9GW/cm^3 for a 1.3ns laser pulse at 1053nm) and adequate birefringence for phase matching a broad range of visible and ultra-violet interactions with a wide acceptance angel and small walk-off. A detailed study of LBO properties has been documented in [2.8].

LBO crystals have been used in numerous nonlinear frequency conversion applications. They have been used to generate second and third harmonics of ≈1μm radiation and can

be temperature tuned for non-critical phase matching [2.9]. They have also seen use for SHG of dye lasers [2.10] and Ti:Saphire lasers [2.11].

2.5.4 Intracavity SHG in Bulk Lasers

There exists a high demand for high-power CW lasers emitting in the visible wavelengths that are not directly possible using standard solid state laser media, both in a 'bulk' or fibre geometry. High power visible lasers are needed in a wide array of fields for a range of applications, including laser processing, projection displays, sensing, defence and medicine. A popular technique to access these wavelengths is through nonlinear frequency conversion of near infra-red fibre and 'bulk' lasers. In the high peak power pulsed laser world this process is sufficient for the requirements demanded. However in the CW regime more complicated laser geometries are required. The nonlinear medium used has to be able to withstand high average powers and be able to handle large mode sizes. The materials used need to have a good thermo-optical and thermo-mechanical properties, but they all generally have low nonlinear coefficients. This weak nonlinearity only allows for a frequency conversion efficiency of a few percent per kilowatt per centimetre of nonlinear medium. When considering the high power pulsed laser sources, external second harmonic generation is easily achieved in single pass configuration. The most popular method for CW sources is through an internal SHG approach. The nonlinear crystal is placed inside the laser cavity (intracavity), optimisation of the pump beam inside the laser rod and the beam size inside the crystal can give good spatial overlap to achieve high efficiencies. This cavity configuration exploits the low intracavity loss and high intracavity powers and is one of the best approaches for generating high powers in the visible wavelengths.

2.5.5 SHG Schemes for CW Fibre Lasers

Fibre lasers have demonstrated excellent power scaling abilities and have been able to achieve power in excess of 1kW as already discussed. The cladding pumped architecture of optical fibres is able to negate the temperature problems that hamper bulk laser media making fibres the choice for power scaling applications. This promises a route to higher powers in the visible spectrum. Schematic configurations of the most common SHG techniques used involving fibre lasers is shown in Figure 2.9.

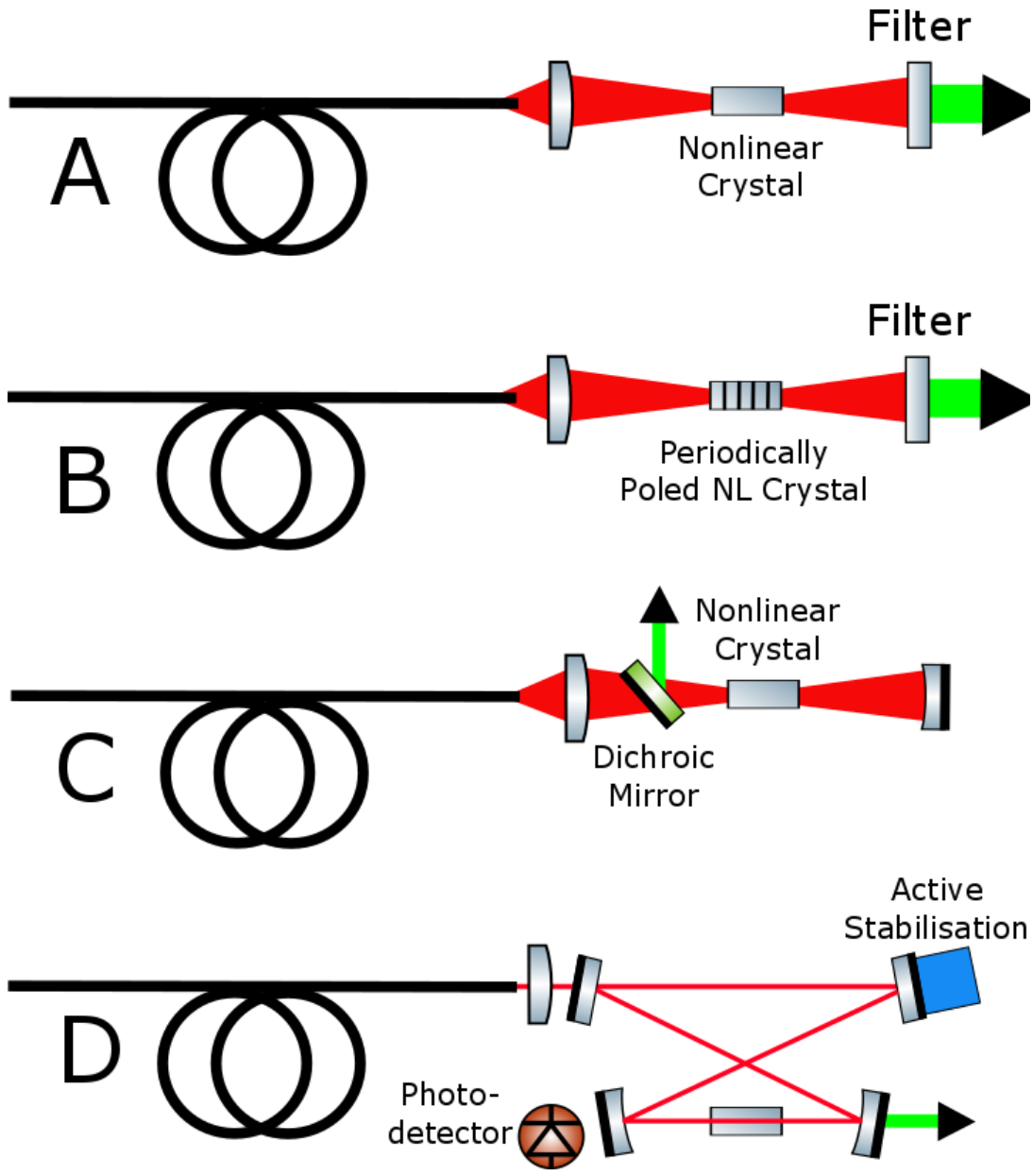

Figure 2.9 Common schematic arrangements for frequency doubling of fibre lasers. (A) Single pass external SHG. (B) Single pass external SHG using a periodically poled nonlinear crystal. (C) Intracavity SHG (D). External resonantly enhanced SHG.

The simplest approach of single pass external SHG, (A), is very simple in its design but struggles to achieve high conversion efficiencies and hence high output powers and is only suited for high power pulsed operation of the fibre lasers. Even then the single pass conversion efficiency is limited to only a few percent meaning that a very high power is needed in the IR signal. Relatively high conversion efficiencies can be achieved if a periodically poled nonlinear crystal is used in a single pass configuration, (B), however thermal effects quickly become apparent at high powers and limit the crystal performance.

The standard intracavity technique used in bulk solid state lasers does not perform well in a fibre laser resonator due to the high intracavity losses now present, (C). The high losses are compensated by the high gain from the active fibres but to extract high powers a very high transmission output coupler needs to be used which results in a low intracavity power; detrimental to intracavity SHG.

The configuration in (D) has seen the greatest success in scaling output powers. This scheme involves an external cavity which can resonate on modes of the fibre laser, this allows for very high intracavity powers to be circulating in the external resonator and subsequent high conversion into the second harmonic. The added complication here is the requirement of active stabilisation of the external cavity to ensure that it is always on resonance with the lasing mode of fibre laser.

In this thesis the resonant cavity technique is applied intracavity to remove the need for active stabilisation but maintain the intracavity powers generated to result in high conversion efficiencies and SHG powers.

2.6 Power Scaling via an Internal Enhancement Resonator

2.6.1 Concept Overview

As is already demonstrated intracavity power enhancement can be achieved with high efficiency and no requirements on cavity stabilisation are required. The concept can be employed in two cavity arrangements, linear and ring. The linear cavity has yielded excellent results [2.12] and this thesis will focus on implementing a ring cavity approach with a different wavelength selection arrangements. Figure 2.10 gives a schematic overview of the concepts involved in the ring cavity. The arrangement consists of three stages. The first is the all fibre gain stage, an active Ytterbium doped fibre is pumped by high power laser diodes; the second is the free space enhancement cavity which allows for high intracavity build up and efficient SHG generation and finally a spectrum narrowing, wavelength selective stage. An advantage of the ring formation over a linear cavity is the improved feedback into the active fibre, where the feedback signal has to travel back through the whole set up in a linear cavity, in the ring the feedback is coupled straight back into the fibre.

The fibre laser can oscillate on longitudinal modes that are defined by the main cavity. The frequencies or wavelengths are imposed by the round-trip path length of the resonator, L as:

$$\lambda_L = \frac{L}{m} \quad or \quad \nu_L = m\frac{c}{L} \tag{2.52}$$

with spacing denoted by:

$$\Delta\lambda_L = \frac{\lambda_L^2}{L} \quad or \quad \Delta\nu_L = \frac{c}{L} \tag{2.53}$$

So, the main ring resonator defines a large number of modes that can resonate, the enhancement cavity will resonate on a smaller number of those modes, the others will experience high loss, leaving only the resonant modes to oscillate. Finally the spectrum narrowing element selects the wavelength of oscillation and reduces the emission bandwidth to be smaller than the phase matching bandwidth of the SHG crystal. This leaves the laser to oscillate on axial modes that match both the enhancement resonator and the spectrum narrowing element. This will lead to a high intracavity power

circulating within the enhancement cavity. As long as the round trip loss of the enhancement cavity is small compared to the round trip loss of the fibre laser these high powers can be attained. A benefit of this arrangement is that there is no requirement for the fibre laser to oscillate on a single mode.

The long round trip path length and small axial mode separation allows for the fibre laser to oscillate on a very large number of axial modes meaning that the laser will oscillate on a large number of modes that are simultaneously resonant in the enhancement cavity. Usually there will be a number of transmission peaks N within the bandwidth Δλ of the wavelength tuning element;

$$N \approx d\Delta\lambda/\lambda^2 \tag{2.54}$$

Where d is the round trip path length of the enhancement resonator. Each transmission peak will have multiple longitudinal modes within it. Care has to be taken in designing the system such that at least one axial mode lies within each transmission peak. This is done by the choosing the specific length of the fibre cavity and enhancement cavity. This will be true when the axial mode separation is smaller than the width of the transmission peak of the enhancement cavity. Hence, the minimum effective length that the main laser cavity can be is defined by;

$$L_{min} \approx dF \tag{2.55}$$

This defines that the main cavity round trip path length must be F times longer than the round trip path length of the enhancement cavity, where F is the enhancement resonator finesse. If the length of fibre required to satisfy this condition is longer than the needed active fibre for good pump absorption passive fibre can be spliced to extend the fibre length. Once the main cavity length is greater than (2.55) there will always be modes to satisfy the resonance condition so that active stabilisation of the cavity length is not required. This results in the laser being immune from any mechanically or thermally induced path length variations.

By design the enhancement cavity can transmit light in both directions. The transmission of the cavity for resonant wavelengths is dependent on the input and output coupler transmission and the power dependant round trip loss. Looking at the concept outline in Figure 2.10 the preferred forward direction of oscillation as indicated by the arrows is not naturally favoured. For the same power levels the loss of the enhancement cavity is greater in the forward direction compared to the backward. This means that a non-

reciprocal device, such as a Faraday isolator, is needed within the ring laser cavity to enforce oscillation in the desired forward direction. Its position should be again after the internal cavity so as to minimise any loss in power entering the cavity.

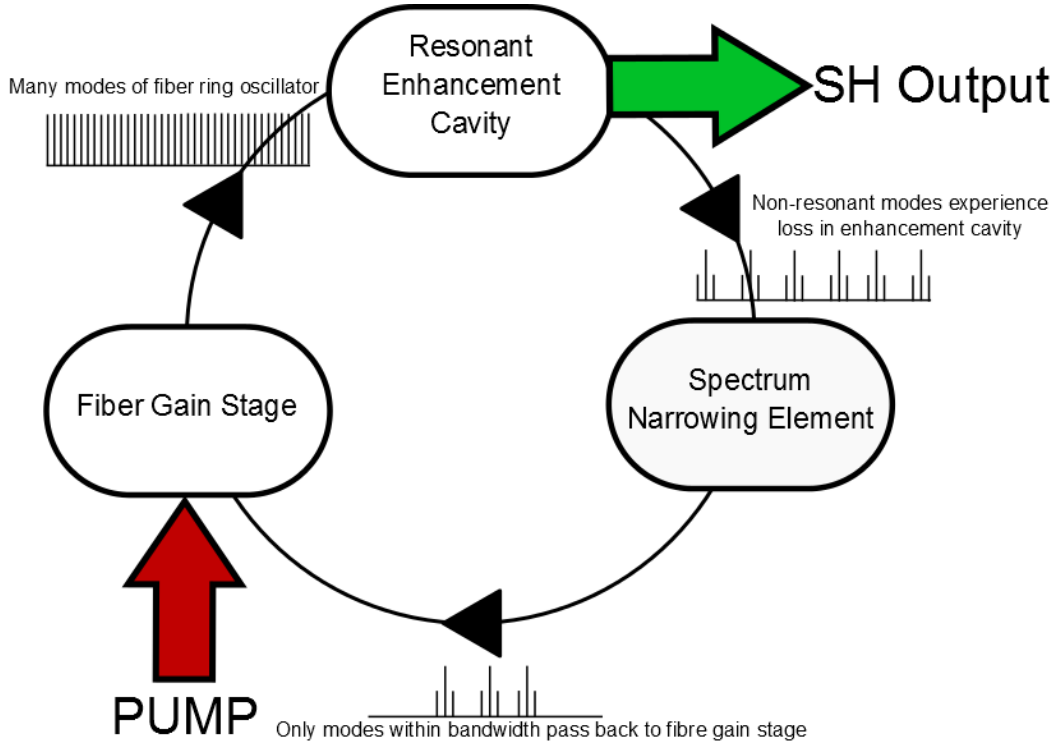

Figure 2.10 Diagram showing the ring fibre laser concept comprised of three stages. The main fibre gain stage generating many axial modes, followed by the enhancement cavity which only resonates on a few of the modes of the main fibre. Finally the Spectrum narrowing element that both narrows the emission bandwidth and can allow for wavelength selection.

2.6.2 Wavelength Tuning Arrangement

2.6.2.1 Birefringent Filter

The linear cavity approach uses a diffraction grating as the spectrum narrowing element. This works very well in that configuration at the HR end of the resonator. However in a ring cavity a diffraction grating working in reflection would complicate the physical arrangement of components so a narrowing element that operates in transmission is preferred. A popular choice in Dye lasers, Ti:Sapphire lasers and Optical Parametric Oscillators (OPO) is the birefringent, or Lyot, filter [2.13]. This consists of a number of birefringent quartz plates that interact with polarised light and can be designed to transmit narrow bands of light. When inserted at close to Brewster's angle the birefringence leads to a wavelength dependant polarisation change and hence transmission loss. Commonly a stack of 2-4 plates is used with thickness decreasing by a

factor of two which allows for the narrowed transmission peaks to be separated well from one another. The thickest plate sets the bandwidth, $\delta\nu_{BF}$, of the transmission peaks and the thinnest plate sets the free spectral range, $\Delta\nu_{FSR}$ this can be calculated in terms of frequency from [2.13]:

$$\Delta\nu_{FSR} = \frac{c}{(n_e' - n_o)L_{thin}} \tag{2.56}$$

$$\Delta\nu_{BF} = \frac{c}{2(n_e' - n_o)L_{thick}} \tag{2.57}$$

where c is the speed of light, L is the plate thickness of the thinnest or thickest plate, n_e' is the extraordinary refractive index and n_o is the ordinary refractive index of the material.

This birefringent filter alone is not enough to narrow the linewidth below 1nm so added to this is a plane-parallel Fabry-Pèrot (FP) etalon. Combining these two elements allows for wavelength selection via the birefringent filter and subsequent narrowing of the transmission spectrum through the FP etalon.

2.6.3 Enhancement Cavity

Efficient SHG is proportional to incident power. Therefore to achieve a high power at the second harmonic one requires a high build-up of the fundamental. By placing the nonlinear crystal inside a low-loss free space resonator this can be achieved as the intracavity power of the enhancement resonator can build to very high values. A diagram of the 'bow-tie' resonator is given in Figure 2.11.

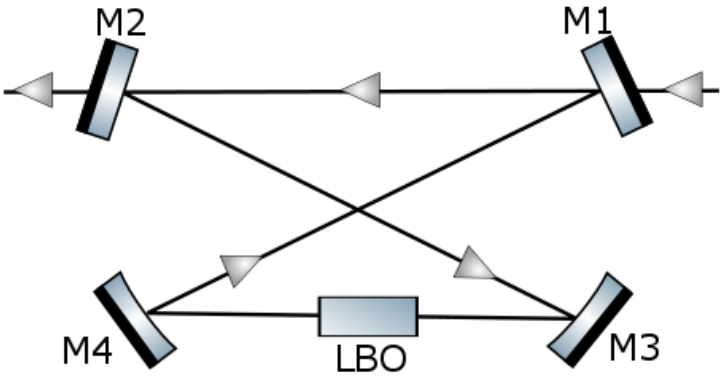

Figure 2.11 Diagram of "bow-tie" enhancement cavity with Brewster cut LBO crystal housed in oven.

Mirrors M1 and M2 are plane mirrors with a reflectivity at the fundamental wavelength R1 = r_1^2 and R2 = r_2^2. The two concave mirrors M3 and M4 have high reflectivity at the fundamental wavelength R3 = R4 = r_{HR}^2 high transmission at the second harmonic. The nonlinear crystal, length L_c is a standard Brewster-angled Lithium Triborate (LBO) crystal inside a temperature controlled oven. r_1, r_2 and r_{HR} are the electric field reflection coefficients at the fundamental wavelength for mirrors M1, M2 and M3 respectively. Chapter 5 of [2.14] provides a detailed description of the theory relating to the efficient operation of the enhancement cavity. The following is a short summary of some of the important parameters.

If the incident electric field on M1 is E_i the amplitude transmitted by the cavity out of M2 E_t is given by:

$$E_t = \sum_{n=0}^{\infty} E_i t_1 t_2 \, (t_1 t_2 t_c e^{i\delta})^n = \frac{E_i t_1 t_2}{1 - \, r r_2 t_c e^{i\delta}} \tag{2.58}$$

where $\delta = \frac{2\pi}{\lambda} d$ is the round trip phase shift, d being the round trip path length, $t_1 = \sqrt{1 - \, r_1^2}$, $t_2 = \sqrt{1 - \, r_2^2}$ are the amplitude transmittances of the mirrors M1 and M2 respectively. The round trip transmission function t_c is denoted by:

$$t_c = \, r_{HR}^2 \sqrt{(1-\alpha)(1-\eta_{SHG})} \tag{2.59}$$

where α is the sum of all the losses excluding the SHG output, denoted by η_{SHG} for a single round trip, and the mirror transmissions.

The power transmission function of the cavity defined as the ratio of the power incident on the cavity M1, P_i and the power exiting the cavity at M2, P_t is given by:

$$T(\delta) = \frac{E_t E_t^*}{E_i E_i^*} = \frac{(t_1 t_2)^2}{(1 - \, r_1 r_2 t_c)^2 + 4 r_1 r_2 t_c sin^2(\delta/2)} \tag{2.60}$$

The function is similar to the transmission function of a simple etalon and just like that case only resonant frequencies close to the resonant condition $sin^2(\delta/2) = 0$ are transmitted. When this conditioned is satisfied the transmission function reaches a maximum:

$$T_{max} = \left(\frac{t_1 t_2}{1 - \, r_1 r_2 t_c}\right)^2 \tag{2.61}$$

To calculate the width of the resonant mode we need to consider the value of the transmission function at half of the maximum. For Eq.2.40 to be satisfied the phase shift $\delta = \frac{2\pi}{\lambda} d = 2\pi m \left(\lambda = \frac{d}{m}\right)$. Following the steps carried out in Chapter 5 of [2.14] we reach an expression for the width of the enhancement cavity mode:

$$\delta\lambda = \frac{2\lambda^2}{\pi d} sin^{-1}\left(\frac{1 - r_1 r_2 t_c}{2\sqrt{r_1 r_2 t_c}}\right) \tag{2.62}$$

Along with the free spectral range (FSR), or in other words the spectral distance between the transmission peaks, which is given by:

$$\Delta\lambda = \frac{\lambda^2}{2\pi d}[2\pi(m+1) - 2\pi m] = \frac{\lambda^2}{d} \tag{2.63}$$

The finesse of the cavity is the ratio of the FSR and the cavity mode width, expressed as:

$$F = \frac{\Delta\lambda}{\delta\lambda} = \frac{\pi}{2sin^{-1}(1/\sqrt{\phi})} \tag{2.64}$$

In which the finesse coefficient is:

$$\phi = \frac{4 r_1 r_2 t_c}{(1 - 4 r_1 r_2 t_c)^2} \tag{2.65}$$

We can express a set of equations as a function of the power P_i which is incident on the input mirror of the enhancement cavity (M1). These include the power transmitted by the cavity P_t which exits the output coupler mirror (M2). The intracavity power that is circulating inside the resonator P_c before it reaches the output coupler. The power lost inside the cavity P_l, which does not include the power converted to the second harmonic output. And finally the power rejected from the cavity P_r which is reflected at the input coupler (M1). These power expressions are shown in the following equations:

$$P_t = P_i T = \frac{P_i (t_1 t_2)^2}{(1 - r_1 r_2 t_c)^2 + 4 r_1 r_2 t_c sin^2(\delta/2)} \tag{2.66}$$

$$P_c = P_i T / t_2^2 = \frac{P_i {t_1}^2}{(1 - r_1 r_2 t_c)^2 + 4 r_1 r_2 t_c sin^2(\delta/2)} \tag{2.67}$$

$$P_l = P_c r_2^2 (1 - t_c^2) = \frac{P_i {t_1}^2 {r_2}^2 (1 - t_c^2)}{(1 - r_1 r_2 t_c)^2 + 4 r_1 r_2 t_c sin^2(\delta/2)} \tag{2.68}$$

$$P_r = P_i - P_t - P_l = P_i \frac{(r_1 - r_2 t_c)^2 + 4 r_1 r_2 t_c sin^2(\delta/2)}{(1 - r_1 r_2 t_c)^2 + 4 r_1 r_2 t_c sin^2(\delta/2)} \quad (2.69)$$

All of the factors containing $sin^2(\delta/2)$ terms in the expression above disappear for resonant wavelengths (frequencies) that satisfy the condition:

$$\lambda_c = \frac{d}{m} \; or \; \nu_c = m \frac{c}{d} \quad (2.70)$$

The resonant cavity performs best when the input coupler transmission is equal to all other losses in the resonator, this is known as the impedance matching condition:

$$r_1 = r_2 t_c \quad (2.71)$$

Assuming that we are operating in the small signal regime, with the circulating power being defined by equation (2.67) and using the round trip transmission function defined in equation (2.61) we can rewrite the impedance matching condition as a function of the power incident on the enhancement cavity at the input coupler M1 and the proportionality constant ϵ.

$$r_1^2 = r_2^2 r_{HR}^4 (1 - \alpha) \left(1 - \frac{\epsilon P_i r_2^2 r_{HR}^2}{1 - r_1^2}\right) \quad (2.72)$$

This equation can be solved for r_1 to give an expression for the optimum, impedance-matched, input coupler transmission:

$$T_1^{i.m.} = 1 - r_1^2 = \frac{\alpha'}{2} + \sqrt{\frac{\alpha'^2}{4} + \epsilon P_i \frac{1 - \alpha'}{1 - \alpha}} \quad (2.73)$$

In which $\alpha' = 1 - r_2^2 r_{HR}^4 + \alpha$ is the total round trip loss, excluding the input coupler transmission. The total round trip loss includes losses in the crystal α and leakage through the output coupler M2 and the concave mirrors M3 and M4.

Looking at only wavelengths that are on resonance, no power will be reflected from the input coupler of the enhancement cavity, $P_r = 0$, and the intracavity circulating power reaches a maximum when:

$$P^{i.m.} = \frac{P_i}{1 - R_1} \quad (2.74)$$

Now the transmission function of the impedance matched resonator will not depend on the loss α and will be equal to:

$$T^{i.m.} = \frac{T_2}{T_1^{i.m.}} \tag{2.75}$$

A comparison of the SHG process in the small conversion regime using an impedance matched enhancement resonator and the SHG using the directly incident laser beam onto the nonlinear crystal (the single pass configuration) gives the power enhancement factor in the resonant cavity:

$$\Omega_\omega = \frac{P_c r_2^2 r_{HR}^2}{P_i} = \frac{R_2 R_3}{1 - R_1^{i.m.}} \tag{2.76}$$

This is the same enhancement factor for SHG. That is the ratio of the resonantly enhanced SHG conversion efficiency to the single pass SHG conversion efficiency.

$$\Omega_\omega = \frac{\eta_{SHG}^{r.e.}}{\eta_{SHG}^{s.p.}} = \frac{\epsilon P_c r_2^2 r_{HR}^2}{P_i} = \frac{R_2 R_3}{1 - R_1^{i.m.}} \tag{2.77}$$

The second harmonic output enhancement factor will be given by:

$$\Omega_{2\omega} = {\Omega_\omega}^2 = \frac{(P_c r_2^2 r_{HR}^2)^2}{\epsilon P_i^2} = \left(\frac{R_2 R_3}{1 - R_1^{i.m.}}\right)^2 \tag{2.78}$$

Since the curved mirrors, M2 and M3, will have very small transmission losses the enhancement factors can be approximated to:

$$\Omega_{2\omega} \approx \left(\frac{1}{T_1^{i.m.}}\right) \tag{2.79}$$

And

$${\Omega_\omega}^2 \approx \left(\frac{1}{T_1^{i.m.}}\right)^2 \tag{2.80}$$

With the transmission of the impedance matched input coupler chosen to be approximately equal to the sum of the round trip losses:

$$T_1^{i.m.} \approx \eta_{SHG} + \alpha' \tag{2.81}$$

2.6.3.1 Cavity Beam Waists

The curvature of mirrors M3 and M4 along with the separation between M1-M2 and M3-M4 and the overall path length of the cavity affect the physical beam waists formed. The bow tie resonator with two curved mirrors forms two beam waist, one between M1-M2 and one between M3-M4. The size of each beam waist is important, the waist formed between the curved mirrors will affect the efficiency of second harmonic generation; the waist between M1-M2 should be matched to the waist of the fibre laser incident on the enhancement cavity. Using the standard ABCD matrix approach we can calculate the beam waists at any position within the enhancement cavity. If we consider the upper arm, the ABCD matrix for the round trip in the resonator with starting point midway between M1-M2 is given by:

$$\begin{bmatrix} A & B \\ C & D \end{bmatrix} = \begin{bmatrix} 1 & \frac{d-d_m}{2} \\ 0 & 1 \end{bmatrix} \begin{bmatrix} 1 & 0 \\ -\frac{2}{R_c} & 1 \end{bmatrix} \begin{bmatrix} 1 & d_m \\ 0 & 1 \end{bmatrix} \begin{bmatrix} 1 & 0 \\ -\frac{2}{R_c} & 1 \end{bmatrix} \begin{bmatrix} 1 & \frac{d-d_m}{2} \\ 0 & 1 \end{bmatrix} \quad (2.82)$$

Where $d_m$is the distance between the curved mirror surfaces, a parameter that when varied will affect the size of the beam waist in the cavity. Using [2.15] expressions for the waist spot size w_0 and its position with respect to the point halfway between the M1-M2 as this is the position at which the beam waist is calculated:

$$w_0 = \sqrt{\frac{\lambda}{2\pi}\sqrt{\frac{4-(A+D)^2}{C^2}}} \quad (2.83)$$

$$\delta z_0 = \frac{A-D}{2C} \quad (2.84)$$

Reordering Eq.2.44 for the waist between the curved mirrors M3-M4 we have

$$\begin{bmatrix} A & B \\ C & D \end{bmatrix} = \begin{bmatrix} 1 & \frac{d_m}{2} \\ 0 & 1 \end{bmatrix} \begin{bmatrix} 1 & 0 \\ -\frac{2}{R_c} & 1 \end{bmatrix} \begin{bmatrix} 1 & d-d_m \\ 0 & 1 \end{bmatrix} \begin{bmatrix} 1 & 0 \\ -\frac{2}{R_c} & 1 \end{bmatrix} \begin{bmatrix} 1 & \frac{d_m}{2} \\ 0 & 1 \end{bmatrix} \quad (2.85)$$

2.7 Conclusions

This chapter introduced a brief overview of the theory behind solid state laser science and specifically that involving the power scaling of fibre lasers and frequency doubling into the visible spectrum through the method of second harmonic generation (SHG).

An in depth look into the requirements for efficient SHG identifies the key requirements needed from the laser source. The technique of internal power enhancement using an internal cavity is outlined and its suitability for efficient SHG highlighted.

2.8 References

2.1. Pask, H.M., et al., *Ytterbium-Doped Silica Fibre Lasers: Versatile Sources for the 1-1.2um Region.* IEEE J. Sel. Top. Quant., 1995. **1**: p. 2-12.

2.2. Clarkson, W.A., *CLEO Short Course: High power fibre lasers and amplifiers*. 2012.

2.3. Dawson, J.W., et al., *Analysis of the scalability of diffraction-limited fiber lasers and amplifiers to high average power.* Optics Express, 2008. **16**(17): p. 13240-13266.

2.4. Hooker, S. and C. Webb, *Laser Physics*. 2010: Oxford Uni Press.

2.5. Armstrong, J., et al., *Interactions betweens light waves in a nonlinear dielectric.* Physical Review, 1962. **127**.

2.6. Sutherland, R.L., *Handbook of Nonlinear Optics*. 1996, New York: Marcel Dekker.

2.7. D. S. Hum, M.M.F., *Quasi-phasematching.* C. R. Physique, 2007. **8**(11): p. 180-198.

2.8. C. Chen, et al., *"New nonlinearoptical crystal: LiB3O5".* J. Opt. Soc. Am. B, 1989. **6**(4): p. 616-621.

2.9. S. P. Velsko, et al., *"Phase-matched harmonic generation in lithium triborate (LBO)".* IEEE J. Quantum Electron., 1991. **9**: p. 2182.

2.10. Kato, K., *"Tunable UV generation to 0.2325 µm in LiB3O5".* IEEE Journal of Quantum Electronics, 1990. **26**(7): p. 1173-1175.

2.11. Beigang, A.N.a.R., *"External frequency conversion of cw mode-locked Ti:Al2O3 laser radiation".* Opt. Lett., 1991. **16**(22): p. 1729-1731.

2.12. Cieslak, R. and W.A. Clarkson, *Internal resonantly enhanced frequency doubling of continuous-wave fiber lasers.* Optics Letters, 2011. **36**(10): p. 1896-1898.

2.13. O'Connor, M.V., et al., *Use of a birefringent filter for tuning a synchronously pumped optical parametric oscillator.* Applied Physics B, 2004. **79**(1): p. 15-23.

2.14. Cieslak, R., *Power Scaling of Novel Fibre Sources*, in *ORC*2012, University of Southampton.

2.15. Kogelnik, H. and T. Li, *Laser beams and resonators.* Applied optics, 1966. **5**(10): p. 1550-67.

CHAPTER 3

3. Fibre Ring Laser

3.1 Fibre Ring Laser Background

Ring lasers have seen many years of research for a wide variety of applications using all fibre and purely free space configurations. Ring lasers have been used to develop single frequency sources, [3.1] [3.2]. When forced to operate in one direction, unidirectional, using some non-reciprocal device such as a Faraday isolator, a travelling wave is formed within the resonator as opposed to a standing wave inside a linear resonator. This traveling wave prevents any spatial hole burning in the laser gain media and makes single frequency operation easier to achieve. All fibre tuneable ring lasers have demonstrated wide output tuning spectra of up to 60nm using wavelength control methods such as Fibre Bragg Gratings [3.3], [3.4], and achieved output powers in the tens of watts [3.5]. High power ring fibre lasers are commonly mode locked with an external seed source [3.6], but high power in the CW regime have also been demonstrated combining a rod-type fibre geometry with a free space ring laser cavity [3.7] Ring lasers are also used for optical gyroscopes where two counter propagating beams are supported and used for a wide array of metrology applications.

The use of fibre ring lasers as a method for scaling output power has not seen a lot of research as there is no easily evident advantage to employing a ring cavity approach over a linear one, both for high powers in the near infra-red (IR) and visible regimes based on the standard methods that exist. What is novel in this work is the implementation of the internal enhancement cavity and the conclusions from previous work that a ring cavity approach will be beneficial.

The ring laser geometry on its own, without an internal resonant cavity, does not perform as well as a linear cavity would for the purpose of a high-power fibre laser based on single mode, double clad, Ytterbium fibre. One of the most efficient and widespread methods for second harmonic generation is through intracavity frequency doubling using a nonlinear medium. Due to the high resonator losses in a high-power fibre laser intracavity frequency doubling is not an efficient way to generate high powers in the second harmonic. A common technique to generate high intracavity powers at the fundamental wavelength is to couple the output of a fibre laser into an external enhancement cavity that can resonate on the fundamental source's longitudinal modes. This can result in power enhancement factors of at least one order of magnitude which can result in high powers generated at the second harmonic when a frequency doubling crystal is placed within the enhancement resonator. The biggest issue with this

technique is the need to actively stabilise the length of the external cavity to ensure that it remains on resonance.

In this work we present a laser geometry that combines the benefits of the two techniques, intracavity frequency doubling and a resonant enhancement cavity, without the drawbacks that are normally associated with them. This is done by placing the enhancement cavity inside the fibre laser resonator. The result is that the many modes that oscillate within the long fibre resonator can oscillate within the enhancement cavity allowing a build-up of intracavity power within the enhancement cavity which does not require active stabilisation as it locks on to modes of the fibre laser.

Looking at the limitations in power scaling of previous work involving internal resonantly enhanced SHG [3.8] it was obvious that a linear laser geometry limits the feedback due to the fact that the feedback signal needs to pass back through all the components within the overall laser cavity. In the case for when we have an internal resonator these loses are quite significant. So as is evident, employing the ring configuration prevents the loss in feedback.

3.2 Ring Laser Prototype

Initial alignment of the system must be done using a wavelength matched seed laser source. Specifically a simple 0.5W Nd:YAP laser. This was chosen as it operates at a wavelength of 1080nm. This is the wavelength on which the fibre ring laser is designed to operate using a diode pump source operating at 975nm so as to match an efficient peak in the absorption spectrum. Operating on the 1080nm emission transition was selected as the available wavelength selection element was limited and also the 1080nm operation of Ytterbium is good for 4 level operation.

The seed source is necessary for two main reasons. Firstly, the initial ring laser alignment is very difficult to realise. A catch 22 arises from the fact that to efficiently recouple the light from the free space path requires the laser to be operating but for it to operate efficient coupling has to be achieved. This is difficult to ensure sufficient coupling with an unmatched alignment source such a Helium-Neon laser. Having the seed source as an alignment aids the alignment of all of the free space optics that form half of the ring laser cavity. This includes the cavity mirrors, isolator and wavelength selection element. The seed source ensures that the transmission peak and bandwidth of the wavelength selective element can be tuned to the maximum reflection peak. The second reason for the seed source is to provide a safety fuse for the fibre when fine tuning of the alignment is being done along with the insertion of the enhancement cavity. Due to the high gain of the Ytterbium fibre it is very easy for the fibre to lase by forming a cavity from the Fresnel reflections of each fibre end. The seed source enforces lasing of the ring cavity. Along with this above a pump power level of 10-15W the fibre laser can exhibit very unstable behaviour arising from self-pulsing which quickly reaches a catastrophic damage level at which the fibre is destroyed.

The seed source is also used to get a measure of the coupling efficiencies at the fibre ends, where we go from free space into fibre and back out. This is a very important value to get as high as possible as it can easily be the biggest loss in the system. Especially when considering recoupling, as we are employing a ring approach to improve feedback, so it must be ensured that as much of the light as is theoretically possible gets coupled back in to the fibre. This will be the biggest effect on the slope efficiency of the ring laser.

Along with the coupling efficiency at the input fibre end, other components in the fibre stage can be measured to determine their losses. This allows for a procedural build-up of fibre components ensuring no losses are introduced at this stage. **Error! Reference source not found.** displays one of the first laser configurations, the enhancement cavity

is missing for now, it will be added in the free space arm at a later stage. As can be seen, the seed light is coupled into the cavity through a beam splitter, initially a 50:50, then guided through the polarisation control stage and coupled into the fibre gain stage.

The fibre gain stage consists of a 2-diode pump combiner with matched passive feedthrough spliced onto the active PM (Panda) Ytterbium fibre, from the commercial supplier NUFERN, specifically the PLMA YDF 10/125 with a core diameter of 10μm and NA of 0.075 and inner cladding diameter of 125μm and NA of 0.46. A counter propagating pump regime is used throughout this work. This is done as the ASE (amplified spontaneous emission) losses are lower in the backward direction and the overall power conversion efficiency, pump to signal is improved. At each end a length of passive fibre is spliced to lengthen the cavity and also to protect the active fibre and combiner in case the fibre ends become damaged or contaminated. As mentioned previously the coupling efficiency and splice losses can be actively measured at each point as the fibre gain stage is assembled.

The output from the fibre is taken along the ring laser path and imaged onto the part of the seed source that is transmitted through the beam splitter which is coupled into an identical fibre coupling stage which is indicated as the reference arm. By matching the position and coupling of the seed source that is directly coupled into the reference arm and the seed light that has traversed through the ring laser path, the ring laser can be aligned to a first estimate. As long as the reference arm is identical in position to the input coupling stage of the ring laser the coupling efficiency can be estimated with confidence. The use of the dummy fibre can be combined with imaging the beam overlap in the far-field using a camera to further improve the alignement. All of this is initially done without any pumping of the fibre gain stage to avoid any damage in the fibre due to imperfect alignment that can result in self-pulsing.

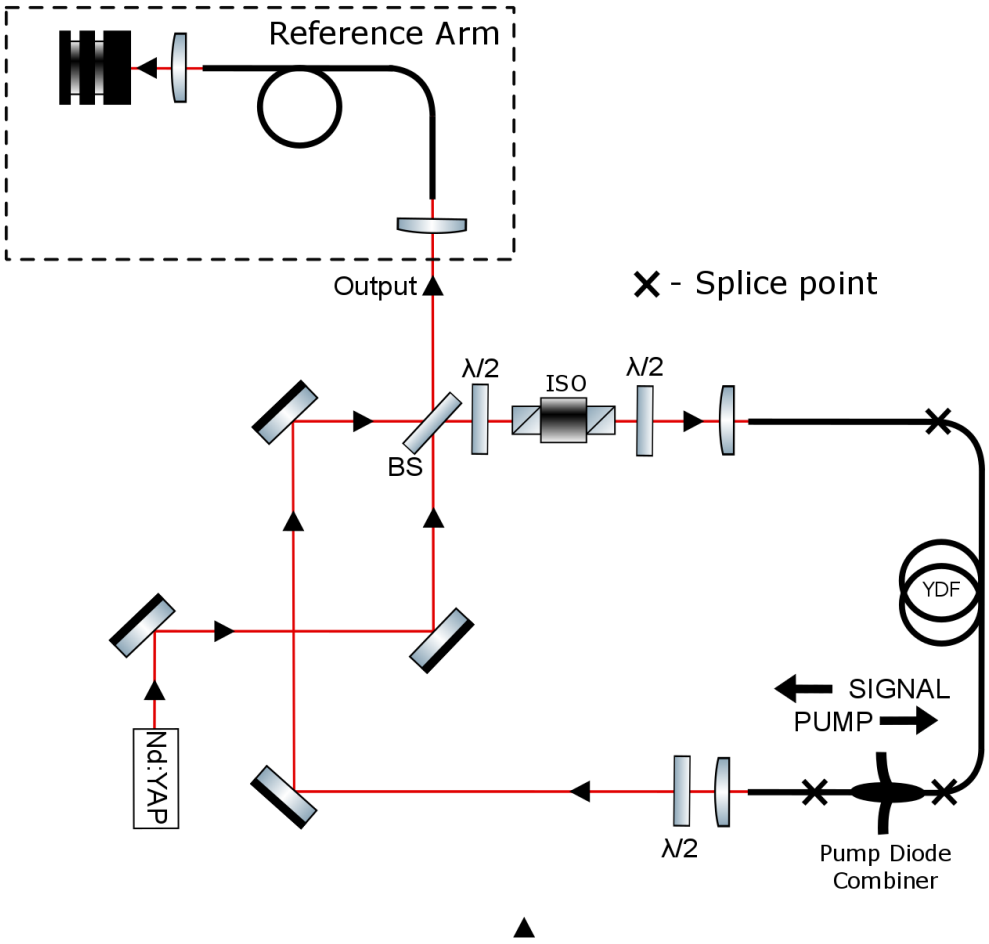

Figure 3.1 Diagram showing the initial ring laser alignment set-up using the alignment seed source and reference fibre arm used to estimate the recoupling efficiency.

The initial results from the attempts to achieve ring laser operation were not successful. It was clear that this was the case from the laser not operating uni-directionally even with the Faraday isolator within the cavity. Looking at the power exiting each fibre end, in the desired, forward, direction and the unwanted, backward, direction a near 50/50 split in output power is observed, shown in Figure 3.2. The reason the power is not exactly 50/50 is due to the seed source propagating in the forward direction, also why the measured power without any pumping is zero. The powers are measured using a pick off mirror placed at the fibre ends, a plane mirror with one side uncoated and the other anti-reflection coated at the signal wavelength. Any unabsorbed pump power is removed using a suitable filter.

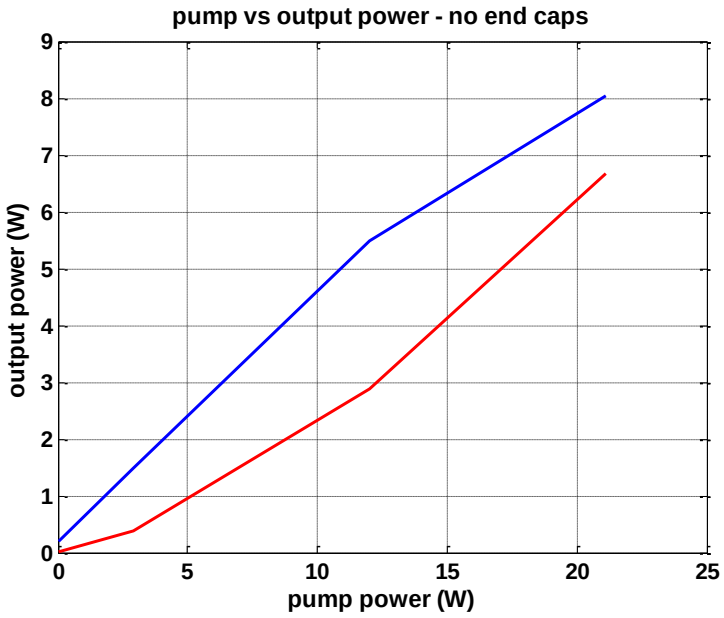

Figure 3.2 Graph of the output power from each fibre end when attempting to realise ring laser oscillation. Blue line is the desired, forward direction, red line is the unwanted, backward direction. The high power measured in the backward direction indicates that ring laser not operational, the fibre is lasing as a standalone linear cavity.

3.2.1 Feedback Suppression

Due to the high gain of the fibre, feedback from the fibre ends needs to be reduced to well below the Fresnel reflection of approximately 4% to facilitate unidirectional lasing of the ring laser. This became evident from the initial attempts to realise ring laser oscillation. A simplified Rigrod analysis of the expected performance of the complete system, when set up for SHG, highlights this. Several assumptions have to be made. This will include the expected coupling efficiency at the fibre end and subsequent re-collimation. This can arise from lens aberration, losses at the lens and imperfect alignment of the lens relative to the fibre along with a mismatch in the desired laser beam radius for ideal focusing by the lens and subsequent re-collimation on exit from the fibre. The expected transmission of the enhancement cavity, T_1, where there will be some loss and the useful power that is converted to second harmonic. Following that is the polarisation control and wavelength selective optics, not indicated on the diagram, T_2.

A schematic is shown in Figure 3.3, this is used to illustrate the power at each stage of the ring oscillator along with the estimated losses and expected transmission.

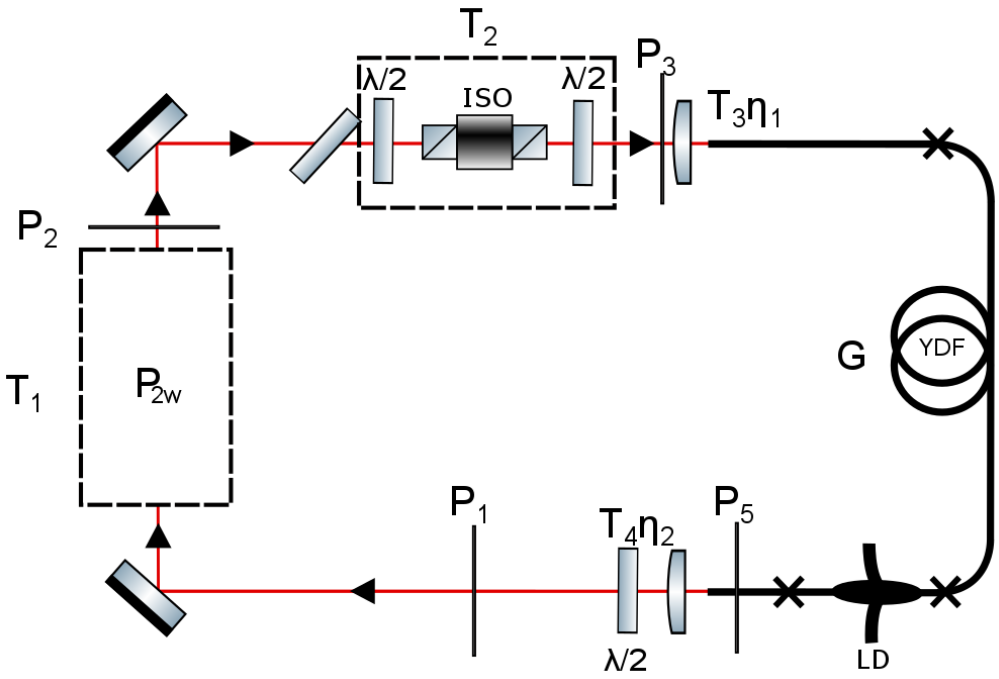

Figure 3.3 Schematic overview of fibre ring laser including internal cavity for frequency doubling. Labelled to highlight the Rigrod analysis performed to understand the need to suppress feedback from the fibre ends due to the high gain of the fibre.

Detailed below in the following equations are the different expected losses at each point in the system and a comparison after each point. Starting at P_1 and working our way through the system we first encounter the loss in the enhancement cavity, which is the conversion to the second harmonic, for this stage we assume there is no loss in fundamental power which will not be true but for the purpose of highlighting the gain in the fibre it is not necessary. For the sake of argument the losses in power can be included in the power converted to second harmonic, P_{2W}:-

$$P_{2W} = P_1 - P_2 \tag{3.1}$$

After which the power is then: -

$$P_2 = T_1 . P_1 \tag{3.2}$$

T1 being the overall transmission coefficient of the enhancement cavity, including the power converted to second harmonic and any losses, here T_1assumed here to be 0.1. Next we encounter the isolator and wavelength selective elements, T_2, assuming a value of 0.5, giving the power remaining as: -

$$P_3 = T_1.T_2.P_1 \tag{3.3}$$

Followed by coupling into the fibre, which includes the transmission of the focusing optics T_3, which for this case will be close to 1 as all the optics will be anti-reflection coated, and the coupling efficiency into the fibre η_1, worst case scenario will be estimated as 0.5, gives the power after as: -

$$P_4 = T_1.T_2.T_3.\eta_1.P_1 \tag{3.4}$$

And then amplification inside the active fibre taking into the account the gain of G gives the power as: -

$$P_5 = T_1.T_2.T_3.\eta_1.P_1.G \tag{3.5}$$

Finally coupling out to complete one round trip, with transmission of the collimation optics T_4=1 and out coupling efficiency η_2=0.5, assumed to be as when coupling in and then arriving at an expression for the threshold of the system: -

$$P_5 = T_1.T_2.T_3.T_4.\eta_1.\eta_2.P_1.G \tag{3.6}$$

$$\frac{P_1}{P_1} = 1 = T_1.T_2.T_3.T_4.\eta_1.\eta_2.P_1.G \tag{3.7}$$

Meaning that the single pass gain of the system based on the assumed values for each element as mentioned above is: -

$$G = \frac{1}{T_1.T_2.T_3.T_4.\eta_1.\eta_2} = 80 = 19dB \tag{3.8}$$

As is evident there is sufficient single pass gain for a very efficient laser, however this high gain coupled with the high efficiency of Ytterbium doped fibres poses a problem when initially aligning the ring resonator. The Fresnel reflections from both ends of the fibre provide enough feedback for the fibre to act as a linear oscillator by itself. This meant that aligning the ring resonator was difficult as there are actually greater losses in the ring system, so the fibre would just continue to lase as a linear fibre laser. In other words, unless a perfect alignment of the system is achieved the fibre will revert to linear oscillation along the cavity formed by the fibre ends. Removing the feedback for lasing from the fibre ends will force the ring laser oscillation to take over.

There are several ways to reduce the feedback from the fibre ends. The best but perhaps the most difficult is to put an anti-reflection (AR) coating on the end of the fibre. This however requires specialist knowledge, equipment and precision as the active core of the Ytterbium fibre used here is 10μm in diameter. When implemented for high power fibre lasers anti reflection coatings will have a damage threshold limit that could be below the fibre damage limit.

In this work two methods were tested, angle cleaving of the fibre ends and the application of end caps, both matched coreless fibre and larger bulk glass. . Each method was tested by building up the initial empty ring laser. That is a fibre/free space ring laser without the enhancement cavity that will be used for SHG. Operating without the enhancement cavity allows for a true comparison of both methods and ensures that the most suitable ring laser configuration is chosen for the most efficient SHG.

3.3 Ring Laser with Angle Cleaves

Angle cleaving is potentially the easiest method in terms of the process, but it can add complications when it comes to alignment back into the system. The concept is simple, by cleaving the end of the fibre at an angle large enough, nominally 8-10^0, to cause the light at the glass air interface to be reflected at an angle that it is incident back into the core at angle that is not able to be guided. When this condition is satisfied the light reflected is either coupled out of the fibre or back into the cladding within which it will be attenuated. Most importantly the light reflected back into the core, that could provide feedback for lasing, is minimised.. A simple schematic shows this in Figure 3.4. The cleave angle is represented as θ_C, this is chosen so that the light that is incident normal to the glass air interface and reflected back can no longer can be guided by the fibre. The diagram highlights the resulting beam deviation that results from angle cleaving.

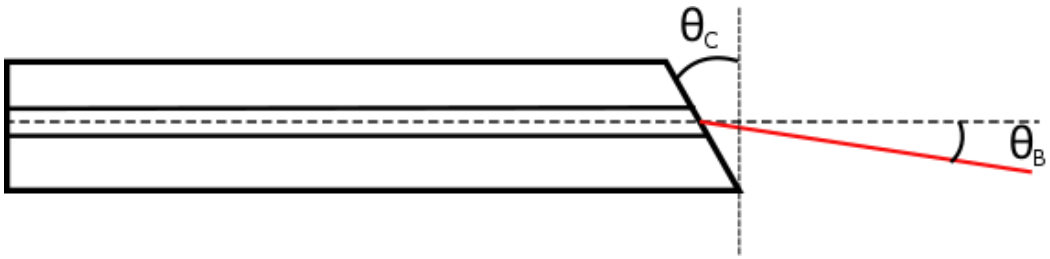

Figure 3.4 Schematic to illustrate a typical angle cleave showing the cleave angle at which the fibre is cut and the beam propagation angle at which the beam deviates from the normal path.

Most mechanical angle cleavers operate by twisting the fibre so that the cleave propagates at some angle, it is difficult to get an exact feel and reproducibility of cleaves

especially at such small angles. Due to the PM fibre having two stress rods that introduce the birefringence needed to maintain the polarisation it is also good to be able to cleave orthogonally to the stress rods so as to avoid any contamination of the end face and ensure good cleaves. For the required accuracy in this case a mechanical cleaver was simply not good enough. Using a fully computerised CO_2 laser cleaver allows for much greater control of the cleave angle, fibre orientation and overall cleave quality. Figure 3.5 and Figure 3.6 are images from the laser cleaver and microscope respectively. The laser cleaver image demonstrates the ease with which the angle can be set. By taking a reference cleave relative to the stress rods in the fibre, the stress rods can be imaged, and the fibre rotated to cleave in a direction that will avoid any contamination from the stress rods to the core. The microscope end face image shows a clean angle cleave with the clear indication of an angle shown by the defocusing at one end of the fibre face, the stress rods are clearly visible to confirm the desired cleave direction along with a very faintly evident core.

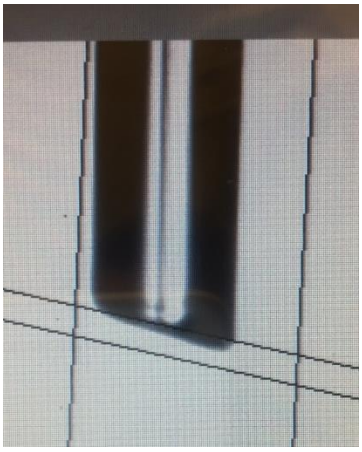

Figure 3.5 Laser cleaver image after angle cleaving fibre.

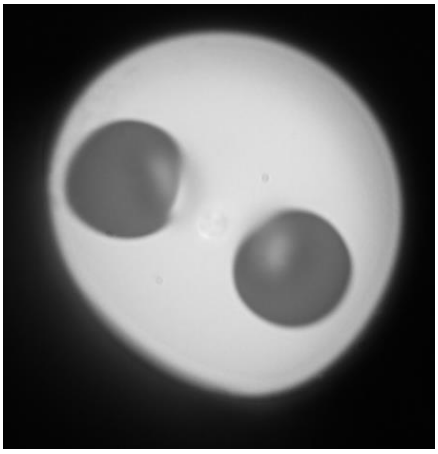

Figure 3.6 End face microscope image of laser cleaver angle cleave confirming cleave precision and direction.

To check the effectiveness of angle cleaving the fibre ends in reducing the reflection coefficient the laser configuration shown in Figure 3.7 was used in an amplifier configuration. By terminating the ring at the output fibre end and monitoring the return power that emerges from the input fibre end using a 4% pick-off mirror the reflection coefficient of the angle cleave can be calculated.

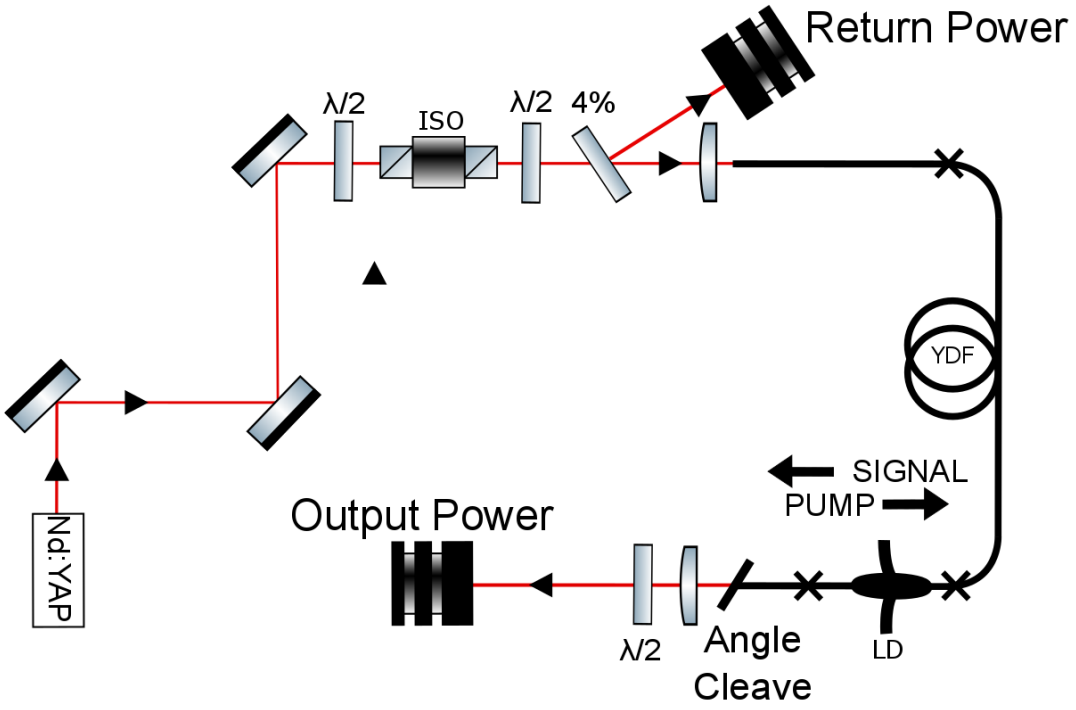

Figure 3.7 Amplifier set-up used for measuring the reflection coefficient of angle cleaves.

The calculated values of the reflection coefficient as pump power is increased are plotted in Figure 3.8. Using a known and fixed seed power and measuring the output power the single pass gain can be calculated for the fibre amplifier. Knowing this gain value and measuring the return power exiting the fibre at the input end the reflection coefficient for the angle cleave can be calculated. A slight decrease can be seen as pump power is increased after which the value stabilises. This happens at low pump powers as there is a mix of the reflection coefficient signal that we need to measure and other reflections along the beam path. It is useful to know that only the values at high enough pump powers are needed to give a good estimate of the reflection coefficient. At high enough pump powers, the reflection from the fibre end can be calculated from:

$$r_{EC} = \frac{(P_R/G)}{P_{OUT}} \tag{3.9}$$

Where P_R is the measured return power in the backward direction measured using the pick off mirror, G is the gain in the fibre, estimated from the amplification of the seed input power to the resulting output power in the forward direction, P_{OUT}.

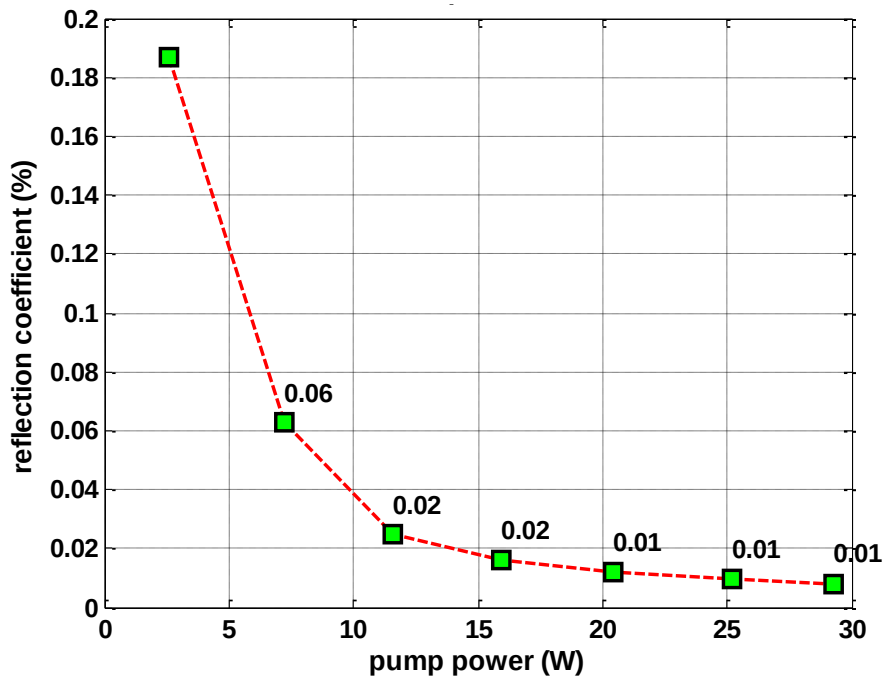

Figure 3.8 Angle cleave refection coefficient, in percent, with increasing pump power.

As the process is reliably repeatable an identical angle cleave is spliced onto the input end and the ring laser configuration implemented as in Figure 3.9. Alignment of the system is performed as described earlier using a reference arm at the output of the ring laser. The seed input mirror/output coupler used here is 85% reflective at the signal wavelength (1080nm). This is chosen to simulate the expected loss that would be experienced by the enhancement cavity through frequency doubling and any power rejected from the cavity due to imperfect coupling. Essentially, when fully operational the conversion from the fundamental IR power to the second harmonic acts as the output coupler of the overall ring laser. Since the performance of the ring laser is first to be investigated without the enhancement cavity present an output coupler loss must be introduced. This gives a good approximation of the feedback power to would be returned in the fibre gain stage. Care must be taken to ensure that the seed light polarisation is aligned to one of the principle axis of the PM fibre to ensure that the light stays polarised and that this is matched to the expected polarisation state of the light in the ring laser.

Once aligned it is not clear if ring lasing has been achieved. For ring lasing to be realised the coupling efficiency at the input fibre end has to be sufficient enough so as to provide feedback. Without it the loss is too great and the fibre can oscillate on a cavity formed by the ends of the fibre, if the feedback from each end is not reduced. Alternatively, with the seed source present the system will act as a single pass amplifier. For this purpose the

temporal response of the laser is monitored along with the output spectrum. Alignment is done using the seed source alone to begin and with it running the pump power is increased.

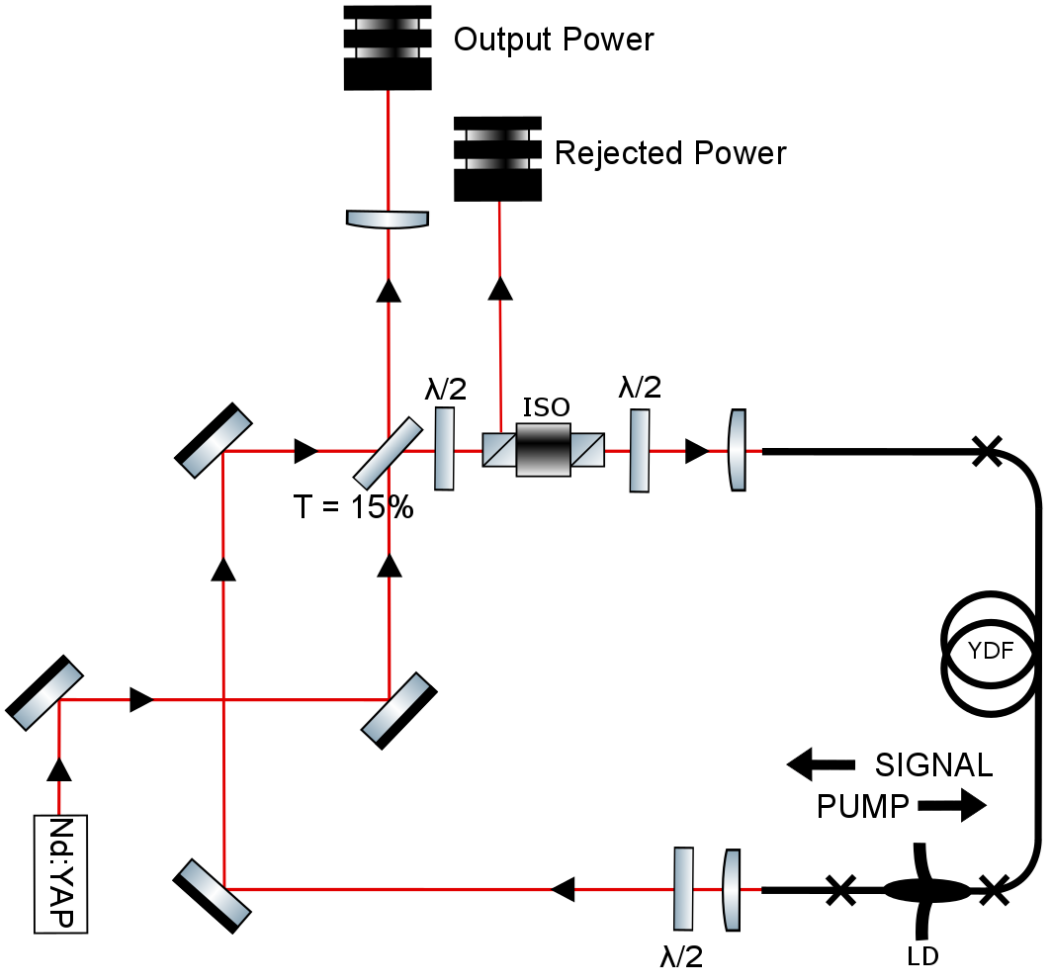

Figure 3.9 First working ring laser configuration. Used to check performance of the overall system and ensure that good feedback suppression at both fibre ends has been achieved.

If the ring is aligned well enough to avoid damage, then looking at the output spectrum gives the clearest indication of when the ring laser threshold is reached and confidence in safe ring laser operation established. As expected with the seed on, initially the system operates as an amplifier for the seed wavelength. Interestingly after a threshold pump power, which varies with coupling efficiency it appears the seed amplifier is now operating along with a broader output form the now operational ring laser. This can be seen when observing the spectrum and how it changes. The spectrum shows a peak for the seed wavelength which is fixed and multiple wavelength peaks which vary with time with a much broader bandwidth. This is expected as the emission spectrum of Ytterbium

is quite broad and there is no wavelength selective mechanism in the system at this stage. Once the seed laser is turned off, its corresponding peak disappears from the spectrum with only the varying broadband output of the ring laser remaining. A collection of images extracted from an optical spectrum analyser (OSA) are displayed in the figures below. Figure 3.10 shows the laser spectra before and after ring lasing achieved with the seed laser switched on at the same power. Figure 3.11 shows two subsequent spectra after the seed had been switched off and the ring laser is operating at an arbitrarily chosen pump power of 16W with a laser output power of 10.2 W in the correct polarisation state.

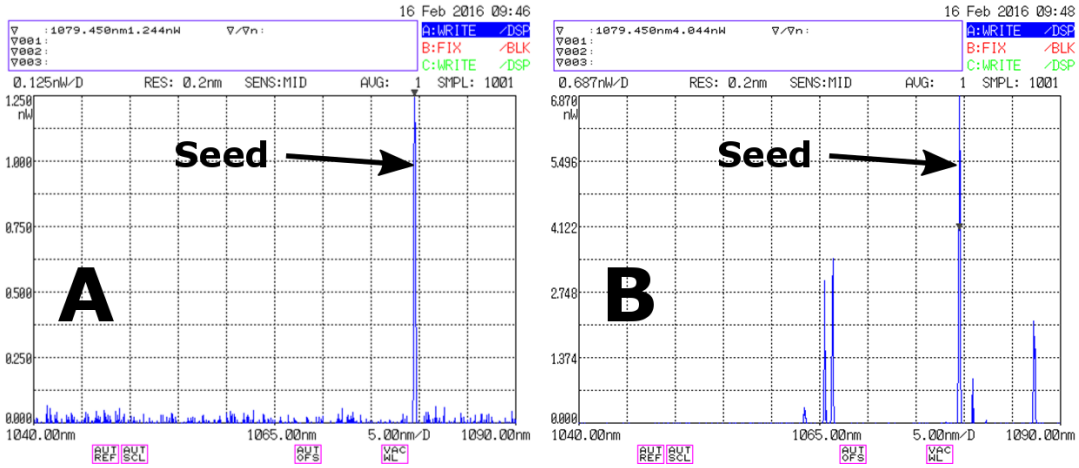

Figure 3.10 Output spectrum showing initialisation of ring laser operation. Spectrum A shows seed wavelength only with no pump into fibre gain stage. Spectrum B shows seed wavelength along with ring laser spectrum of multiple peaks along emission spectrum, pump power now several factors above threshold.

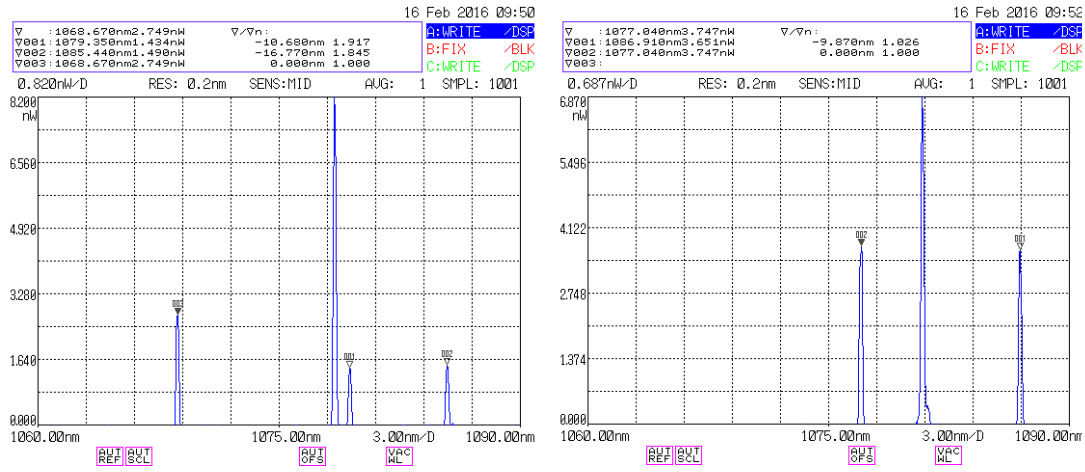

Figure 3.11 Output spectra of the angle cleaved fibre ring laser. No wavelength selective element present and seed source switched off, hence peak at 1079nm no longer present. Variation in spectra peaks on the order of seconds.

The power efficiency of the ring laser is plotted in Figure 3.12. It was evident that the polarisation state of the output radiation was not perfect with a small fraction in the orthogonal polarisation state and rejected at the entrance of the isolator. This fraction of power which is rejected is another loss in the system and hence needs to be kept to a minimum as it will not be fed back to the laser and will be rejected by the enhancement cavity. For this reason, and to give a more detailed report of the power performance of the laser, the output power including and excluding the power in the orthogonal polarisation is plotted. Along with this, for comparison, the slope efficiency for the amplifier set-up is also plotted. In this amplifier configuration, the seed is left on and the ring blocked turning the ring laser into a seeded fibre amplifier. This is a useful comparison to ensure that the ring laser is performing reasonably well, any big deviation below the amplifier performance would indicate big losses somewhere in the system, most likely at the input fibre end or even misalignment. It can be seen that the ring laser operates at a maximum output power of 18.5W (19.5W including the rejected power which does not match the polarisation state enforced by the isolator) with a slope efficiency of 65% (68 with rejected power) which is just a little below the 72% achieved in an amplifier configuration. All these values are below the theoretical limit of Ytterbium, with some Ytterbium fibre lasers operating close to 80% efficiency. However, considering the fibre/free space arrangement and multiple PM fibre splices and diode combiner, it is a satisfactory starting point.

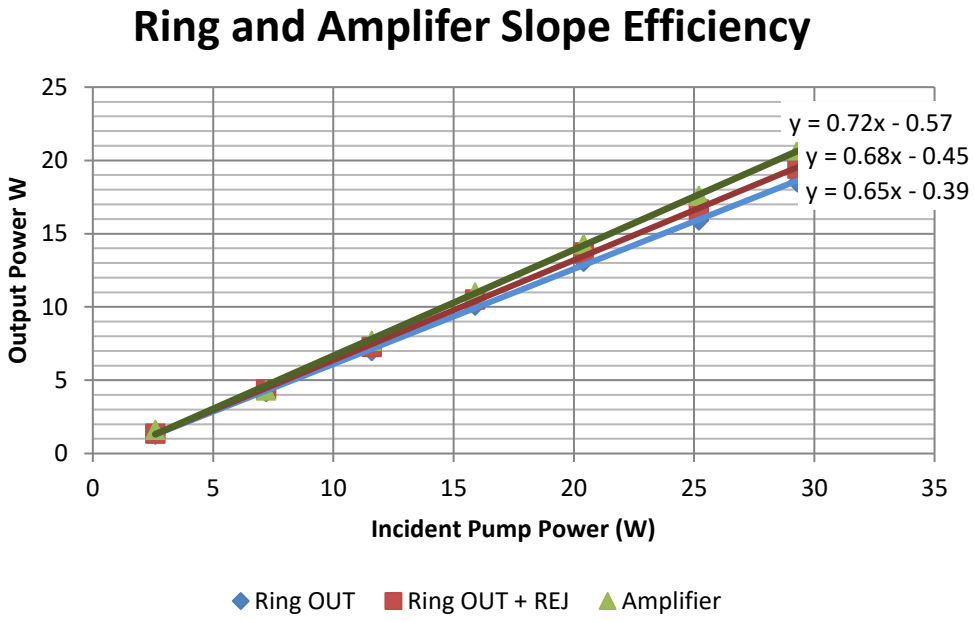

Figure 3.12 Slope efficiencies for amplifier and ring laser configuration to assess the performance of the angle cleaves.

3.4 Ring Laser with End Caps

A big alignment issue with angle cleaving when constructing the ring laser is the need to correct the beam deviation from a straight line at the exit of the fibre and then again at the input end. This will also require a good mechanical arrangement to keep the end of the fibre fixed in place. End-capping the fibres allows for a flat cleave at the fibre to air interface and hence maintains the straight-line beam path. This greatly simplifies the initial alignment and allows for faster replacement of fibre ends if something goes wrong.

An end cap is made by splicing a very short length of coreless fibre or bulk glass to the fibre end. As there is no core the light cannot be guided in the end cap as it is in the fibre and the beam expands as it propagates towards the end cap to air interface. There the 4% reflection is still present but on the return path back towards the active fibre the beam has expanded significantly and can no longer couple back efficiently into the core. By choosing the correct length of end cap to allow for this increase in beam waist, the light fed back into the fibre is dramatically reduced. Most commonly the length of the end cap is at least long enough to allow for the beam to double in size when in travels through the coreless fibre/glass end cap. If we consider a standard double clad fibre with a core of 10μm and inner cladding of 125μm the length of the end cap would need to be approximately 0.8mm to allow the beam to diverge to a diameter of half the inner cladding. A simple schematic to illustrate this is shown in Figure 3.13, here the end cap is a coreless fibre matching the diameter of the active fibre.

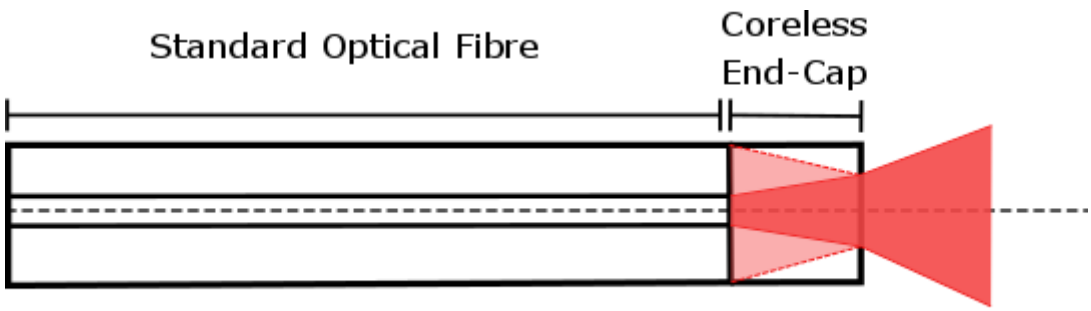

Figure 3.13 Schematic showing a simple end cap, with the beam propagation inside the end cap illustrating the growth in beam waist as some light is reflected back towards the core.

3.4.1 Fibre End Caps

The process to end-cap an optical fibre is easiest when the end cap is of a similar size in diameter to that of the active fibre that is to be end-capped, see Figure 3.13. The fibres are spliced using standard splicing methods after which the end-cap fibre is cleaved to the desired length. Difficulties arise in splicing two different fibres, one is coreless, and cleaving back the end cap to the desired length which needs to be as short as 0.8mm, as discussed earlier. With conventional cleavers/splicers the reproducibility is not very good.

The end cap performance is tested in the same way as for the angle cleaves. First one end cap is spliced onto the output and then a second on the input. By looking at the return power at the input end of the fibre using the pick off mirror the effect of the reduction in feedback can be seen and measured. Figure 3.14 shows the powers exiting both ends of the fibre, the blue line being the forward (desired) direction and the red the return. With no end caps present the power out of each end is almost in a 50:50 ratio. With two end caps that ratio is greatly reduced. The set-up here is operating in a single pass amplifier arrangement.

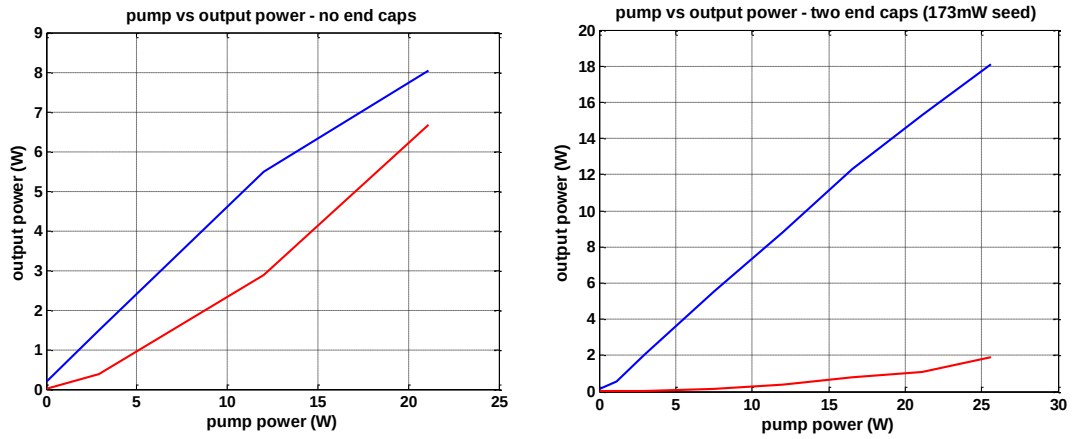

Figure 3.14 Two plots indicating the reduction in power travelling in the return direction when end caps are added to the system. A clear indication of the reduction in feedback at the fibre ends. The system is operating in a single pass amplifier configuration. Blue line indicates power in the forward direction, red line is power in the reverse direction.

Figure 3.15 is a plot of the reflection coefficient (in %) from the fibre end caps with increasing pump power. After reasonable amplification the coefficient of reflection is measured to be close to 0.06%. This is again a vast improvement on flat cleaves and similar to the performance of the angle cleaves. The reasons behind the pump power dependence is the same as previously for the case of angle cleaves.

However, this initial approach to end-capping the fibres seemed to have a detrimental effect on the performance of the ring laser. This can be seen when comparing the slope efficiency for the system plotted in Figure 3.16. Here the slope efficiency is down to 39%, way below what is acceptable. The reason for this was the effect of the end caps on beam quality and recoupling. It proved harder to reproduce good end-caps that maintain a good beam quality, which is what is achieved with angle cleaves and simple flat cleaves. Poor beam quality will affect the performance of the collimating and focusing optics. This degradation in beam quality led to a dramatic drop in coupling efficiency to below 50%. It became evident that the process by which the active fibre was spliced to the coreless endcap was not repeatable and not sensitive enough to not affect the beam quality. This loss of power that can be fed back into the fibre on recoupling can explain the drop in laser efficiency, decreasing from the amplifier value of 71% to 39%. This low efficiency will not be suitable for generating high power in the second harmonic. In the simplest case this power lost in the IR will be power lost in the second harmonic, to achieve the highest green power possible we need to start with as much IR power as possible, and such a low slope efficiency will not allow for this. Looking at the reasons behind this, it was evident that a lot of the power was lost on recoupling. This will result in a lot of power incident on the fibre end which when not coupled will only serve to transfer heat and cause physical instability of the fibre tip, reducing the performance further or even damage.

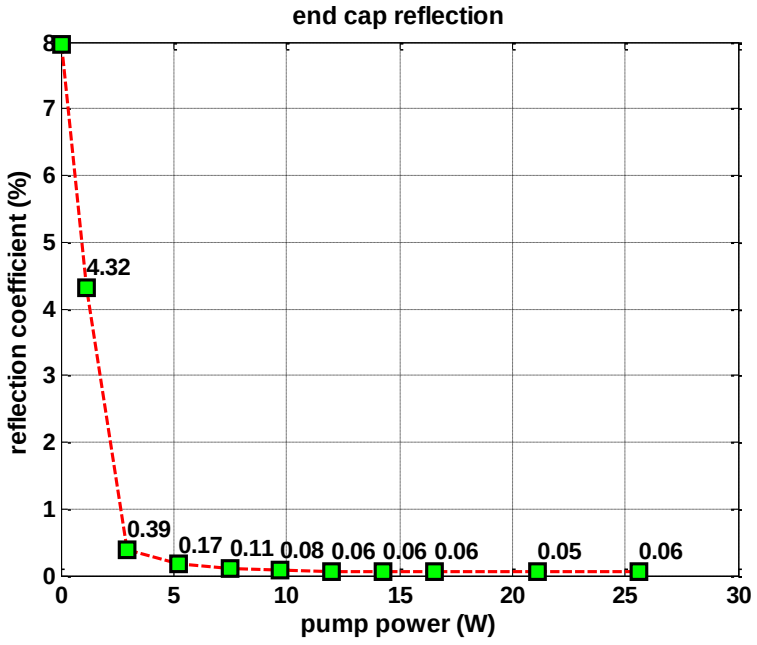

Figure 3.15 The feedback suppression performance of the fibre end caps expressed as the reflection coefficient (in %) at the end cap at the high power output end of the fibre gain stage.

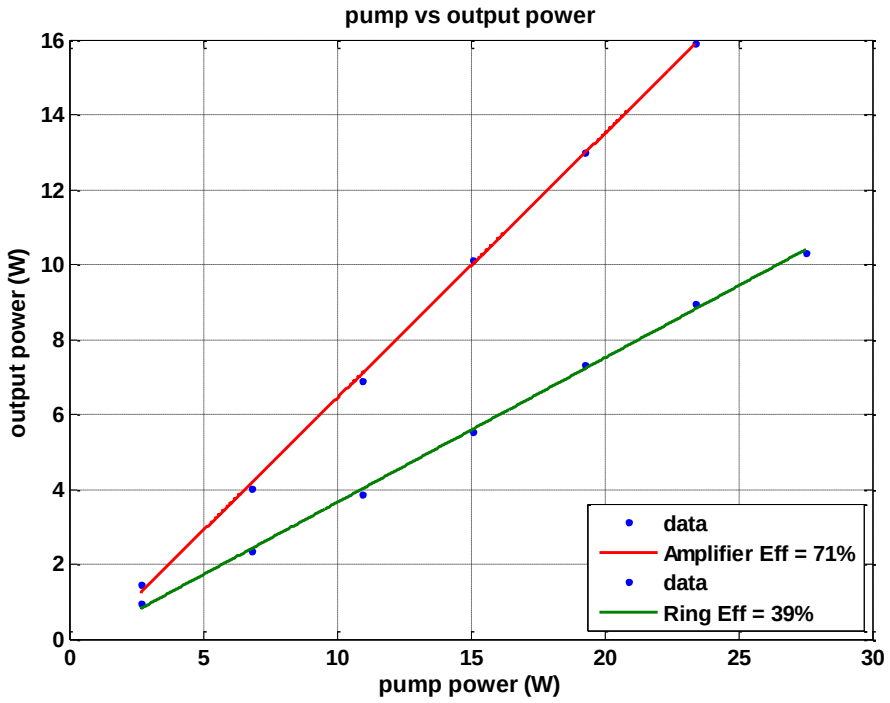

Figure 3.16 Slope efficiency of amplifier and ring laser configurations to test the performance of the fibre end caps.

3.4.2 Bulk End Caps

An alternative approach is to splice a larger piece of fibre or even bulk glass onto the active fibre. The beam can grow to an even larger diameter resulting in potentially better reduction in the end reflection. As mentioned previously splicing the two mismatched fibres proved problematic and the performance of the fibre end caps was poor in terms of losses on recoupling. Here a bulk piece of silica glass is fused onto the end of the fibre. This was done via the use of a CO_2 laser and a custom arrangement. The bulk glass is heated to melt the surface and first few millimetres of depth. The fibre is cleaved and polished then driven into the softened glass by a mechanical stage. This fuses the fibre into the glass and by means of a camera the quality of the splice can be observed visually. To allow ease of production the end cap is spliced onto a piece of passive fibre which is matched to that of the active fibre. An actual fused end cap is shown in Figure 3.17. The end-capped passive fibre is subsequently spliced into the system. The bulk end caps also add improved stability of the fibre ends. By using glass big enough to fit into standard lens mounts the end caps can be fixed into place far better than the fibre end caps which would hang over the ends. A picture of the mounted end cap is shown in Figure 3.18. The potential for thermal handling is also greatly improved. Since the bulk end cap is far

longer in length and total volume the beam can increase further in size and the heat per unit area will be reduced when comparing to a matched fibre end cap.

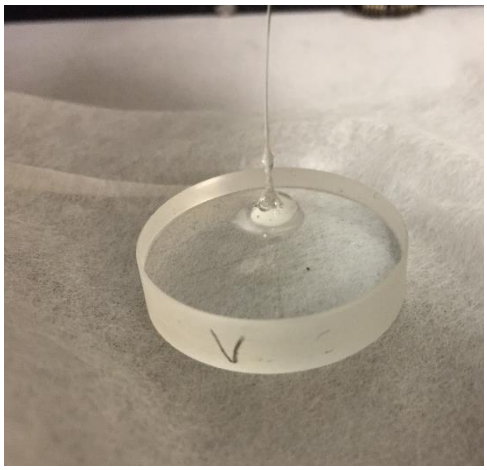

Figure 3.17 A bulk glass end cap with AR coating spliced onto a piece of passive fibre. Ready to be spliced onto the active fibre.

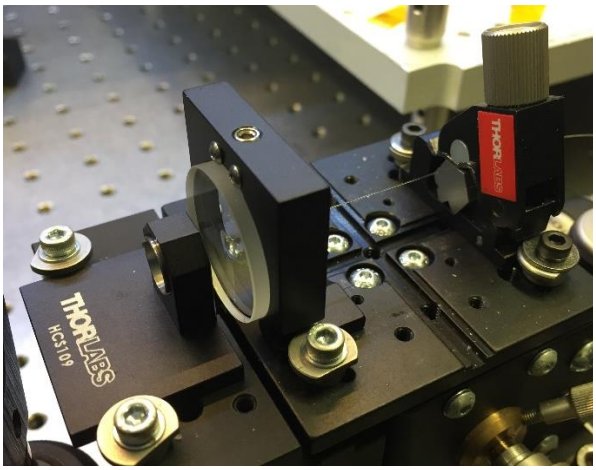

Figure 3.18 A bulk glass end cap inside a fixed optical mount and in position within the laser system.

The performance of the bulk end caps is assessed through the laser efficiency of ring laser. The results are displayed in Figure 3.19. The laser operates with a slope efficiency of 62%. This was done after the increase in available pump power and no thermal rollover can be seen when pumped to nearly 100W. There was no degradation at high powers due to any heating as the increased end cap size has helped maintain temperatures at the fibre ends low. Measuring the temperature using a thermal camera as a rough estimate, the end face temperatures did not exceed 30-40°C.

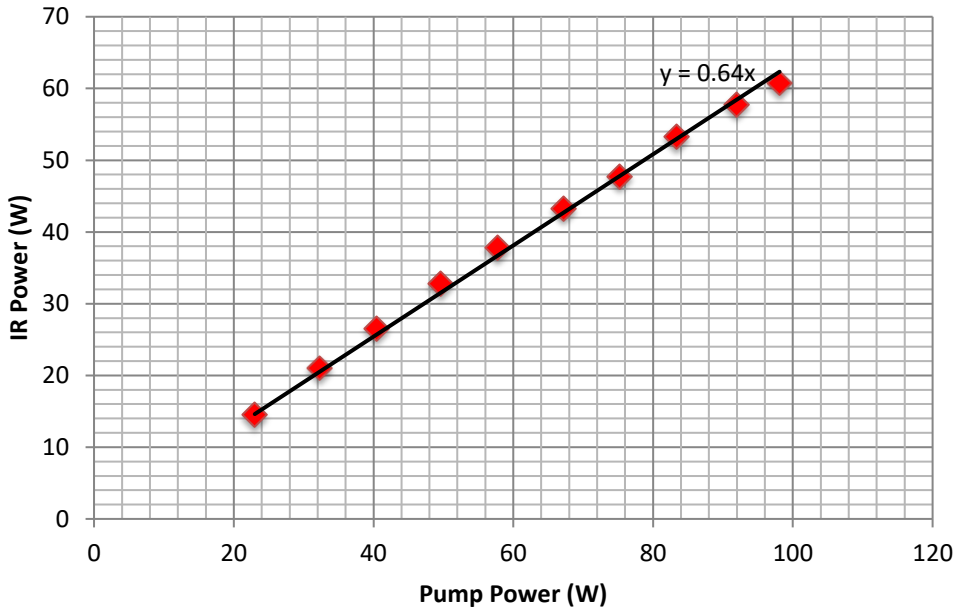

Figure 3.19 Slope efficiency of ring laser using bulk glass end caps.

This improvement in performance over the fibre end caps is encouraging and will provide a satisfactory IR source for power enhancement inside the internal resonant cavity and subsequent SHG. At maximum pump power 60W of IR signal is available, assuming a big loss on coupling into the cavity so that only 50% of the power is coupled in, due to imperfect mode matching or polarisation loss, 30W can be coupled into the enhancement cavity, based on results from [3.8]. An enhancement factor of 10 can be expected resulting in a circulating power of 300W. Taking a single pass second harmonic conversion efficiency of 4% for the nonlinear crystal will result in 12W of second harmonic output.

3.5 Losses in the System

Before adding the enhancement cavity and wavelength control mechanism a brief study into the main losses of the system was carried out. Figure 3.20 is a diagram of an example case of the ring laser operating at an output power of 18.5W with a slope efficiency of 65%, this is the angle cleaved configuration from section 3.3. The coupling loss at the fibre input is measured using the seed source before amplification. As discussed, the T=15% beam splitter acts as both input coupler of the seed light and output coupler of the ring laser. This loss is close to the expected loss in the enhancement cavity when frequency doubling is occurring. From the experiment the biggest loss is at the isolator

due to power being present in the orthogonal polarisation direction. In fact, the polarisation extinction ratio (PER) was measured to be 12dB. This is lower than expected from a PM fibre laser. The loss can occur within the fibre gain stage due to imperfect splices of the active and passive fibres. As there are three splice points in total this kind of loss can occur at any of them or be a combination of all three. Another potential issue is imperfect alignment of the polarisation orientation upon exit from and entry into the fibre gain stage.

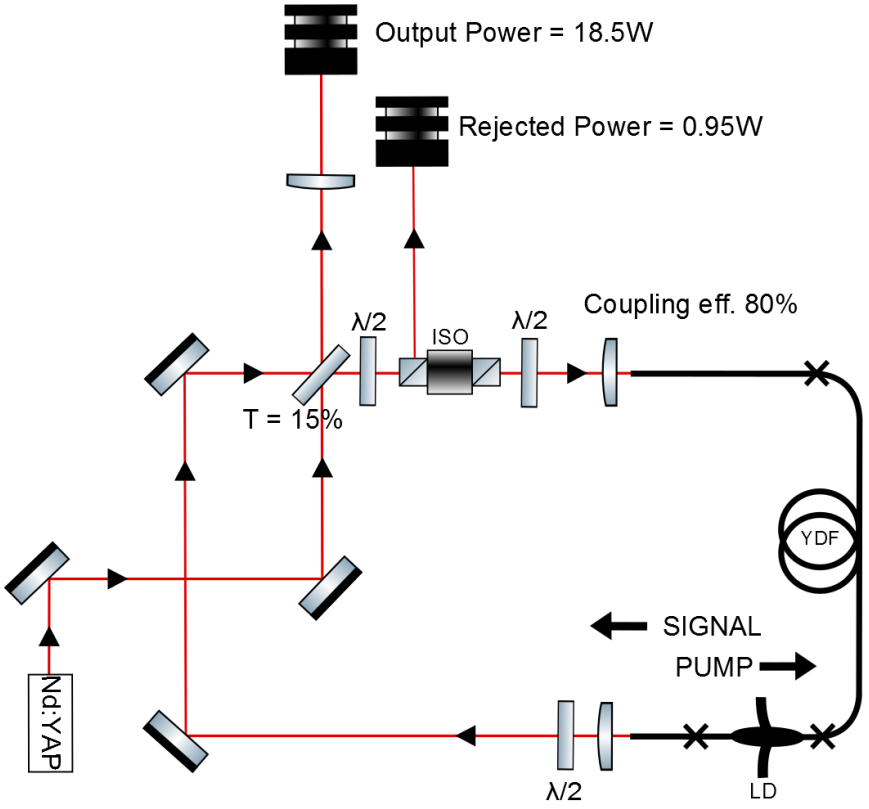

Figure 3.20 Diagram of an example case of the ring laser operating with a measure of the biggest losses in the system, at the isolator and on coupling, before the inclusion of a wavelength control mechanism and internal cavity.

Nevertheless, although the polarisation loss is significant, in the case above around 5% of the total power is lost at the first polariser of the isolator, in affecting the output power and slope efficiency knowing the extent to which it affects the system and its potential causes will help eliminate it as a source of potential problems further in the development of the system.

It highlights that the best position for the enhancement cavity will be immediately after the fibre gain stage, in what is termed the 'high-power' end of the system. This means

that the enhancement cavity can make use of the maximum power generated in the system before any losses are experienced in the polarisation control stage.

3.6 Wavelength Control

Looking at the initial ring laser configuration it is clear that an ideal wavelength control mechanism would be operating in transmission. This will avoid adding any extra mirrors in the system and simplify alignment. As discussed in the previous chapter a multi-layer birefringent filter array will also add the potential for easy wavelength tuning by rotating the filter about the axis of beam propagation. Unfortunately the bandwidth narrowing produced from a 3-stage birefringent filter plate at this wavelength was too broad for the SHG requirements. Adding a Fabry–Pérot etalon still allowed potential secondary peaks to be oscillating, which is where the laser will hop to as it tries to find the path with least losses.

A more robust solution is to use a Volume Bragg Grating (VBG) in reflection. A VBG can give very narrow bandwidth, below 1nm, and suffers from very low loss with the reflectivity at the peak wavelength greater than 95%. When the Bragg condition is met for a certain angle the light is reflected back and for other angles passes straight through. Different angles will reflected different wavelengths within a certain wavelength range allowing for some possibility of wavelength tuning. Angle tuning in a ring laser will be difficult as any beam deviation will result in misalignment of the laser. A VBG is a Bragg grating that has been written inside a bulk transparent material in the form of a cube. Usually diffraction gratings are written along the surface of a material whereas here the grating is written within the volume of the material. They can be made in fairly big dimensions allowing beam diameters of around 1mm to be used, as will be the case here. This combined with the high damage threshold of the material allows for stable high power operation.

Due to the superior expected performance of VBG and the ease with which it can be implemented into the system it was chosen as the first option for the wavelength control mechanism in the ring laser. The VBG used was centred at 1080nm for close to normal incidence with an expected reflection bandwidth of 0.5nm. As the VBG operates in reflection it is necessary to add three more mirrors into the main laser cavity to fold the beam back into the desired path whilst giving control over the angle of incidence onto the VBG. The VBG angle is aligned using the seed source which operates on the desired wavelength that the ring laser will operate. The possibility for wavelength tuning

remains but requires the addition of a wavelength tuneable seed source as changing the wavelength would require angle tuning the VBG and hence misalignment. A tuneable seed source can help realign the ring laser for each desired wavelength. Figure 3.21 shows the ring laser set up with the position of the VBG. The seed source path used in alignment of the VBG is also indicated.

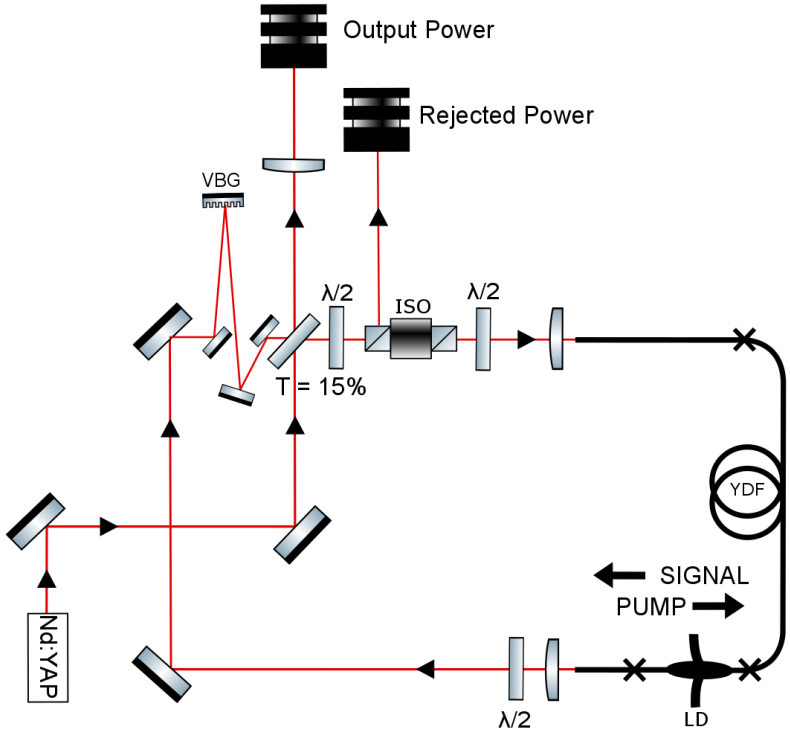

Figure 3.21 Schematic of ring laser set-up with VBG in place and seed source path indicated as used in alignment.

Looking at the spectrum of the output infra-red light it can be seen that the VBG performs even better than expected with a central peak at 1079.55nm and a FWHM bandwidth of 0.035nm, shown in Figure 3.22.

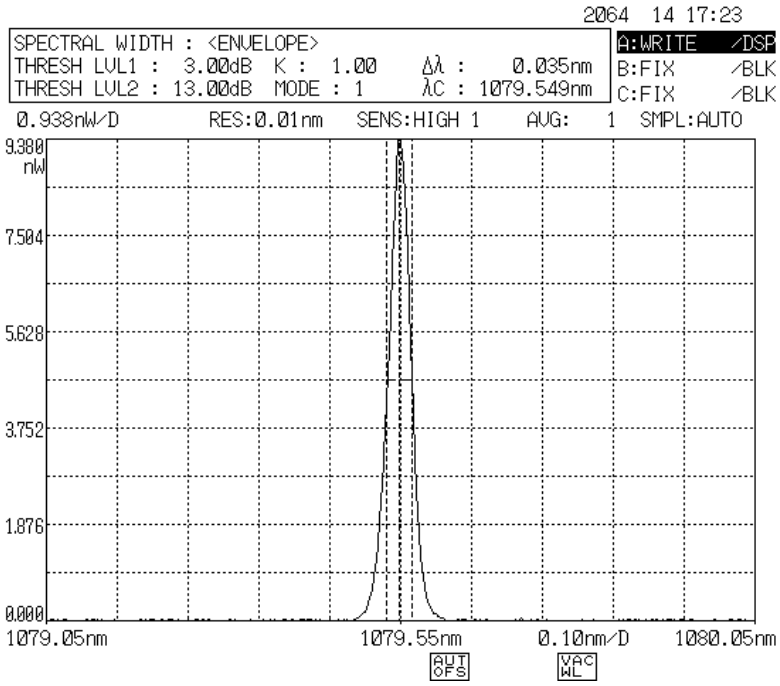

Figure 3.22 Infra-red output spectrum using a Volume Bragg Grating (VBG).

3.7 Conclusions

This chapter presented the initial design and development of the stand-alone ring fibre laser. It addressed the main issues that need to be overcome in order to have the capability of second harmonic generation (SHG) via the use of internal enhancement resonator. The biggest stumbling block, not obvious on first thought, is the difficulty in enforcing unidirectional oscillation of the ring laser. Due to the hybrid free space/fibre design, the feedback from both fibre ends needs to be reduced sufficiently to prevent lasing of the fibre independently. This in turn required an alignment system that can act as a fuse in this alignment and be used later for inclusion of the enhancement cavity. Two methods of feedback suppression are presented and tested with the results of the bulk end capped fibres proving the greater potential over the easier to assemble angle cleaving technique. Finally a suitable wavelength control tool, comprising of a Volume Bragg Grating is added into the system to select the lasing wavelength whilst providing a suitably narrow bandwidth for efficient SHG.

3.8 References

3.1. Polynkin, A., *Single-frequency fiber ring laser with 1W output power at 1.5µm.* Optics Express, 2005. **13**(8): p. 3179-3184.

3.2. Lu, C., *Stable single grequency Er-doped all-fiber ring laser with fiber Bragg grating Fabry-Perot filter.* Chinese Oprics Letters, 2005. **3**(4): p. 212-214.

3.3. Song, Y.W., *40-nm-wide tunable fiber ring laser with single mode operations using a highly stretchable FBG.* IEEE Photonics Technology Letters, 2001. **13**(11): p. 1167-1169.

3.4. Feifei, Y., et al., *60-nm-Wide Tunable Single-Longitudinal-Mode Ytterbium Fiber Laser With Passive Multiple-Ring Cavity.* IEEE Photonics Technology Letters, 2011. **23**(22): p. 1658-60.

3.5. Auerbach, M., et al., *10W Widely tunable narrow linewidth double-clad fiber ring laser*, in *Conference on Lasers and Electro-Optics*2002.

3.6. Baumgartl M., e.a., *66W average power from a microjule-class sub-100fs fiber oscillator.* Optics Letters, 2012. **37**(10): p. 3.

3.7. Royon, R., et al., *High power, continous-wave ytterbium-doped fiber laser tunable from 976nm to 1120nm.* Optics Express, 2013. **21**(11): p. 13818-13823.

3.8. Cieslak, R. and W.A. Clarkson, *Internal resonantly enhanced frequency doubling of continuous-wave fiber lasers.* Optics Letters, 2011. **36**(10): p. 1896-1898.

CHAPTER 4

4. Frequency Doubling in an Internal Enhancement Cavity

4.1 Full Alignment Technique

The alignment of the whole system has to be done in a specific order and crucially the most important tool to do this safely and efficiently is the seed source. As mentioned, the seed source serves as multifunctional component of the system, allowing measurement of feedback suppression from fibre ends, initial alignment and also as a fuse when fine tuning the enhancement cavity. When aligning the enhancement cavity the feedback back into the ring laser can drop and by having the seed source running will prevent the fibre from self-pulsing. The seed source forces the fibre to operate as an amplifier so that when misaligned any self-pulsing is avoided. The laser is aligned in the following order, first without the enhancement cavity to ensure polarisation and bandwidth requirements are met and subsequently the bow-tie cavity is added. The first step is the more advanced and requires careful alteration of the polarisation orientation of the seed source and ring laser.

4.1.1 Stage 1 – Polarisation and Bandwidth

The first stage is the alignment of the overall ring laser cavity, i.e. both the fibre and free space parts. The entire alignment is done with the seed source which is matched in wavelength to that which the ring laser will oscillate, 1080nm, shown in Figure 4.1. Starting with the amplifier arrangement, as discussed in Section 3.3 and shown in Figure 3.7, the reduction in feedback from the fibre ends is confirmed along with a measurement of the coupling efficiency at the input fibre end. For the best alignment coupling efficiencies of over 80% were measured, not including the Fresnel losses and losses at the fibre splice points. The VBG angular tuning position can accurately be set along with the polarisation orientation of the isolator. The seed source is also linearly polarised, as will be the ring laser. This allows for alignment of the polarisation direction relative to the stress rods of the PM fibre, which is necessary to ensure that polarisation is maintained. The beam-splitter which is used to couple in the seed source and acted as the output coupler by simulating the expected loss in the enhancement cavity is now replaced by a thin film polariser plate (TFP). The TFP is positioned at Brewster's angle so that there is no loss for the linear polarisation state which the ring laser is operating on in transmission. The seed source is polarised in the orthogonal direction which requires care when aligning the ring path with the seed laser. Two pick-off mirrors are added into the system, plane-plane uncoated glass windows. The first just before the input fibre end will serve as an alignment tool, by overlapping the seed beam with that

of the beam that has traversed through the ring laser. The second is at the high-power output fibre end and serves as a pick-off mirror to measure the power exiting the fibre when the ring is operational. This is useful to get a measure of the efficiency at which the ring laser is operating and once the enhancement cavity is in position can quantify the power that is successfully coupled into it.

The second stage is insertion of the enhancement cavity, there are many ways to do this which will be discussed later but the method employed was to position each mirror one by one with the input coupler being the last mirror positioned, checking the performance of the empty cavity and then inserting the nonlinear crystal. The empty cavity performance is a good check if the resonance condition can be achieved and monitor the IR spectrum incident on the internal cavity and that after the VBG.

The whole alignment process is ordered in such a way as to eliminate potential problems, then eliminate or quantify any losses that will affect the performance of the whole system so that they can be accounted for when monitoring the second harmonic output and its efficiency.

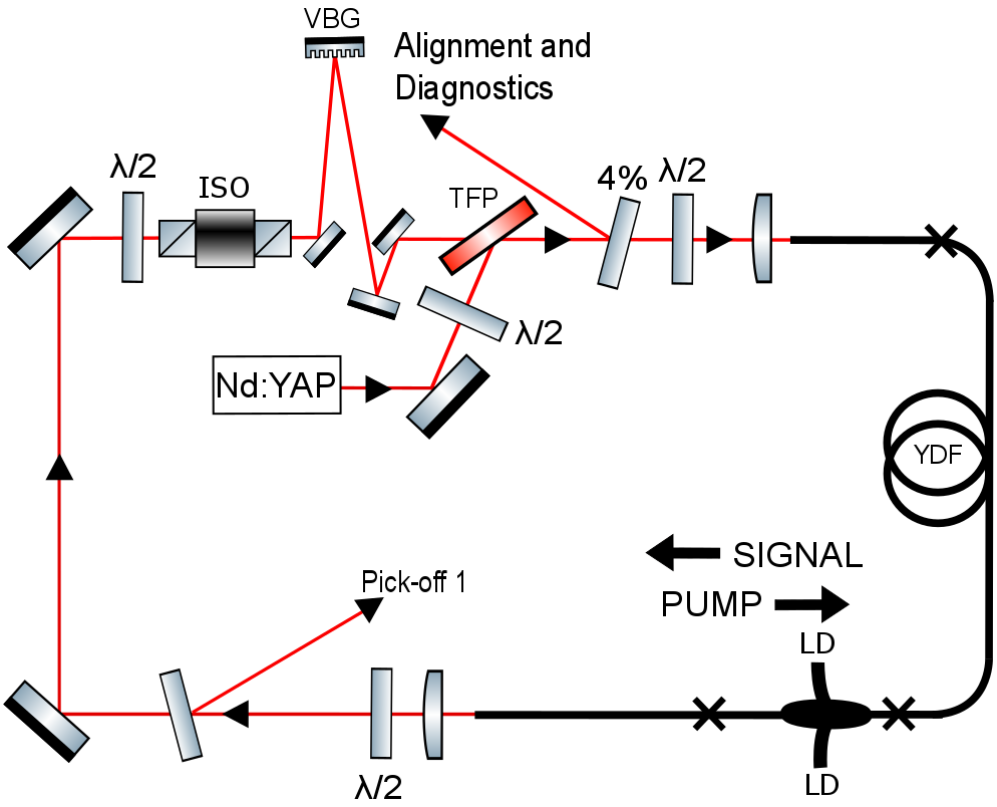

Figure 4.1 Diagram of the laser set-up at Stage 1 of the alignment procedure. Here the linear polarisation direction of the ring laser is aligned to be in the plane of the table and rotated to match the orientation of the stress rods of the PM fibre at the entry and exit ends. This stage also positions the VBG at the correct angle and ensures narrow bandwidth performance at the signal wavelength. The isolator position has changed for ease of physical placement of the components.

As mentioned the use of the TFP as an input coupler for the seed source without impacting the ring oscillation requires the seed to be linearly polarised like the ring laser but in the orthogonal direction. A few careful steps must be taken when performing the alignment to ensure that the polarisation states of the seed and ring oscillator will be correct. This is outlined in the following steps with the aid of Figure 4.2, Figure 4.3 and Figure 4.4. For simplicity and to make each figure clearer the VBG has been omitted from the diagrams as it is always in the same position and its alignment is not altered as the polarisation alignment is performed. The first pick-off mirror has also been omitted for clarity.

The first stage of the alignment is shown in Figure 4.2 where only the seed source is used without any pumping and amplification inside the fibre gain stage. The seed source is linearly polarised and coupled into the ring path via a steering mirror and the thin film polariser (TFP) indicated in the diagram. Its polarisation orientation is controlled by a half-wave plate ($\lambda/2_d$) before the TFP. After coupling into the fibre with a sufficiently high efficiency the orientation of the polarisation relative to the PM fibre stress rods is aligned using the half-wave plate before the fibre ($\lambda/2_a$). The polarisation orientation exiting the fibre gain stage is aligned using the half wave-plate at the output ($\lambda/2_b$). The Faraday isolator is aligned so that the polarisation that exit from it is in the p-polarisation state that will be transmitted by the TFP.

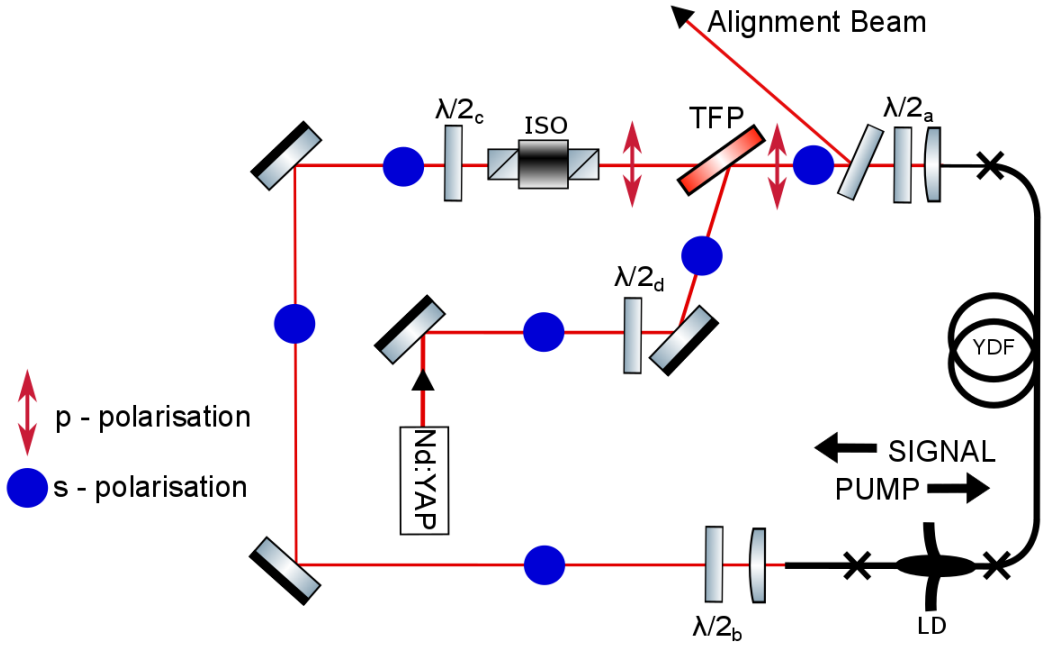

Figure 4.2 First stage of polarisation alignment using seed source. No pumping and only seed light used to align components for ring oscillation. Rotation of waveplate before isolator permits seed light to propagate through and also pass through TFP for alignment.

This requires the half-wave plate before the isolator ($\lambda/2_c$) to rotate the polarisation by 45 degrees to ensure that it passes through the first isolator polariser without loss, is rotated by the 45 degrees inside the isolator and then exits through the second isolator polariser without loss and orientated for the TFP. This now results in the initial seed polarisation direction to be orthogonal to that that has passed through the ring path. Taking the alignment beam from the pick-off mirror just before the fibre input, the ring beam can be aligned to couple into the fibre.

Now, what is clear is that the seed polarisation and the ring polarisation will be orthogonal, meaning that some alignment of the polarisation orientation is required to 'switch' from operating as an amplifier to achieving ring laser oscillation. Once the beam direction is aligned the half wave plate before the isolator is rotated by 45 degrees so that the seed beam is rejected at the first isolator polariser, see Figure 4.3. Applying a small amount of pump power will result in amplifier operation to begin with the output being the first polariser. However, at a certain pump power, ring laser threshold, if the ring beam is perfectly aligned then laser operation will switch over from amplifier to laser and a drop in the rejected power will be observed at the first isolator polariser as the ring laser polarisation orientation is orthogonal.

The rejected polarisation is used as an alignment tool as fine adjustment of the steering mirrors and fibre can be done to increase the coupling of the ring laser by reducing the power rejected at the polariser. Essentially there are two simultaneous processes going on, amplification and lasing. Once the rejected power is down to a low enough level to be sure that amplification is minimised, easily comparable by looking at the total power generated from the first pick-off mirror, the seed source can be turned off. The small amplified seed power rejected at the first polariser drops and only ring oscillation remains. Once the seed source is switched off the ring laser is aligned, as shown in Figure 4.4. Further very minor adjustments can be made to increase the output power. Care must be taken so as to avoid any damage if misalignment occurs, no seed source means that if the feedback is lost into the fibre gain stage self-pulsing behaviour can develop and cause damage to the fibre ends.

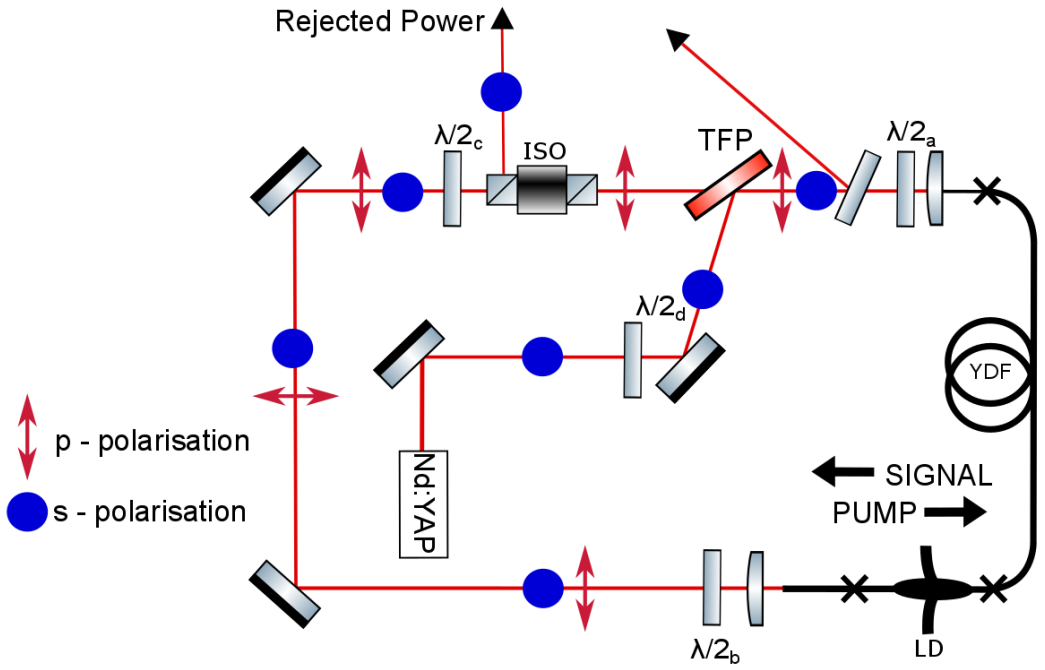

Figure 4.3 Second stage of aligning the polarisation of the ring laser. The seed polarisation is rotated so as to be rejected at the first isolator polariser. Pump power is applied and both ring oscillation and seed amplification is operational.

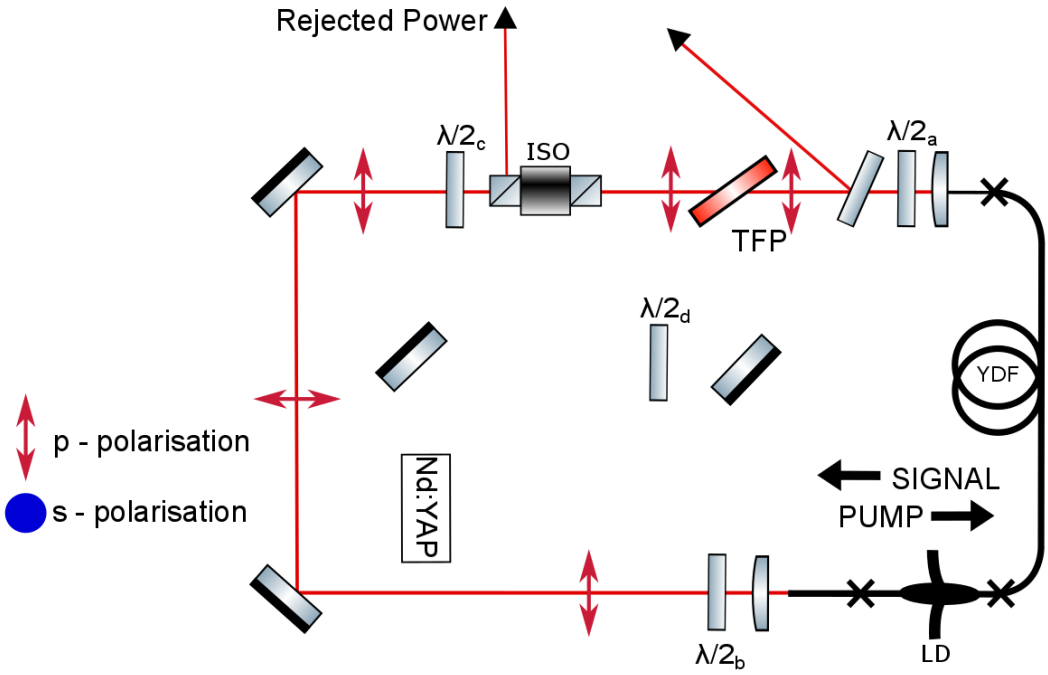

Figure 4.4 Final stage of polarisation alignment. Seed source is turned off leaving only ring oscillation operational and laser aligned.

4.1.2 Stage 2 – Internal Enhancement Cavity

Once the ring laser has been aligned with the wavelength and polarisation control to ensure a narrow enough bandwidth for SHG and ensuring that the polarisation of the IR signal light is in the plane required by the nonlinear crystal the enhancement cavity can be set-up.

The internal cavity mirrors are placed in position one by one. The first mirror placed is the output coupler followed by the first and second curved mirrors, in the case where a 6-mirror cavity is used the folding mirrors are placed in order of the beam path. The beam that exits the cavity is guided into the diagnostic tools as this is where the rejected beam path will travel. The final input coupler mirror is placed and the light rejected is guided into the marked out rejected beam path. Initially the cavity is empty to check the laser performance.

Since the ring laser will not oscillate until the cavity is exactly aligned and the cavity will not resonate until the ring laser is oscillating the amplified seed source is used once again to set-up the individual mirrors and bring them into alignment to achieve coupling into the cavity. To ensure that there are a few possible modes within the amplified seed, one of the cavity mirrors which form the seed laser is placed onto a piezo electric scanning mechanism.

After the enhancement cavity is aligned and the whole ring laser is operational without the safety of the seed source the nonlinear crystal is moved into position. As the empty cavity is aligned before the crystal goes in only a slight realignment is required to bring it back into resonance.

4.2 Internal Enhancement Resonator Design

4.2.1 300mm Cavity Design

As the ring laser was operating with a collimated beam radius of around 1mm in initial experiments the first enhancement cavity design had to be long enough to match the beam radius. This requirement was necessary to ensure the beam divergence along the free space path was kept low to ensure that the beam on recoupling does not expand beyond the maximum radius allowed for efficient coupling back into the fibre. Selecting mirrors with curvature of 300mm would allow for the ring laser beam waist to resonate

and give a focused waist in the lower arm of around 50μm. Figure 4.5 is a plot of the beam waists in the upper arm (red line) and lower arm (green) line with varying separation between the curved mirrors. Ideally, for good stability and ease of alignment the cavity would be designed so that the curved mirrors are a little apart and the chosen beam waists roughly in the middle of the plot. However here we have no ability to alter the beam waist of the ring laser, for the upper arm, so the mirror separation required is very close to the edge of stability where it is equal to the mirror curvature. A change in the fibre laser collimating lens will affect the Rayleigh length. This will in turn affect the recoupling efficiency. For practical reasons the collimating lens is fixed in its focal length and hence the beam waist.

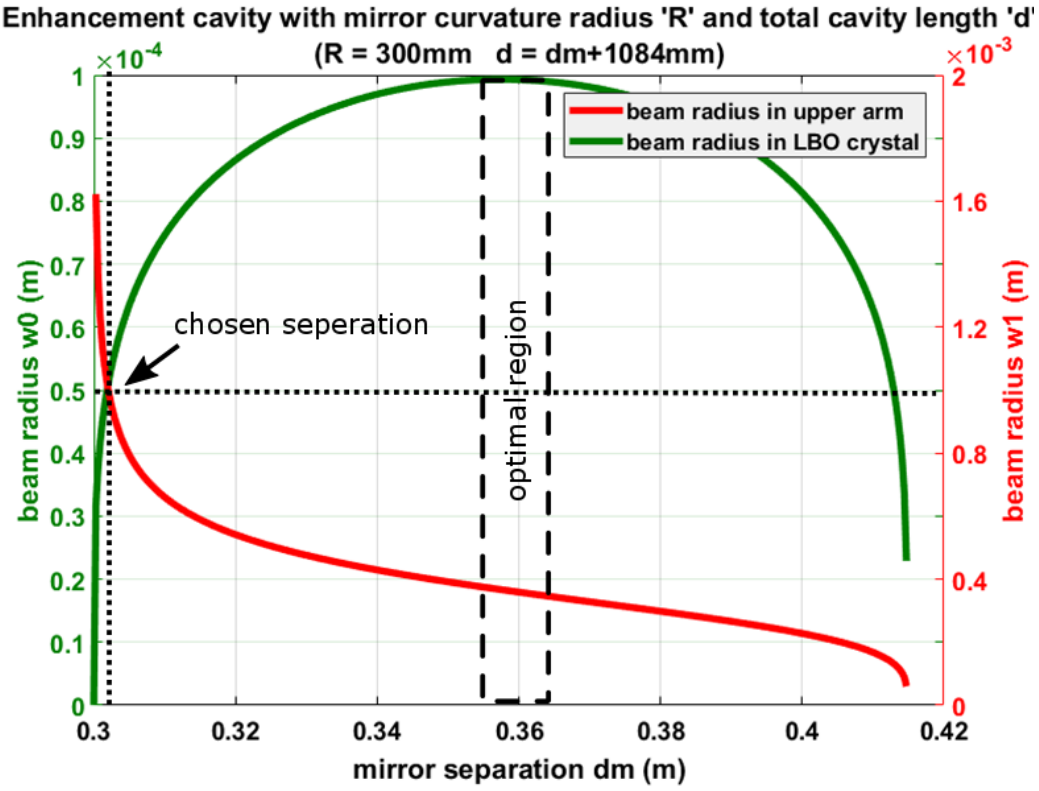

Figure 4.5 300mm enhancement cavity graph plotting out the change in beam waist in the upper arm of the enhancement cavity, red line, and the change in beam waist formed in the lower arm at the nonlinear crystal, green line. The beam size varies as the separation of the curved mirrors, (dm), is changed

A problem for a cavity with a long curvature radius is that the overall cavity length increases. In this case, for Rc = 300mm the overall cavity length was designed to be 1.7m. This resulted in two extra mirrors needed as part of the enhancement cavity so as to allow it to be folded and fitted within the overall system. The folding of the cavity is needed as the angle at the curved mirrors need to be kept as small as possible so as to avoid any astigmatism being introduced in the beam as it will be detrimental to the SHG

efficiency. Figure 4.6 is a diagram of the empty cavity. M1 is the input coupler with a transmission at the signal wavelength, λ=1080nm, of T=5.5%. M2 is the output coupler with transmission at the signal wavelength of T=1%. M3 and M4 are the curved mirrors RC=300mm, HR coated at 1080nm. The curved mirrors had a transmission at the second harmonic wavelength of T=67%. Mirrors M5 and M6 are HR coated at the signal wavelength. The distance between M1 and M2 is 275mm, M2 and M5 is 277mm, M5 and M4 is 290mm, M3 and M6 is 290mm, M6 and M1 is 277mm. This configuration results in an angle of 8 degrees at the curved mirrors which is small enough to avoid any astigmatic effects.

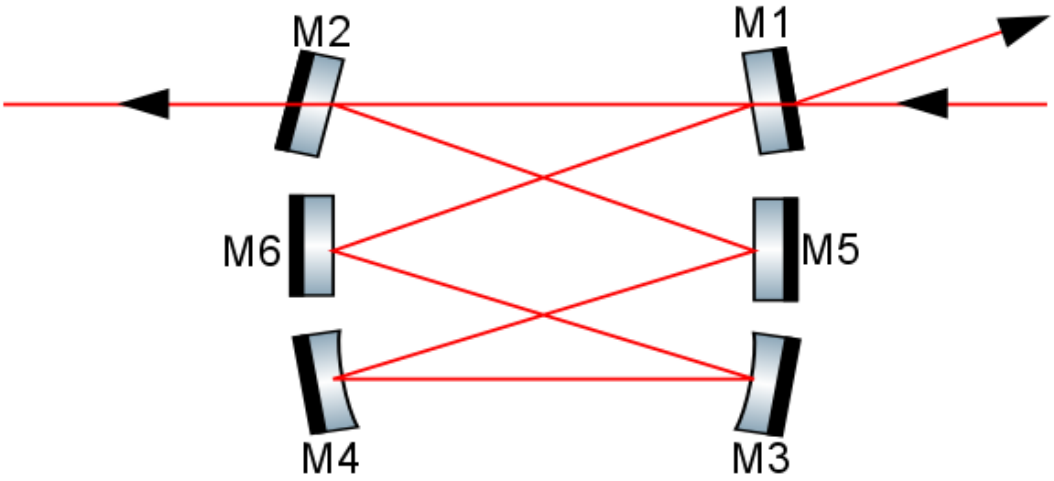

Figure 4.6 Schematic of empty 6-mirror enhancement cavity indicating beam propagation. Curved mirror radius of 300mm.

4.2.1.1 Empty Cavity Performance

As a preliminary experiment to test the cavity stability and help with alignment the laser was operated with an empty enhancement cavity. It allows for an initial check of the fibre gain stage performance in terms of total power, polarisation, feedback power and spectrum. Figure 4.7 shows the rejected power at the enhancement cavity for the IR power generated and incident on it. It is important to note that since the cavity is empty the impedance matching condition will not be met so the power rejected with an empty cavity will be higher.

For this cavity arrangement the fibre gain stage generated a maximum of 56W of light at the signal wavelength of 1080nm from a pump power of 98W with an overall slope efficiency of 58%. Of this 56W a total of 36W is rejected at the input coupler. The remaining 20W is coupled into the enhancement cavity. The intracavity power

circulating inside reaches a maximum of 520W at peak pump power giving an enhancement factor of 26 relative to the power coupled in. This is calculated from the transmitted power from the enhancement cavity and the transmission of the output coupler. Looking at the polarisation extinction ratio reveals a value of 12 dB, measured at the output of the fibre before interaction with the enhancement cavity. . This confirms that there is a loss in power due to some of the IR radiation not being in the polarisation state for which the second harmonic crystal is orientated and will be lost at the enhancement cavity. Essentially this power is wasted as none of it can be used for conversion.

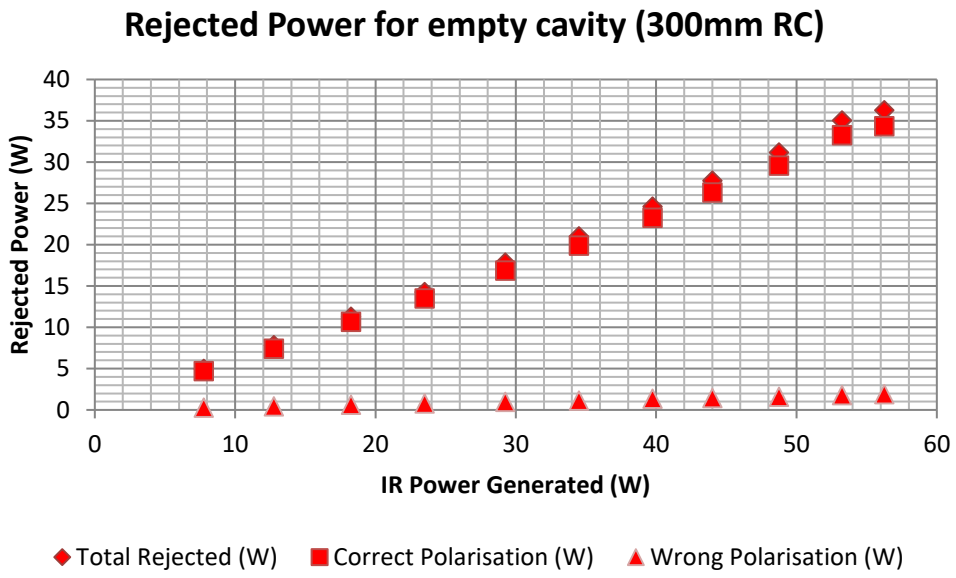

Figure 4.7 Graph of the rejected power at the input coupler of the enhancement cavity compared to the generated power incident. The graph is used to show that the majority of the power generated in the fibre is in the polarisation orientation for which the nonlinear crystal is orientated, and this ratio does not get worse with increasing pump power. Since the majority of power rejected is in the polarisation state required we can rule out polarisation as a reason for not being able to couple more light into the cavity.

4.2.2 200mm Cavity Design

A smaller cavity with mirror curvatures of 200mm was also set-up, shown in Figure 4.8 to investigate if it would be possible to operate the laser with an even smaller beam waist inside the crystal. Analysing its performance can also give a confirmation that the closer we are to the instability region the more difficult it will be to generate efficient second harmonic. Once again the plot in Figure 4.9 gives the possible beam waist for varying curved mirror separation.

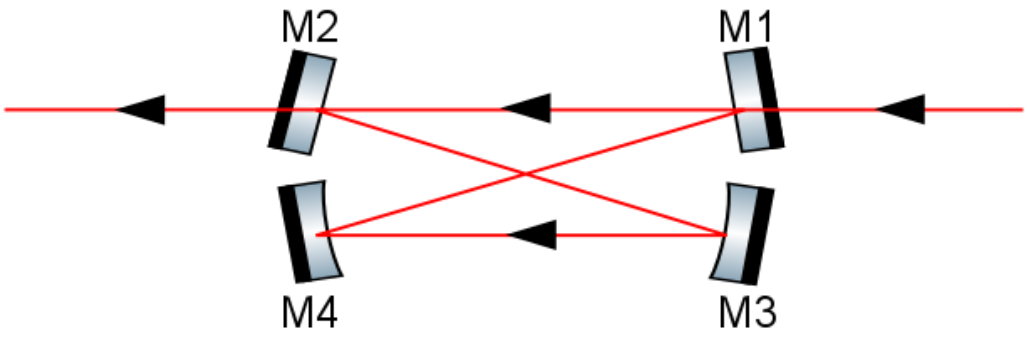

Figure 4.8 Empty 4-mirror enhancement cavity with curved mirrors of radius 200mm.

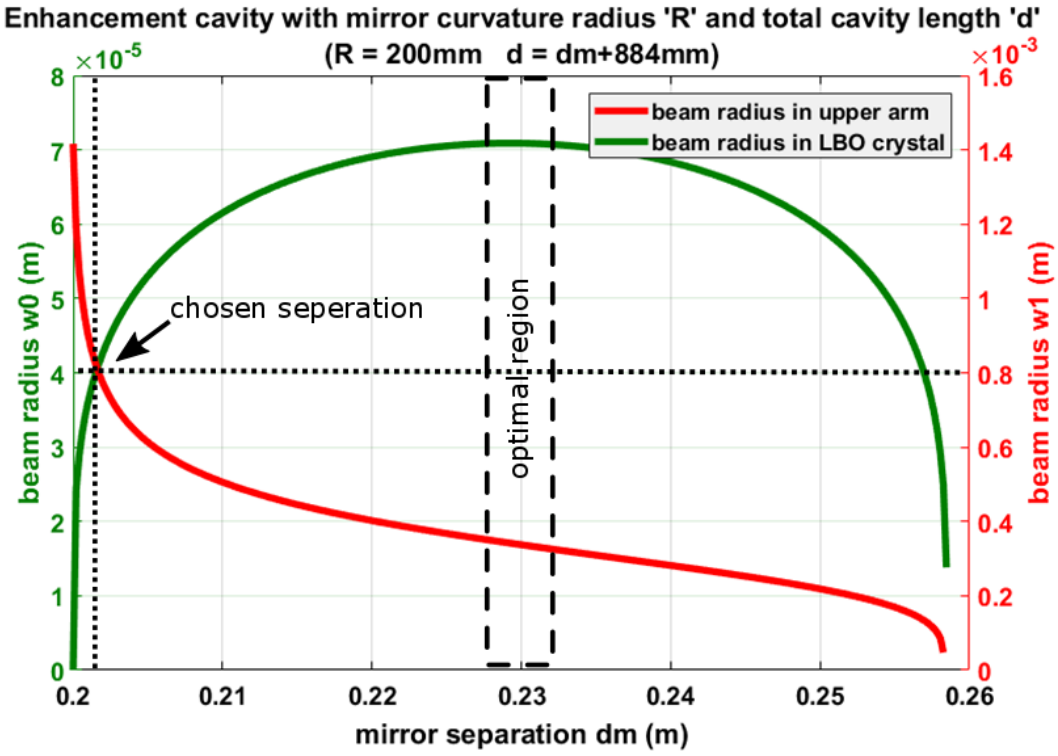

Figure 4.9 200mm enhancement cavity graph plotting out the change in beam waist in the upper arm of the enhancement cavity, red line, and the change in beam waist formed in the lower arm at the nonlinear crystal, green line. The beam size varies as the separation of the curved mirrors, (dm), is changed

The shorter radius mirrors result in a shorter enhancement cavity that does not require folding mirrors as is the case for the 300mm radius mirrors. M1 is the input coupler with a transmission at the signal wavelength of T=5.5%. M2 is the output coupler with transmission at the signal wavelength of T=1%. M3 and M4 are the curved mirrors RC=200mm, HR coated at 1080nm and AR coated at the second harmonic of 540nm. This configuration again results in an angle of 8 degrees at the curved mirrors which is small

enough to avoid any astigmatic effects. The distance between M1 and M2 is 240mm, M2 and M3 is 222mm, M4 and M2 is 222m and the distance between M3 and M4 is varied around 200mm to give the most stable operation. This gives a total enhancement cavity length of 884mm.

4.2.2.1 Empty Cavity Performance

Once again, the laser is operated with the empty cavity and the powers generated and rejected are shown in Figure 4.10. For the maximum launched pump power of 98W the laser generated 49W of signal power of which 39W is rejected at the input coupler. 10W is coupled into the cavity and the intracavity power circulating reaches a maximum of 357W resulting in an enhancement factor of 34 with 3.5W being fed back to the fibre gain stage. The main result to take away from this result is to compare the difference in the power coupled into the cavity with that for the larger, 300mm cavity. As expected the larger cavity allows for a larger beam waist in the upper arm which is more closely matched to that of the ring laser. This affects the overall efficiency of the ring laser, as less power is fed back into the ring oscillator.

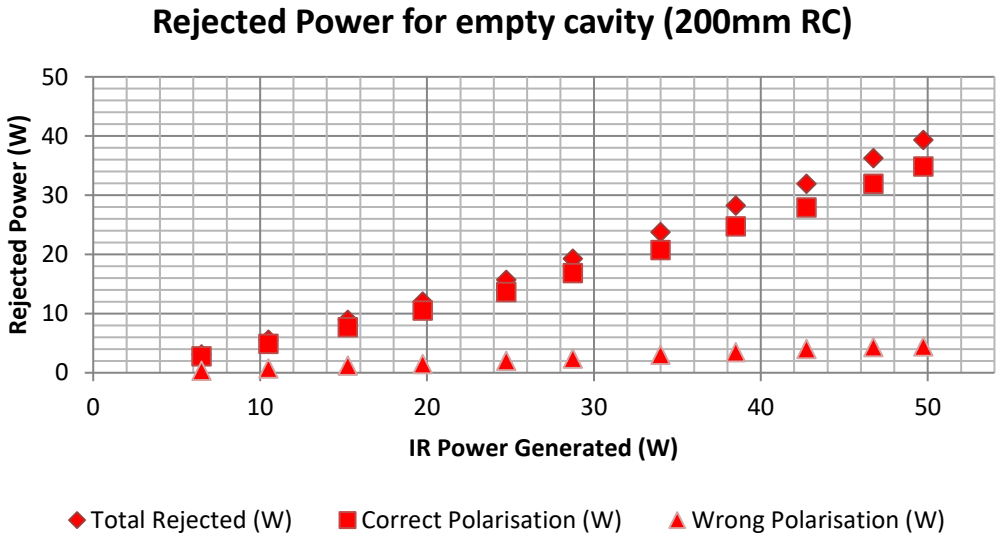

Figure 4.10 Rejected power at the 200mm radius of curvature mirror cavity. The graph is used to show that the majority of the power generated in the fibre is in the polarisation orientation for which the nonlinear crystal is orientated, and this ratio does not get worse with increasing pump power. Since the majority of power rejected is in the polarisation state required we can rule out polarisation as a reason for not being able to couple more light into the cavity.

4.3 Results

This section presents the main results obtained from the various experiments with the ring laser configuration. The results are divided first by differentiating the fibre feedback suppression method used, angle-cleaved fibre ends or end-capped fibre ends. This separates the results into two laser devices, the first preliminary experiment with angle cleaves at lower pump powers and the bulk end capped laser with a scaling of the pump power.

Within each laser configuration two arrangements of the internal enhancement cavity are investigated, a 6-mirror cavity with curved mirror radius RC=300mm and a 4-mirror cavity with RC=200mm, the design considerations for which were carried out in Section 2.6.3. Changing the radius of curvature of the internal cavity mirrors affects the allowed beam waist that can resonate inside the cavity and the focused beam waist inside the LBO cavity. A key factor in efficient operation of the laser is to ensure good spatial mode matching between the collimated beam exiting the fibre gain stage and the supported beam waist inside the enhancement cavity, TEM_{00} mode. Altering the cavity sizes investigates this effect as altering the separation changes the size of the TEM_{oo} mode. This allows to tune the internal cavity mode size to best match that of the fibre oscillator.

Within the second laser, using bulk end caps, a first look into scaling down the overall size of the laser device is investigated by decreasing the collimated IR beam waist and compacting the system. By reducing the free space path to efficiently support a smaller beam waist improvements in overall conversion efficiency is expected.

4.3.1 Laser 1 - Angle Cleaved Larger Beam Waist

The first experiments with the full laser set up were conducted with angle cleaved fibre ends. The bulk glass end caps were developed further into the project and their performance is analysed in a subsequent section. The angle cleaves showed good promise when operating the ring laser without an enhancement cavity, looking at the feedback reduction achieved and the ring laser performance was encouraging. The two cavity arrangements, with differing mirror curvatures, were built to investigate the mode matching capabilities of both designs and a comparison of their performance was carried out. Figure 4.11 shows the full ring laser set-up configured for a 4-mirror enhancement cavity, with the curved mirrors of radius=300mm. It is important to indicate the pick-off mirrors that are added to observe the incident power on the cavity

and also the feedback power, these are required to get a measure of exactly how the laser is performing as the only output without them is the generated second harmonic exiting the enhancement cavity.

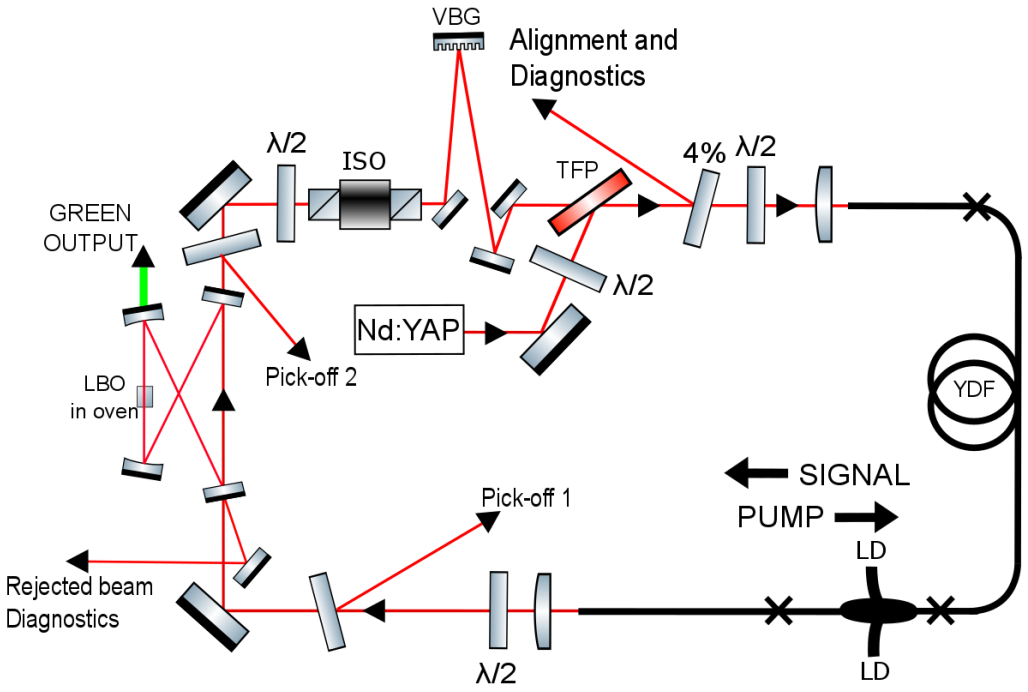

Figure 4.11 Ring laser set-up with 4-mirror enhancement cavity and diagnostic pick-off mirrors used for alignment and analysis if rejected light and fibre gain stage performance.

4.3.1.1 4-Mirror Enhancement Cavity

The first enhancement cavity was built using the smaller curvature mirrors as, with radius of 200mm.. Mirrors M1 and M2 are the input and output couplers, respectively. Mirror M1 is a flat mirror with reflectivity (R) at the signal wavelength (1080nm) of 95%. Mirror M2 is also a flat mirror with a higher reflectivity of 99% at the signal wavelength. The curved mirrors, M3 and M4 are highly reflective (HR) at the signal wavelength and anti-reflection (AR) coated for the second harmonic (540nm). The separation of the curved mirrors could be varied using mechanical stages to optimise the second harmonic power. The LBO crystal is inside an oven which is used to maintain the temperature slightly above room temperature. The LBO crystal is orientated for type-I critical phase matching. The reflectivity of M1 is chosen so that its transmission will equal the expected loss in the enhancement cavity, which is the leakage for feedback from M2 and the expected single pass second harmonic conversion efficiency of 4%. This is the impedance matching condition for the enhancement cavity.

For the maximum available pump power of 40W this cavity generated 2.55W of second harmonic signal with a slight rollover in the output power becoming evident, see Figure 4.12, at high pump power. This was for a total of 21W of IR power generated in the fibre gain stage and 9.2W coupled into the enhancement cavity with the remaining 11.8W rejected at the input coupler. The cavity needed slight realignment with increasing pump power which indicated an instability in the spatial mode matching due to the beam waist fluctuating. As pump power is increased the IR beam waist will increase and hence the size of the mode incident on the cavity will change. This requires an adjustment of the curved mirror separation to better match the allowed beam waist inside the cavity to that incident on it. Measuring the threshold power proved difficult due to the low feedback into the fibre, exiting the enhancement cavity, at low pump powers. This insufficient feedback results in damage in the fibre. To avoid this issue the seed source was used at low pump powers until the pump power was taken to a significant value above threshold. All of the results below were taken without the seed source operating.

The enhancement cavity generated 120W of intracavity circulating power at the maximum pump power, shown in Figure 4.13, with 1.2W being fed back into the fibre gain stage from the cavity. This represents an enhancement factor of 13 for the 9.2W that is coupled into the enhancement cavity. The ring laser IR slope efficiency, see Figure 4.14, is 54.5%, which is below the potential efficiency for a conventional Ytterbium fibre laser and also lower than the demonstrated slope efficiency when the ring laser was operated without an enhancement cavity. This drop in slope efficiency immediately suggested a loss at the recoupling stage in the laser, from free space to fibre. When experimenting without an enhancement cavity to see the tolerances on beam waist at recoupling a slight increase in the beam radius could cause decreases in slope efficiencies as seen here. All this indicates to incorrect beam size at the fibre being the main cause.

It can be seen from Figure 4.15 that roughly 50% of the power generated inside the fibre gain stage is rejected at the input coupler of the enhancement cavity. This is an indication of below optimal performance of the laser.

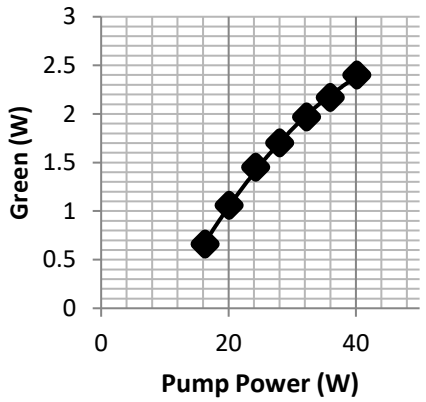

Figure 4.12 Plot of generated second harmonic against pump power for 4-mirror cavity with curved mirror radius RC = 200mm. Fibre ends terminated with angle cleaves.

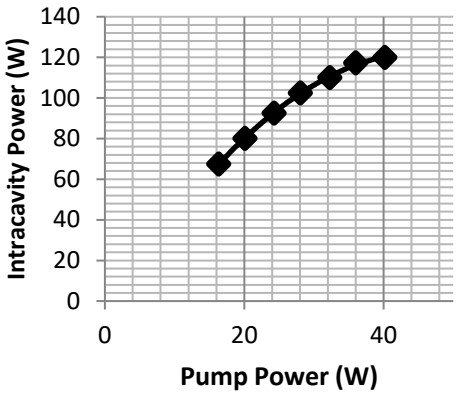

Figure 4.13 Plot of intracavity circulating power versus pump power for 4-mirror cavity with curved mirror radius RC = 200mm. Fibre ends terminated with angle cleaves.

Further investigation showed that a mismatch between the spatial modes of the ring laser and that of the expected mode size in the enhancement cavity was observed. The beam wasit could be measured form the rejected light of the entrance of the enhancement cavity. This problem was expected when designing the enhancement cavity in Section **Error! Reference source not found.**. As the mode sizes that the system operates on are very close to the limit of stability it proves difficult to get the spatial mode matching exact. Finally analysing the enhancement cavity performance relative to its frequency doubling potential, the single pass second harmonic efficiency increase from 1% to just over 2% with increasing intracavity power, shown in Figure 4.16.

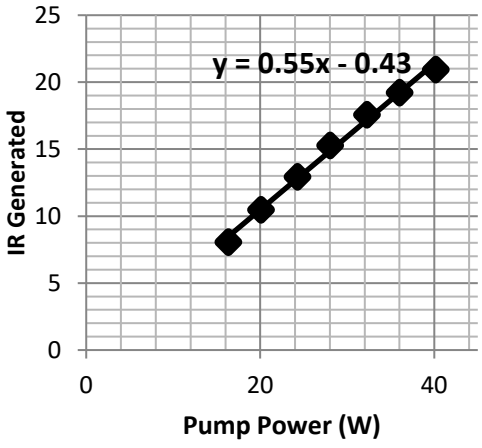

Figure 4.14 Plot of generated signal power incident on 4-mirror enhancement cavity versus pump power. Measured using pick off mirror to indicate the power efficiency of the ring laser. Fibre ends terminated with angle cleaves.

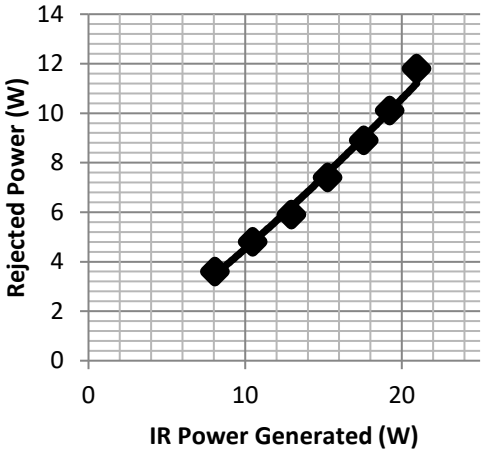

Figure 4.15 Plot of generated signal power incident on 4-mirror enhancement cavity versus rejected power at the input coupler.

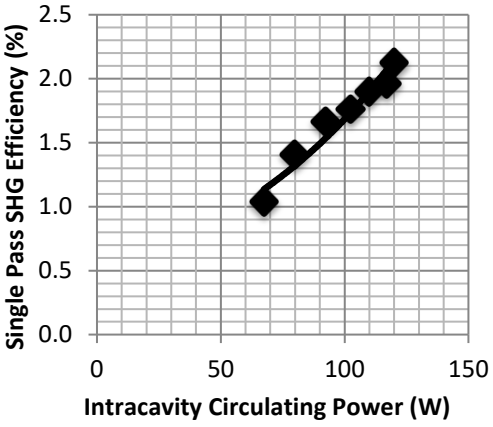

Figure 4.16 Single pass second harmonic conversion efficiency relative to intracavity circulating power.

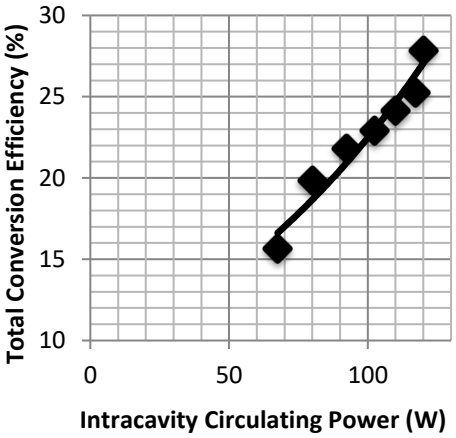

Figure 4.17 Graph of the total conversion efficiency versus intracavity power. The cavity efficiency is calculated from the coupled IR power relative to green generated.

This is lower than expected, typical single pass efficiency for LBO is closer to 4%. Whilst the total conversion efficiency, coupled IR power relative to generated green power, reaches a peak value of 28% at the maximum pump power, Figure 4.17.

4.3.1.2 6-Mirror Enhancement Cavity

The second enhancement cavity configuration was built using the larger radius curved mirror, r=300mm. Due to the large collimated beam radius of the ring laser a large curvature radius mirror was chosen for the mirrors that form a waist inside the LBO crystal. As the graph in Figure 4.5indicates, for a signal beam radius of 1mm a beam radius of 50μm is formed in the lower arm.

Mirrors M1 (R=95% at 1080nm) and M2 (R=99% at 1080nm) are the input and output couplers respectively, both flat. Mirrors M3 and M4 are the curved mirrors, with radius of 300mm. Both of them are HR (>99.9%) at the signal wavelength, 1080nm, but were not AR coated at the second harmonic wavelength (R≈33% at 540nm). Hence why all of the second harmonic power values documented are specified as power generated taking into account the fraction of light reflected at the curved mirrors. To complete the cavity mirrors M5 and M6, both flat HR (>99.9% at 1080nm), are needed to fold the enhancement cavity in to fit within the overall ring laser. The LBO crystal is mounted inside of an oven to be able to control its temperature, not shown in the diagram.

This cavity produced 3.4W of second harmonic for a pump power of 40W before the power started to roll off and the enhancement cavity became unstable. The power evolution can be seen in Figure 4.18. This was from a total of 21W of IR power generated in the fibre gain stage with 10.3W coupled into the enhancement cavity and the remaining 10.7W rejected at the input coupler. Due to the need to realign the cavity as the power was increased the plot is not smooth and slightly exponential, as would be expected.

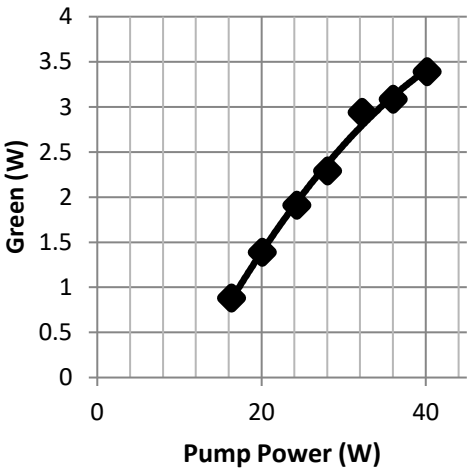

Figure 4.18 Plot of generated second harmonic against pump power for 6-mirror cavity with curved mirror radius RC = 300mm. Fibre ends terminated with angle cleaves.

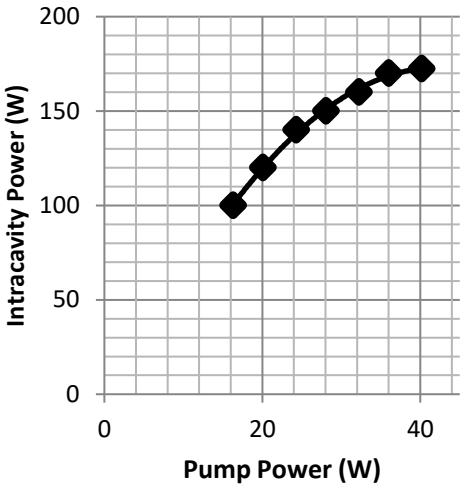

Figure 4.19 Plot of intracavity circulating power versus pump power for 6-mirror cavity with curved mirror radius RC = 300mm. Fibre ends terminated with angle cleaves.

The enhancement cavity generated a maximum intracavity circulating power of 172.5W for the 10.3W coupled into it, an enhancement factor of 16.7, shown in Figure 4.19. This is an improvement on the smaller enhancement cavity along with the power coupled in and the subsequent second harmonic power generated. All of this can be explained due to the slight improvement in the spatial mode matching that the larger enhancement cavity allows. The ring laser IR efficiency, see Figure 4.20, was down on the expected performance at 55% when comparing with the potential expected from the amplifier experiments. Roughly 50% of the power generated in the fibre was lost at the input coupler, see Figure 4.21, and the trend was increasing as the pump power was going up. All of these limits in performance once again suggest a non-optimal set-up with the biggest problem being the difficulty in achieving good spatial mode matching inside the enhancement cavity. The loss in IR efficiency suggested a loss at the recoupling part of the system. Looking at the frequency doubling performance of this larger cavity we see

a similar single pass conversion efficiency as that of the smaller one, Figure 4.22. With a slight increase in the IR power coupled into the cavity and subsequent increase in the intracavity power the total conversion efficiency is slightly higher than that of the smaller cavity, rising to 32% at maximum output power. It is evident that spatial mode matching is one of the limiting factors in the current configuration. The increase in mirror curvature increased the maximum possible beam waist that could be supported by the enhancement cavity. For this configuration of the ring laser with what is quite a large beam radius of 1mm, necessary due to path length in free space, a big enhancement cavity is needed in terms of both mirror curvature and subsequent path length to allow an even bigger waist to form in the upper arm. This adds a complication as further increasing the size of the enhancement cavity prevents it from fitting inside the ring laser. Knowing this an alternative to achieving a good spatial mode overlap is to decrease the beam radius that the ring laser operates on. To do this would require to scale down the whole system and ensure that the Rayleigh length of the decreased beam radius is longer than the free space path of the ring laser.

The second big factor affecting performance is the power generated in the fibre. There was no difference between the two enhancement cavities suggesting that the problem is in the fibre gain stage and more precisely it arises from potential loss at recoupling due to the angle cleaves and their performance at high powers. As pump power was increased the output power became unstable, which could be due to thermal fluctuations of the fibre ends. To investigate if the angle cleaves were an issue the laser was rebuilt using bulk glass end-caps which could be held more rigidly in place and would dissipate heat building up at the glass/air interface better.

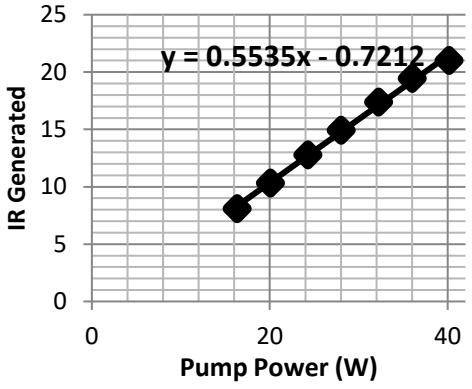

Figure 4.20 Plot of generated signal power incident on 6-mirror enhancement cavity versus pump power. Measured using pick off mirror to indicate the power efficiency of the ring laser. Fibre ends terminated with angle cleaves.

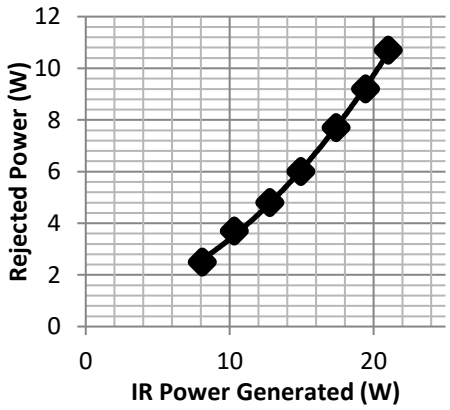

Figure 4.21 Plot of generated signal power incident on 6-mirror enhancement cavity versus the power rejected at the input coupler.

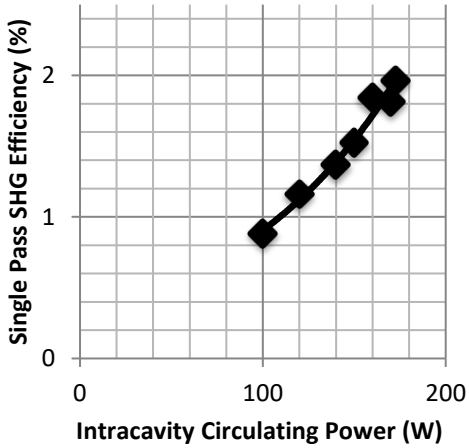

Figure 4.22 Single pass second harmonic conversion efficiency relative to intracavity circulating power.

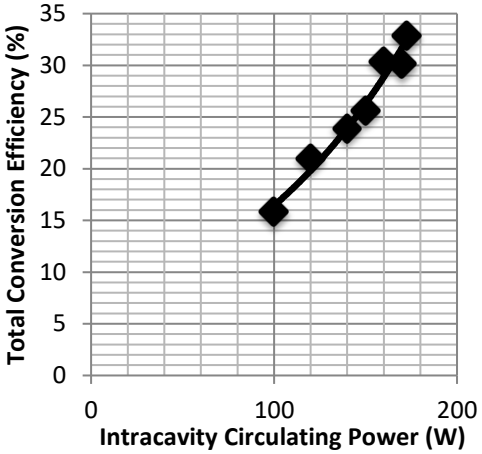

Figure 4.23 Graph of the total conversion efficiency versus intracavity power. The cavity efficiency is calculated from the coupled IR power relative to green generated.

4.3.2 Laser 2 - Bulk End Capped Ring Laser

The first laser configuration demonstrated good frequency doubling potential and the internal cavity was able to generate enhancement factors over 10 for both cavity sizes. One obvious limit on the maximum output power was the slope efficiency on which the fibre was operating, down to 55%. The power scaling potential was also not promising as instability in alignment was observed at pump powers of only 40W. Both of these issues are related to the recoupling of the feedback signal bask into the fibre after passage through the free space part, the enhancement cavity, isolator and VBG.

In parallel with the angle cleaved fibre end development, a system to produce bulk glass end caps were developed, shown in section 3.4.2. The bulk end caps were able to be mounted in a far more stable and robust way so as to avoid any thermal drift of the fibre ends and when compared to the fibre end caps operated with a better slope efficiency, over 60% compared to 39% for the matched fibre end caps. These two potential improvements indicate that an increase in second harmonic output power can be achieved. The angle cleaves were replaced with bulk end caps and the ring laser aligned in the same manner as before to produce the following results.

Once again both cavity sizes are investigated to see if the effect of imperfect spatial mode matching is evident. This time, for the smaller internal cavity, RC=200mm, the overall size of the ring laser was reduced by decreasing the focal length of the collimating and recoupling lenses at the fibre ends from 15.29mm to 11mm. This will reduce the collimated IR beam radius from 1mm to 800μm and should improve the mode matching and increase the output power for the smaller enhancement cavity.

The available pump power is now increased by over two times that of what was available before to 100W, delivered via two 50W 975nm fibre coupled laser diodes using a 2 to 1 tapered fibre combiner as before.

4.3.2.1 6-Mirror Enhancement Cavity

The 6-mirror cavity performed best for the angle cleaved laser and it was the first set up investigated in the bulk end cap laser configuration. The cavity was designed in exactly the same way as before, shown in Figure 4.6 and all the mirrors were identical as previously mentioned. A flat input coupler with reflectivity of 95% and flat output coupler reflectivity of 99%. Curved mirrors with radius RC=300mm and the LBO crystal in an oven orientated for type-I critical phase matching. The curved mirrors are again placed on high precision micrometre mechanical stages to provide fine control of the beam waist inside the LBO crystal. Two HR flat mirrors are still required to fold the enhancement cavity to allow it to fit inside the main ring resonator.

For the maximum incident pump power of 98W the laser generated 17.4W of second harmonic output from 60.8W of generated IR power, 40.4W of which was successfully coupled into the enhancement cavity, with the remaining 20.4W rejected at the input coupler. The power evolution plot is shown in Figure 4.24 where no obvious rollover in output power is seen. Perfecting the alignment procedure along with the improved stability of the bulk end cap fibre terminations allowed for better power measurements near the laser threshold.

Extending the analysis of the rejected power from the previous experiments provides further information into potential reasons as to why more power is not coupled into the cavity. In this case 66% of the generated IR power is coupled into the enhancement cavity an improvement on the 50% measured for the angle cleaved ring laser. Figure 4.25 displays the IR power rejected for increasing pump powers, it displays the total power and the ratio between the powers in the two orthogonal polarisation states that were present. Ensuring that the IR power is polarised in the orientation that the ring laser is aligned for and the LBO crystal is orientated for would help rule this out as potential limitation in second harmonic output power. The majority of the power rejected is again in the 'correct' state, that being the orientation for which the crystal is aligned and the ring laser should be operating on. This is an indicator that even though there is some depolarisation in the fibre gain stage the majority is in the correct orientation. The polarisation extinction ratio of the IR signal before being incident on the cavity was measured to be 14dB.

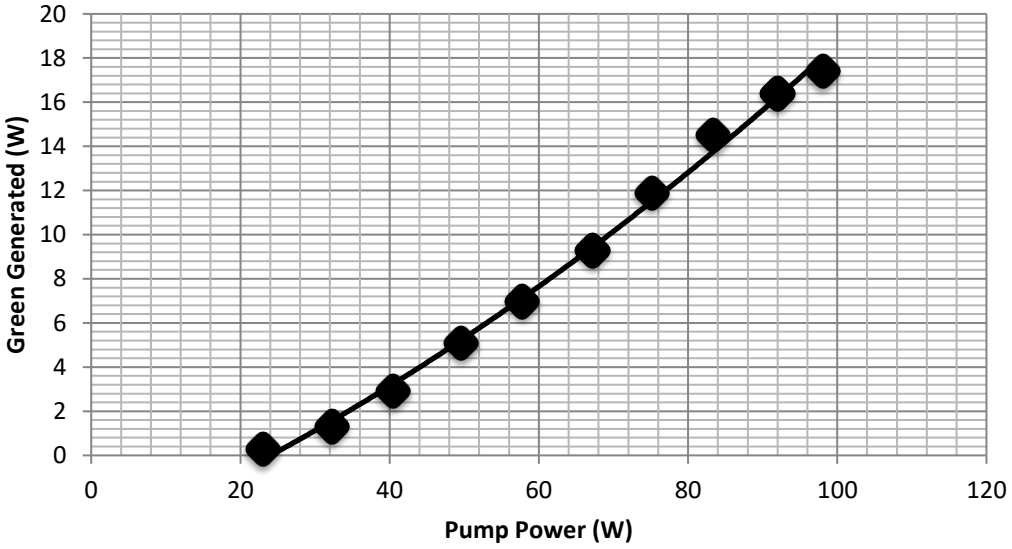

Figure 4.24 Plot of generated second harmonic against pump power for 6-mirror cavity with curved mirror radius RC = 300mm. A maximum of 17.4W of second harmonic power is generated for maximum pump power of 98W. Fibre ends terminated with bulk end caps..

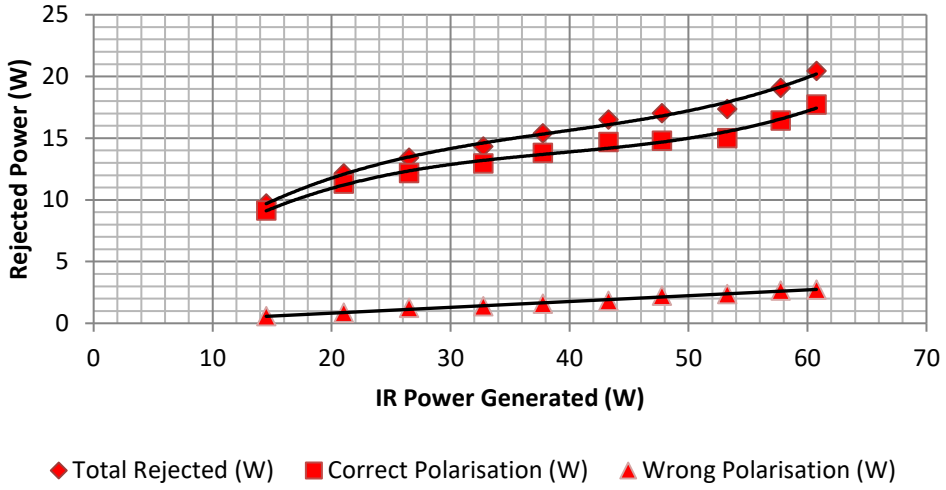

Figure 4.25 Plot of the rejected IR powers in both polarisations against the generated IR power incident on the enhancement cavity.6-mirror enhancement cavity, RC = 300mm, bulk glass end caps, with collimated IR beam radius 1mm.

The ring laser was operating more efficiently with the slope efficiency having increased from the 55% for the angle cleaved laser to 62%, Figure 4.26, for this bulk end cap configuration. For the maximum 40.4W of IR power coupled into the enhancement cavity 420W is circulating intracavity, an enhancement factor of 10.4. This decreases from a factor of 15 at lower pump powers. The decrease in the enhancement factor compliments the increase in the nonlinear efficiencies of the enhancement cavity. Observing the feedback power, see Figure 4.27, indicates a rollover at higher pump powers without any obvious detrimental effect on the slope efficiency or output power, this is correlated to the decrease in enhancement factor of the circulating power.

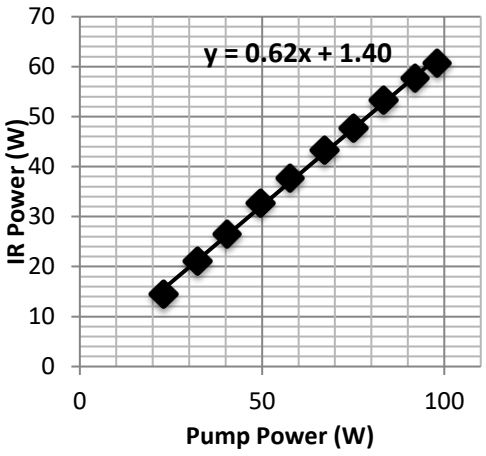

Figure 4.26 Plot of generated signal power incident on 6-mirror enhancement cavity versus pump power. Measured using pick off mirror to indicate the power efficiency of the ring laser.

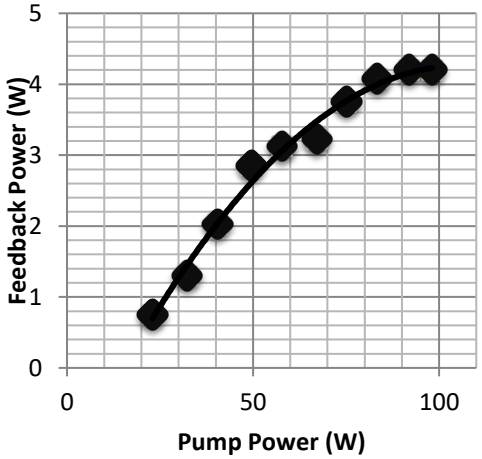

Figure 4.27 Feedback power exiting the enhancement cavity.

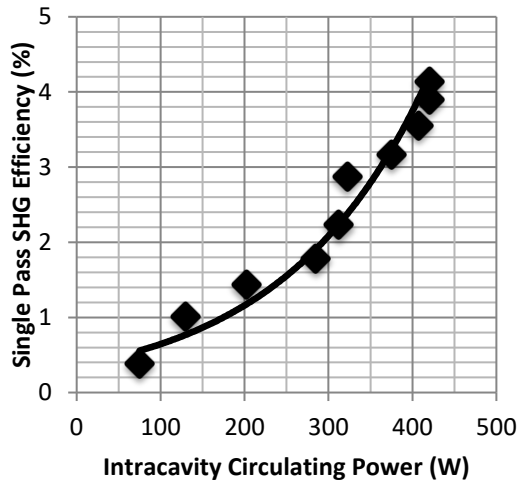

Figure 4.28 Single pass second harmonic conversion efficiency relative to intracavity circulating power

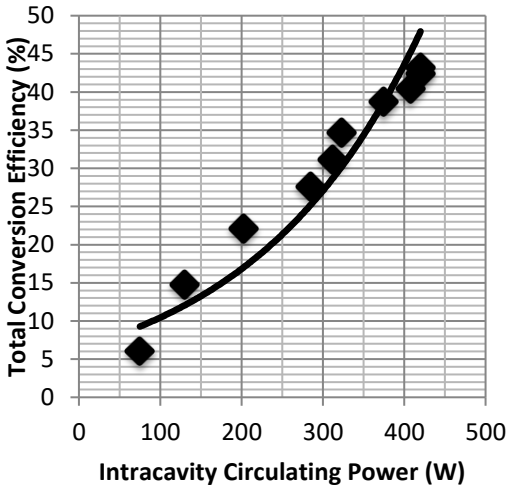

Figure 4.29 Graph of the total conversion efficiency versus intracavity power. The cavity efficiency is calculated from the coupled IR power relative to green generated

As is expected, for higher pump powers the enhancement cavity becomes more efficient in second harmonic generation. Figure 4.28 and Figure 4.29 display the single pass harmonic efficiency and the total conversion efficiencies respectively. Here the single pass efficiency reaches a maximum value of 4.1% and the total conversion efficiency, w.r.t. pump power, reaches 43% with increasing pump power. Both values are a significant improvement of the performance of the angle cleaved laser and indicate a far more efficient laser system.

The spectrum of the second harmonic output and the incident IR signal are plotted in Figure 4.30 and Figure 4.31 respectively. The spectrum of the input IR signal shows a clear main peak at 1079.7nm with a bandwidth of 0.1nm FWHM. Two secondary peaks can be seen that are being suppressed sufficiently well enough by the VBG highlighting the importance of having a robust method to narrow the bandwidth of the signal light for efficient SHG. The spectrum shows a peak at 539.9nm with a bandwidth of 0.1nm FWHM. The spectrometer used lacks sufficient sensitivity to produce a detailed enough measurement hence the spectrum appears uneven due to the resolution of the machine being lower than the bandwidth of the signal to be measured. Nevertheless both output spectra highlight the excellent performance of the VBG for wavelength control.

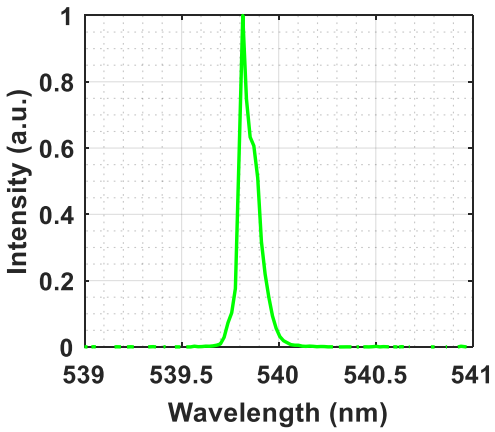

Figure 4.30 Second harmonic output spectrum. FWHM 0.1nm.

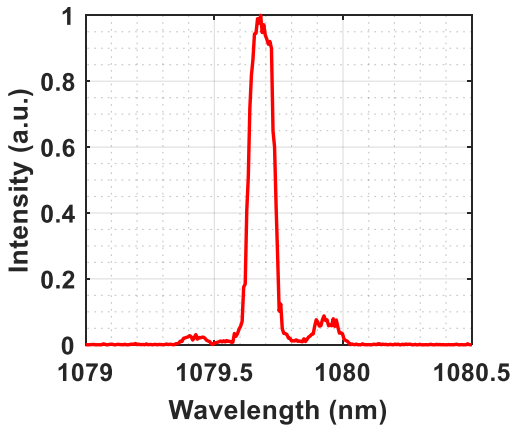

Figure 4.31 Incident IR signal spectrum. FWHM 0.1nm.

The second harmonic output beam quality (M^2 parameter) was measured to be 1.09 and 1.02 in the x and y directions respectively. The very slight difference between the two values could be due to imperfect positioning of the IR beam onto the curved mirrors which could introduces astigmatism in the beam. However, the beam quality of the second harmonic signal is still excellent as would be expected from the beam quality of the signal light as it emerges from a single-mode fibre. Figure 4.32 and Figure 4.33 show the beam waist measurements with a Gaussian beam fit.

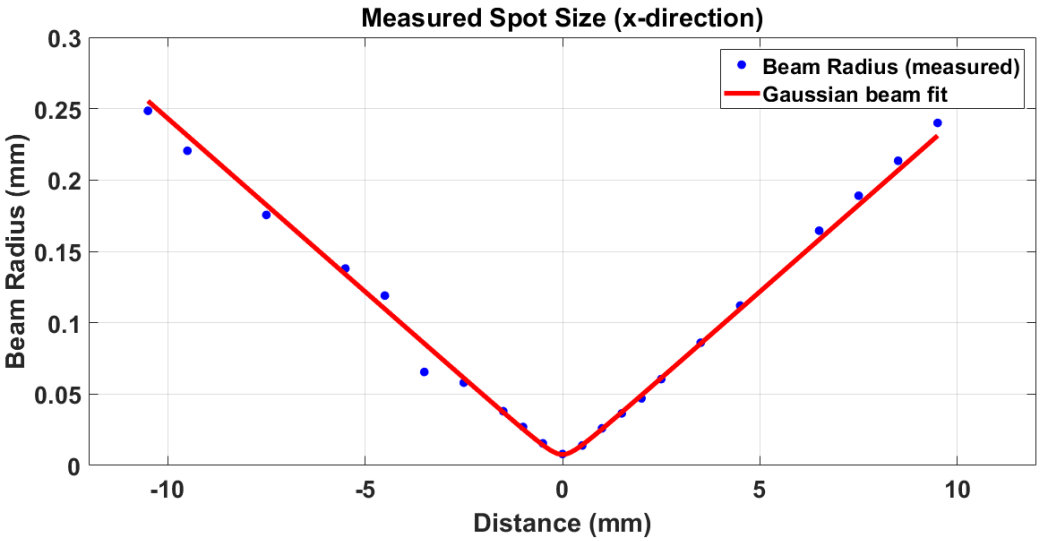

Figure 4.32 M2 (x-direction) of the output second harmonic beam for a 6 mirror enhancement cavity with curved mirror radius of 300mm, M2 is 1.09.

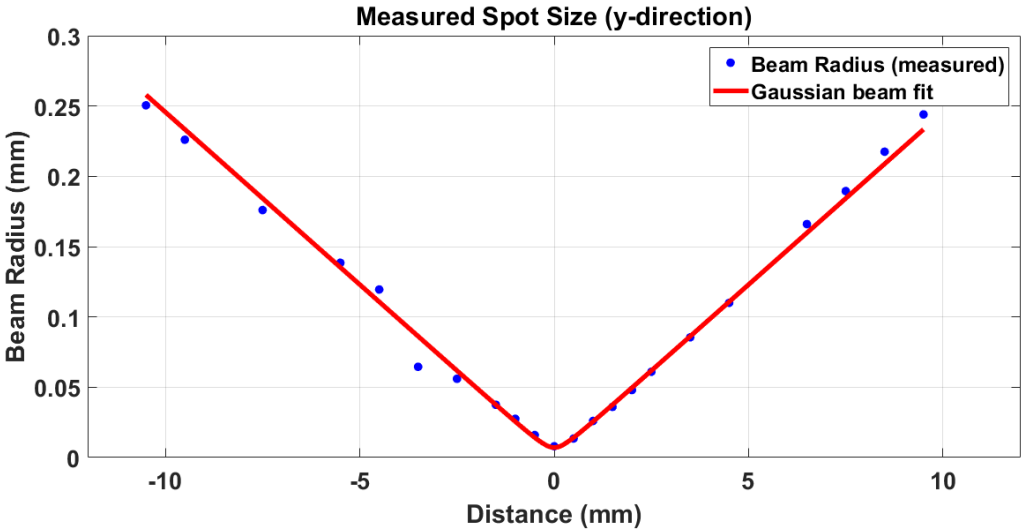

Figure 4.33 M2 (y-direction) of the output second harmonic beam for a 6 mirror enhancement cavity with curved mirror radius of 300mm, M2is 1.02.

The axial mode content of the output spectrum can be influenced by many factors such as changes in the cavity length due to mechanical or temperature induced fluctuation of components. However, due to the large number of closely spaced axial modes simultaneously resonant in the enhancement cavity this will ensure a very stable output. Figure 4.34 displays a measure of the signal intensity noise for a period of 10ns to 120 seconds measured using a photodetector. The R.M.S. error is less than 1% over the time period measured indicating a good noise performance.

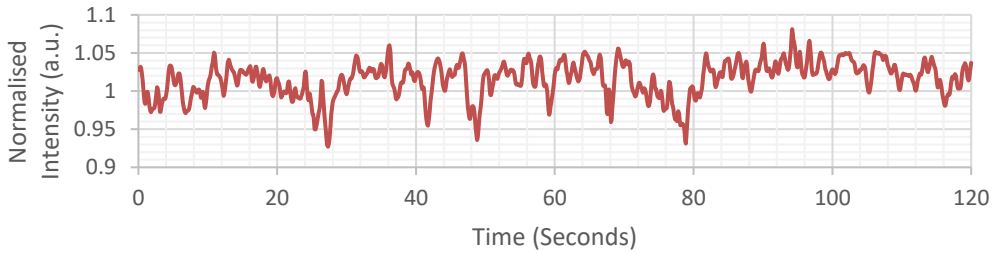

Figure 4.34 Normalised intensity noise, RMS error <1%.

4.3.2.2 4-Mirror Enhancement Cavity

From the previous results obtained using the 4-mirror enhancement cavity it is expected that its performance will be worse than that of the 6-mirror cavity for the same identical ring laser configuration. As discussed, this is due to a bigger mismatch in the spatial mode overlap between the collimated IR beam and the beam supported by the enhancement

cavity. This also affects the alignment of the enhancement cavity when it comes to stability as the optimum separation of the curved mirrors lies very close to the edge of the allowed beam waist.

This section presents results for the 4-mirror cavity in the original ring laser configuration as used for a 6-mirror cavity and compare it with a ring laser set-up operating on a reduced collimated IR beam waist. This was done by reducing the focal length of the collimating and recoupling aspheric lenses from a focal length of 15.29mm to 11mm. The reduction in beam waist requires a reduction in the free space path of the ring laser, to be close to or below the Rayleigh length of the new collimated beam waist so as to avoid recoupling losses arising from beam divergence.

A) Original beam waist

The 4-mirror cavity was set up as previously shown, comprising of a plane input coupler with reflectivity R=95% and a plane output coupler with reflectivity R=99% both at the signal wavelength 1080nm. The two curved mirrors were HR coated at the signal wavelength and AR coated at the second harmonic, wavelength 540nm, with a radius of curvature of 200mm. The angle of incidence onto the mirrors was 8 degrees to avoid any astigmatism. The curved mirrors were again placed onto a micrometre precision translation stages for control of the mirror separation.

For the maximum pump power of 98W coupled into the fibre gain stage 11W of green second harmonic output was generated. This was for an incident IR signal power of 60.25W of which 38.05W was successfully coupled in and 22.2W rejected at the input coupler. The output power evolution curve is shown in Figure 4.35. No evident rollover can be observed while the curve is not perfectly smooth as the cavity required slight adjustment of the curved mirror separation as pump power was increased. Measurements near the laser threshold were difficult as the cavity was unstable and pulsing of the signal was seen until enough power could be fed back to the fibre gain stage. Hence at low pump power the seed source needed to be used to prevent any damage of the fibre. All of the data presented is without the seed source.

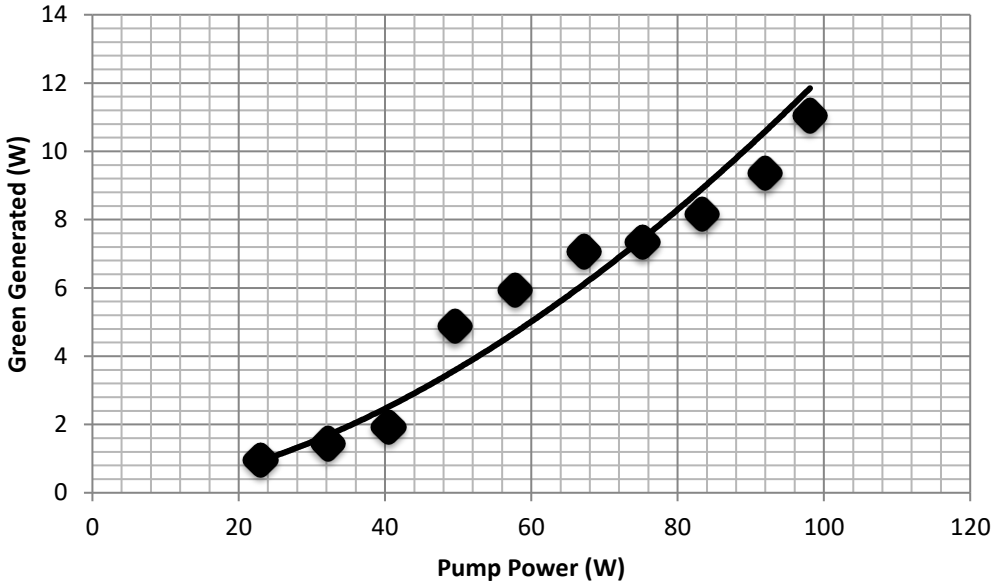

Figure 4.35 Plot of generated second harmonic against pump power for 4-mirror cavity with curved mirror radius RC = 200mm. Fibre ends terminated with bulk end caps. Incident collimated IR beam waist of 1mm.

Looking at the rejected power, Figure 4.36, 63% of the incident IR power is coupled into the enhancement cavity, a slight decrease on the 6-mirror performance. Once again the majority of the rejected power is in the 'correct' polarisation state and the PER was again close to 14dB indicting that the change in cavity does not affect polarisation and it is not the biggest factor in the overall efficiency.

The ring laser operates with a 62% slope efficiency for the generated IR signal, similar to the 6-mirror cavity, see Figure 4.37. For the maximum 38.05W of IR power coupled into the cavity an intracavity circulating power of 353W is generated, an enhancement factor of 9 which has decreased from 15 at lower pump powers. This results in a lower feedback power, shown in Figure 4.38, compared to the 6-mirror cavity without a detrimental effect on the IR slope efficiency. Due to the minor re-alignment adjustments required as pump power was increased the feedback power curve is not as smooth as expected and this pattern is repeated in the results for the nonlinear efficiencies.

Figure 4.39 and Figure 4.40 show the single pass conversion efficiency and the total conversion efficiency. Both are below the values achieved for the 6-mirror cavity, with a maximum single pass efficiency of 3.1% and total conversion efficiency of 29%. Both of these values add to the expected result that the 4-mirror cavity would perform less effectively due to imperfect spatial mode matching, this explains the strange behaviour

seen in the data. There seems to be a plateau in the feedback power for a range of pump powers which affects the conversion to second harmonic and circulating power. More power is rejected which leads to decreases in intracavity power and less conversion to the second harmonic.

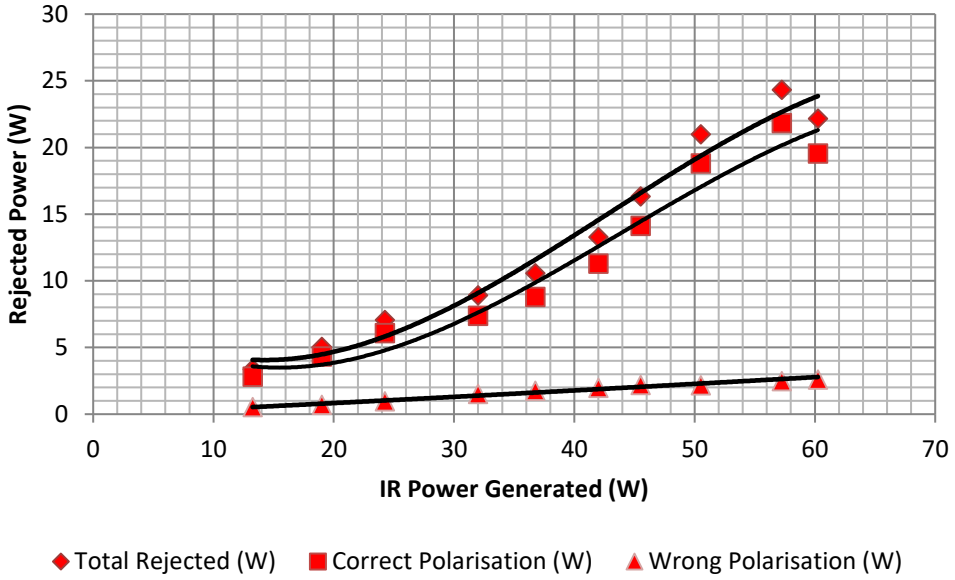

Figure 4.36 Plot of the rejected IR powers in both polarisations against the generated IR power incident on the enhancement cavity.4-mirror enhancement cavity, RC = 200mm, bulk glass end caps, with collimated IR beam radius 1mm.

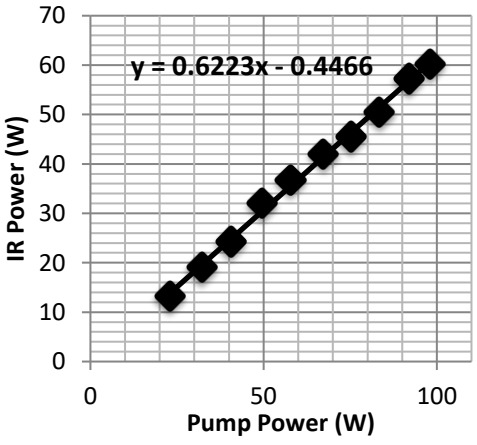

Figure 4.37 Plot of generated signal power incident on 4-mirror enhancement cavity versus pump power. Fibre ends terminated with bulk end caps. Beam radius of 1mm.

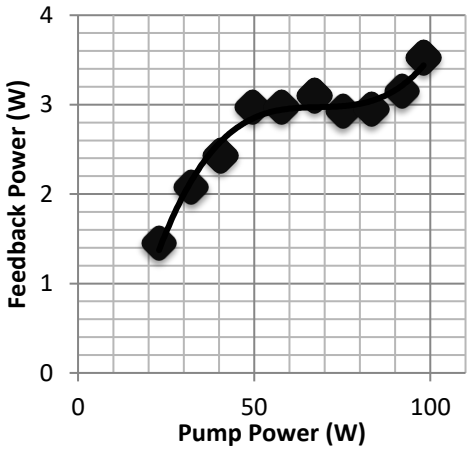

Figure 4.38 Feedback power exiting the enhancement cavity.

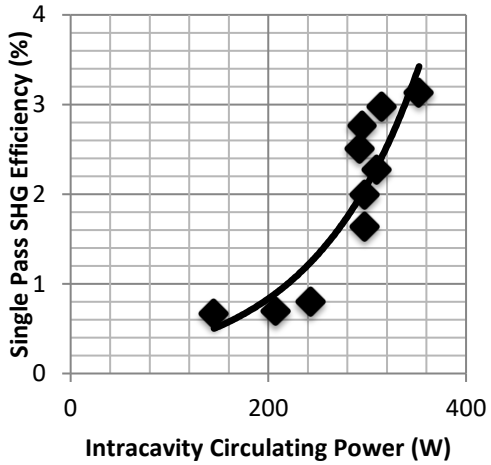

Figure 4.39 Single pass second harmonic conversion efficiency relative to intracavity circulating power

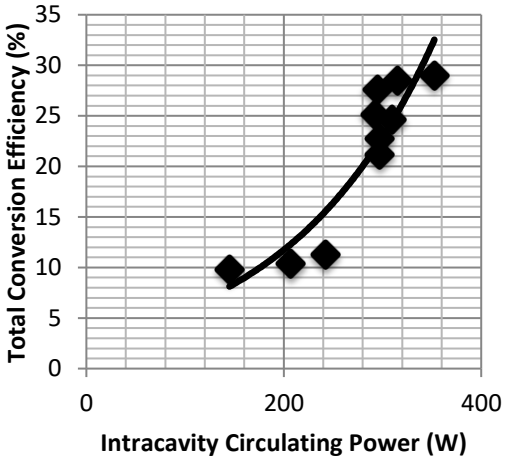

Figure 4.40 Graph of the total conversion efficiency versus intracavity power. The cavity efficiency is calculated from the coupled IR power relative to green generated

B) Reduced beam waist

As mentioned previously, the 4-mirror enhancement cavity with R=200mm curved mirrors, operated very close to the limit of the allowed beam waists for the upper and lower arm in the cavity. This results in a very narrow waist being formed in the LBO crystal and a more unstable enhancement cavity overall. One way to improve this is to decrease the collimated beam waist that the ring laser operates on. That is the beam waist of the IR signal which should be matched to the beam waist in the upper arm of the enhancement cavity. To do this the aspheric lenses that are used for collimation and recoupling at the fibre ends were changed from f=15.29mm to f =11mm, reducing the beam radius from 1mm to 800μm. As can be seen from Section 4.2.2, Figure 4.9, this moves the cavity into a more stable operating region and increases the size of focused beam waist in the LBO crystal from 30μm to 40μm. All of these changes will yield a more stable and more efficient cavity.

One downside to the decreasing the ring laser beam waist is that it reduces the Rayleigh length of the collimated beam waist and requires a reduction in the overall free space beam path of the laser. The Rayleigh length goes down from 3.2m to 1.66m. This requires a reconfiguration of the free space components within the ring laser to make them as compact as possible so that the free space path can be kept to within the new Rayleigh length or at least as close as possible. To simplify alignment as well as improve the compactness of the whole laser the VBG and isolator arrangement are switched and

Figure 4.41 shows the schematic of the final laser system. It was difficult to fit everything including the enhancement cavity within the 1.66m and the free space path length was closer to 2m. This would result in a potential loss at recoupling and hence ring laser IR efficiency as the collimated beam waist would grow in size due to diffraction by the time it reaches the recoupling lens, but the expected loss will not affect the performance significantly. It will impact the IR efficiency but it would still not be the biggest limiting factor in the overall second harmonic power generated.

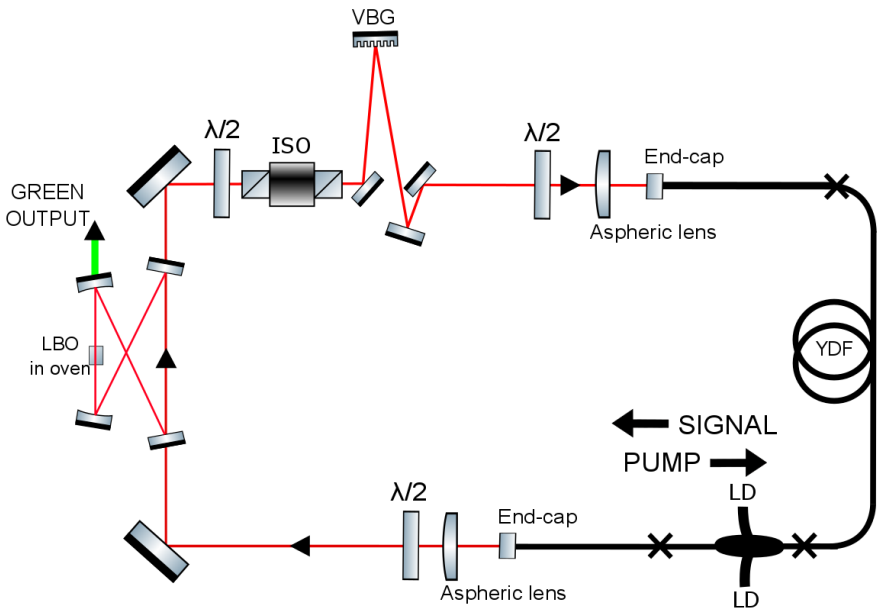

Figure 4.41 Schematic diagram of the full laser set-up with a 4 mirror enhancement cavity and LBO crystal aligned for critically phase matched second harmonic generation

Along with the schematic diagram Figure 4.42 to Figure 4.44 are photographs of the laser when operating. Figure 4.42 is a photograph of the overall system when operating at roughly 50% pump power with a generated green power of 8W. The fibre gain stage can be seen on a water-cooled plate on the right hand side with the pump diodes, pump combiner and all the necessary splice points positioned underneath. The fibre part of the system is indicated by the black outline with the free space path represented by the red outline. The two parts of the free space section, the wavelength and polarisation control (highlighted in blue), and enhancement cavity (highlighted in green) are represented in more detail in Figure 4.43 and Figure 4.44 respectively. In the wavelength control picture the beam path taken by the seed source is represented by the dotted line which is coupled into the system via the use of the thin film polariser, the procedure for which is

described earlier in Section 4.1. The final pick-off mirror used for alignment of the ring laser and diagnostics is also seen along with the path taken by the alignment beam. This alignment beam is used to ensure the spatial overlap of the ring beam with the seed beam in initial alignment along with ensuring that the ring beam quality and waist size is suitable for recoupling by adding a dummy fibre arm.

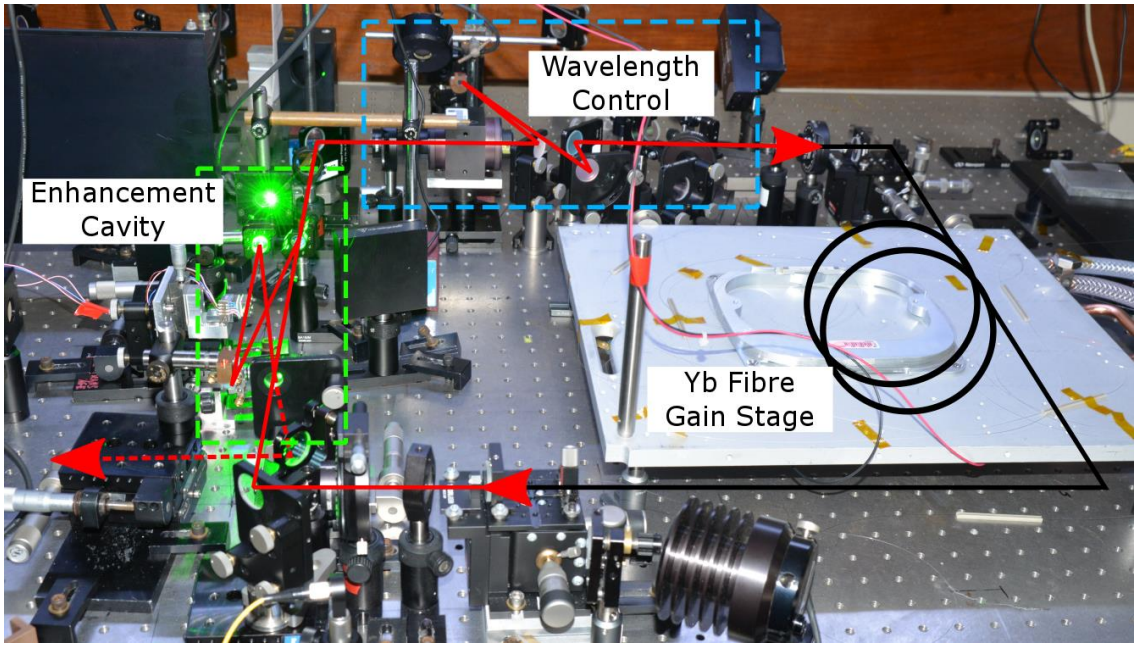

Figure 4.42 Photograph if the complete laser set-up indicating the fibre and free space parts, specifically highlighting the enhancement cavity and wavelength control sections. Both are shown later in expanded views.

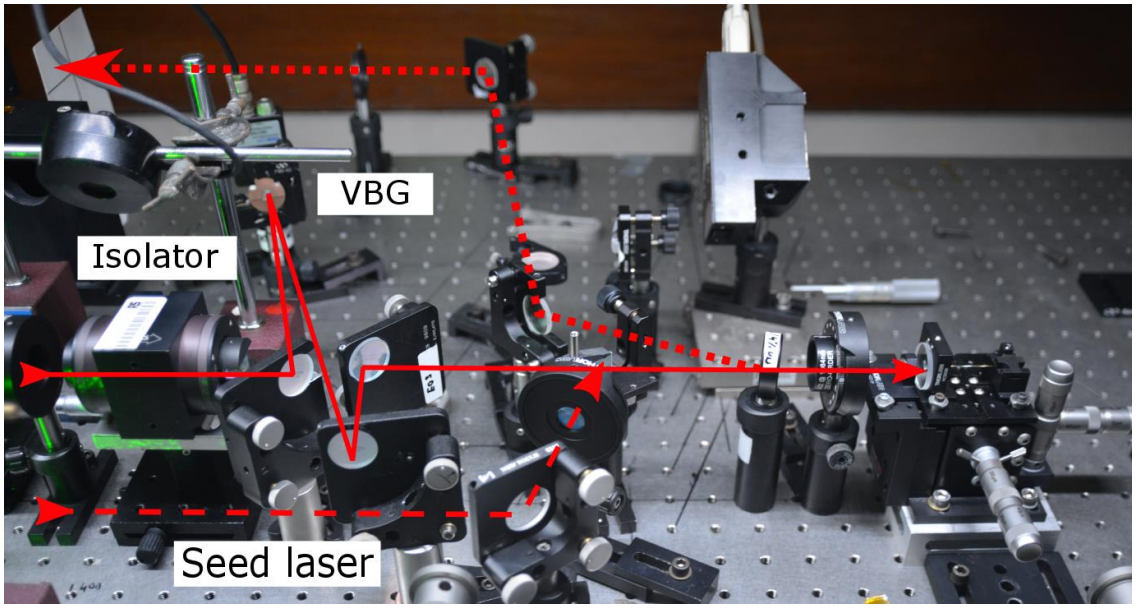

Figure 4.43 Photograph to show the seed laser input and wavelength control optics in more detail. The seed beam is coupled into the ring path using a thin-film polariser. Solid line is the path of the ring laser, after passing through the enhancement cavity. Dashed line is path of seed source. Dotted line is pick-off beam used for alignment and diagnostics.

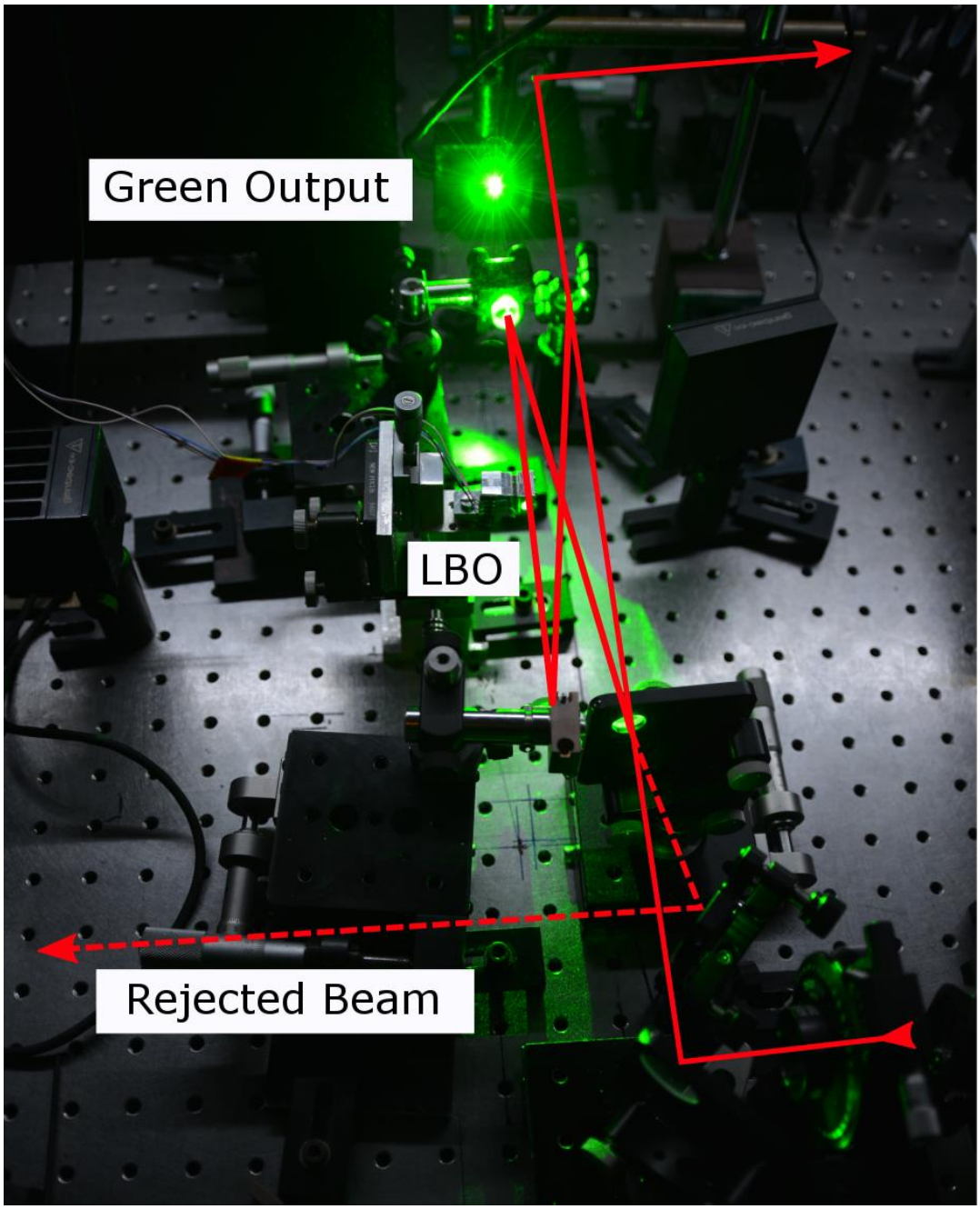

Figure 4.44 Detailed view of 4-mirror enhancement cavity when operating showing green output with indication of ring laser beam direction (solid line) and rejected beam (dashed line).

The enhancement cavity picture indicates the path taken by the input IR beam as it is coupled into the cavity and then feedback into the laser (solid red line) along with the rejected beam reflected form the input coupler (dashed red line).

For the maximum pump power of 98W coupled into the fibre gain stage 15.3W of green second harmonic output was generated. An increase of nearly 40% compared to the large beam waist ring laser in the previous section. This was for an incident IR signal power of 53.25W of which 32.55 was successfully coupled in and 20.7W rejected at the input coupler. The output power evolution curve is shown in Figure 4.45. No evident rollover can be observed while the curve is fairly smooth and no realignment was necessary as pump power was increased. As the cavity showed good stability measurements closer to the threshold could be taken without the need for the seed source.

Looking at the rejected power, Figure 4.46, we can see that 61% of the generated IR power is couple into the cavity with the majority of that in the 'correct' polarisation state again eliminating any polarisation problems being a major factor in the limit of output power. Comparing this with the larger beam waist laser results for both cavity sizes there is not a big difference in the proportion of generated IR light coupled in.

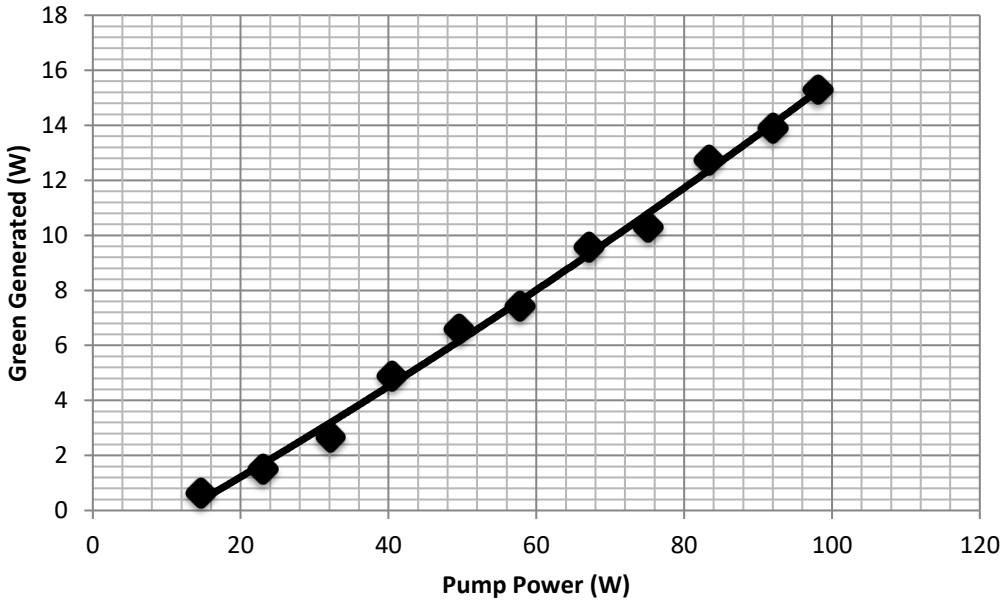

Figure 4.45 Plot of generated second harmonic against pump power for 4-mirror cavity with curved mirror radius RC = 200mm. Fibre ends terminated with bulk end caps. Incident collimated IR beam waist of 1mm.

As expected the decrease in the IR signal beam waist and the difficulty in scaling down the length of the free space path has reduced the IR laser efficiency to 55%, Figure 4.47. Due to the greater beam diversion of this smaller beam waist there is evidently a loss at

recoupling which is affecting the slope efficiency. The feedback power, exiting the enhancement cavity is slowly increasing in line with pump power, Figure 4.48, and is reaching the same levels as that of the 6-mirror and 4-mirror cavities with the larger beam waist. What is evident is that the reduction in input beam waist has increased the nonlinear conversion efficiency of the internal cavity for a decrease in the amount of IR signal power generated. This proves that scaling down the laser both in terms of collimated beam waist and free space cavity length improves the spatial mode matching for the focused beam inside the LBO crystal.

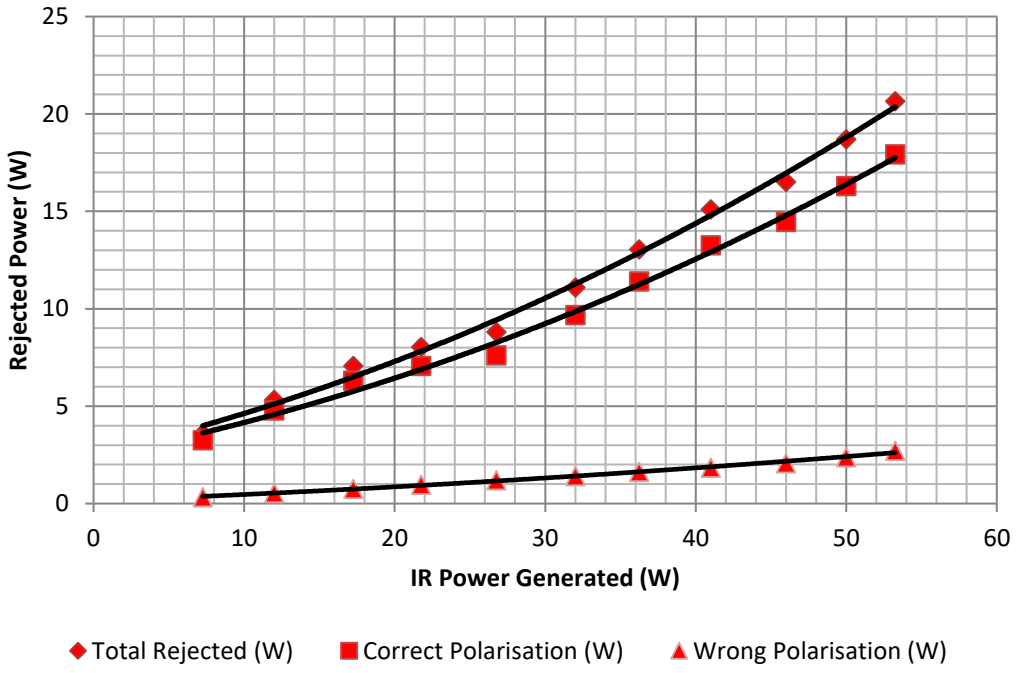

Figure 4.46 Plot of the rejected IR powers in both polarisations against the generated IR power incident on the enhancement cavity.4-mirror enhancement cavity, RC = 200mm, bulk glass end caps, with collimated IR beam radius 800μm.

The single pass second harmonic efficiency reaches a maximum value of 3.7% for an intracavity circulating power of 415W, Figure 4.49, which is close to that achieved previously with the larger beam waist 6-mirro enhancement cavity. Where this cavity performs best is the total conversion efficiency it achieves, shown in Figure 4.50. For the maximum intracavity circulating power of 415W the cavity achieves a conversion efficiency of 47%, the highest of any of the cavity configurations tested. As expected from the enhancement cavity design the other cavity configurations formed a tighter focused beam waist inside the LBO crystal, showing that scaling down the IR signal collimated

beam waist is a right step towards increasing the overall output power and efficiency of the laser system. Unfortunately the limit in pump power has not allowed to investigate the limit of the results here, the trend in total conversion efficiency is seen to be increasing with no sign of levelling off, certainly at higher powers the impedance matching conditions will change and hence the powers at which the cavity operates efficiently will be different.

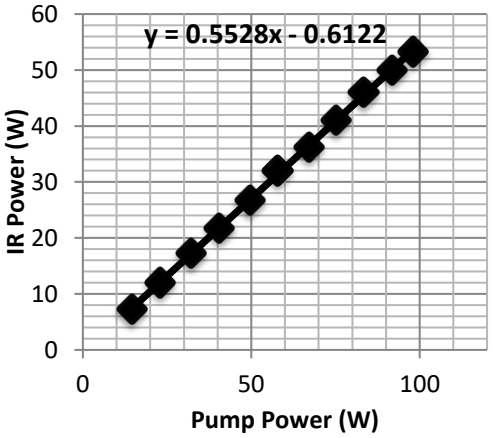

Figure 4.47 Plot of generated signal power incident on 4-mirror enhancement cavity versus pump power. Measured using pick off mirror to indicate the power efficiency of the ring laser. Fibre ends terminated with bulk end caps. Beam radius of 800μm.

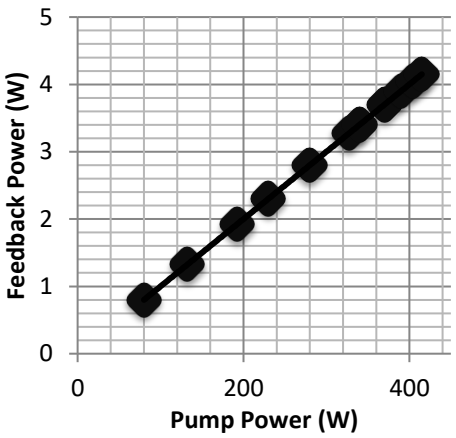

Figure 4.48 Feedback power exiting the enhancement cavity.

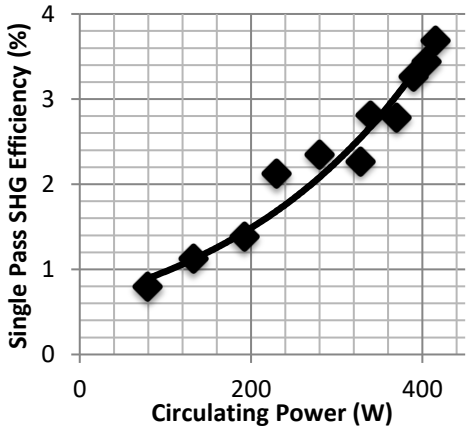

Figure 4.49 Single pass second harmonic conversion efficiency relative to intracavity circulating power

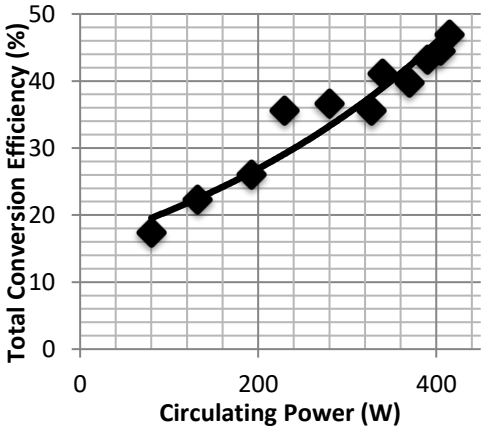

Figure 4.50 Graph of the total conversion efficiency versus intracavity power. The cavity efficiency is calculated from the coupled IR power relative to green generated

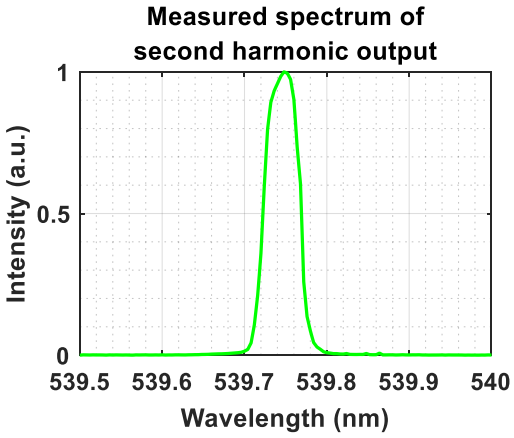

Figure 4.51 Green spectrum. FWHM 0.04nm.

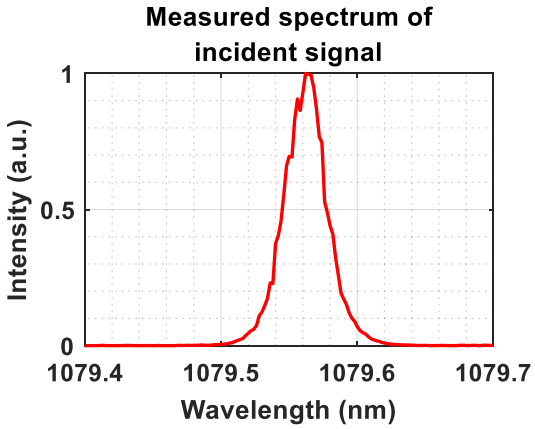

Figure 4.52 IR Spectrum. FWHM 0.03nm.

Looking at the spectrum of the signal and second harmonic, it is clear to see that the laser is performing just as well as previously, shown in Figure 4.51 and Figure 4.52, with a good narrow bandwidth in the IR signal and subsequently in the frequency doubled output. The second harmonic signal has one clear peak at 539.8nm with a bandwidth of 0.04nm, while the input IR spectrum has one clear peak at 1079.58nm with a bandwidth of 0.03nm. Better alignment of the VBG or perhaps the overall system has resulted in a much clearer peak without any evident power in the side peaks that were seen before. This is a clear indication of the better laser performance and a factor in the improvement in the second harmonic conversion efficiency. It supports the theory that in the previous configurations the proportion of light in the secondary peaks although small was being wasted and not converted to second harmonic. Even though the intracavity power in the IR and the power coupled was higher the conversion efficiency was lower. This result highlights the importance of the wavelength control mechanism used in this laser to ensure a good efficiency for the output power generated.

Looking at the output and signal beam, Figure 4.53 and Figure 4.54, we see a good diffraction limited Gaussian output beam with a beam quality factor (M^2) of 1.09 in the x-direction and 1.02 in the y direction. The power stability although slightly worse than previous is still adequate with an R.M.S. error of 1.67% over the time period of 10ns to 120s, shown in Figure 4.55.

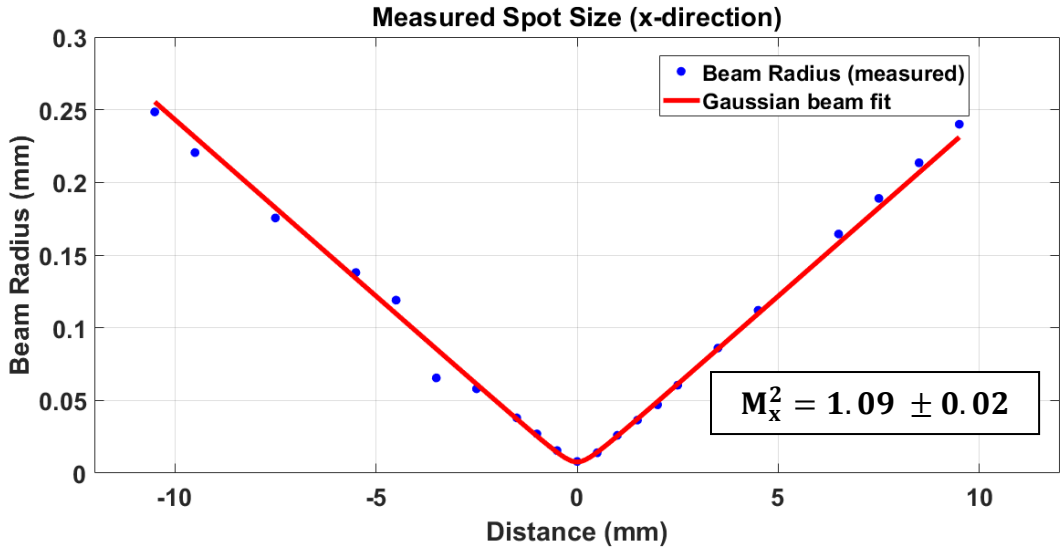

Figure 4.53 Measured beam radius of green output with a Gaussian beam fit and M^2 measurement in the x-axis. 4 mirror enhancement cavity with curved mirror radius of 300mm.

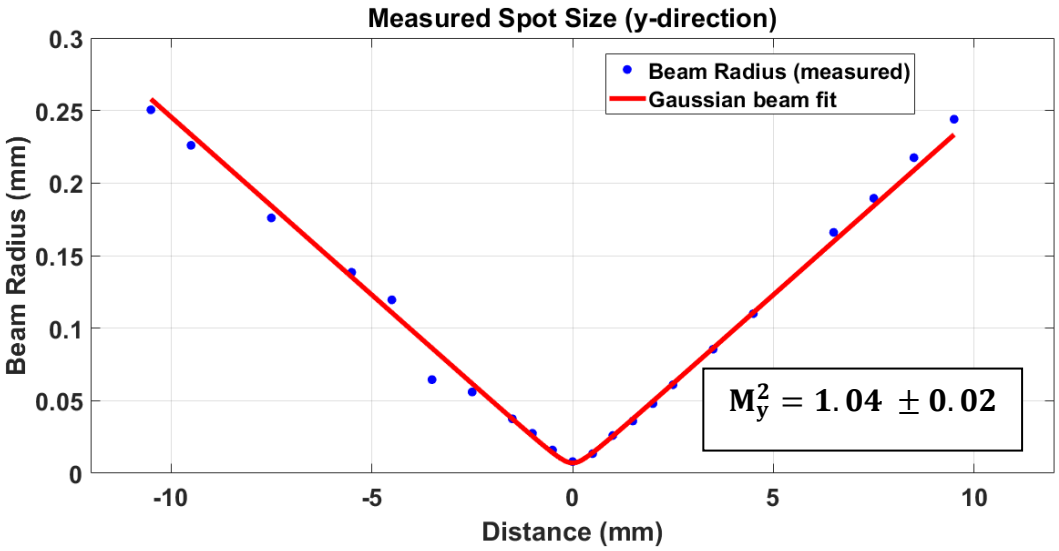

Figure 4.54 Measured beam radius of green output with a Gaussian beam fit and M^2 measurement in the y -axis. 4 mirror enhancement cavity with curved mirror radius of 300mm.

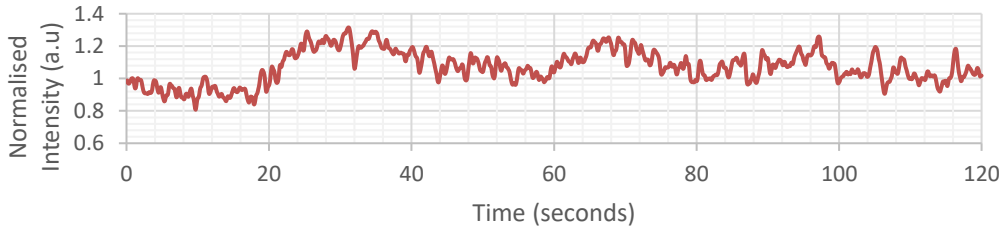

Figure 4.55 Power stability for 4-mirror enhancement cavity with reduced beam waist of 800µm. Time period 10ns to 100s.

4.4 Conclusions

This chapter presented the results obtained for a resonantly enhanced intracavity frequency doubled ring fibre laser including a detailed description of the unique alignment technique required.

The results are summarised in Table 4.1. Two lasers were built differing in the available pump power and more significantly in the feedback suppression mechanism used at the fibre ends. Within each laser two different cavities were experimented to see how significant the mode matching between the IR beam and the supported cavity is. To take this further using the 200mm radius of curvature cavity the whole laser was scaled down in size to support a smaller beam waist in the IR beam.

Laser 1 demonstrated the concept of this work in operation but was very limited in performance. It is clear when comparing with Laser 2 that the angle cleaves simply cannot perform well enough and especially as the pump power is increased. The ring laser slope efficiency is low in both cavity arrangements yielding only 55% in both cases. The larger 300mm radius of curvature cavity was able to couple in more light, generate a higher intracavity power and subsequently generate more second harmonic, reaching 3.4W for a diode pump power of 40W, achieving a single pass SHG efficiency of 2.0% and total conversion efficiency of 32%.

Laser 2 was a clear indication of the superior performance of the bulk glass end caps over the angel cleaves. Operating on the larger beam radius of 1mm the 300 cavity again performed better in all parameters. Both lasers operated with an IR slope efficiency of 62% but the 300mm cavity was able to couple in more power and subsequently generate a higher intracavity power and ultimately achieve a maximum green output of 17.4W for a diode pump power of 98W. This was achieved with a single pass SHG efficiency of 4.1% and total conversion efficiency of 43%. The superior performance of the 300mm cavity confirmed the theory that it is better suited to mode matching and more stable so to investigate this further the 200mm cavity arrangement was rebuilt using a smaller IR beam radius of 0.8mm to better mode match into the cavity. The results again confirmed the expected improvement in the performance of the enhancement cavity with more power coupled in and a high green output power of 15.3W generated for a diode pump power of 98W. This cavity did not surpass the output power generated by the 300mm cavity but the total conversion efficiency is superior. The smaller beam radius affected the IR slope efficiency down to 55% from 62%, so actually for a similar IR performance a greater green output power is expected. The drop in slope efficiency was due to the

greater beam divergence for the smaller beam radius and the difficulty in decreasing the free space path to negate this effect.

Parameter	Maximum Value				
	Laser 1 Angle Cleaves			Laser 2 End Caps	
Curved mirror radius	200mm	300mm	200mm	200mm	300mm
Collimated beam radius	1mm	1mm	1mm	0.8mm	1mm
Pump power	40W	40W	98W	98W	98W
Power generated in fibre gain stage.	21W	21W	60.3W	53.25W	60.8W
Power coupled into cavity	9.2W	10.3W	38.1W	32.55W	40.4W
Percentage of power rejected	56%	51%	37%	39%	34%
Circulating power (at max. Green output)	120W	175W	353W	415W	420W
Power feedback from enhancement cavity	1.2W	1.75W	3.53W	4.15W	4.2W
IR slope efficiency	55%	55%	62%	55%	62%
Green power generated	2.3W	3.4W	11.0W	15.3W	17.4W
Single pass SHG efficiency	2.1%	2.0%	3.1%	3.7%	4.1%
Total conversion efficiency (IR to Green)	28%	32%	29%	47%	43%
Pump efficiency (Pump to Green)	6.3%	8.4%	11.3%	15.6%	17.7%
Enhancement factor (at max. Green out)	13	17	9	13	10

Table 4.1. Summary of all of the key parameters for the different ring laser configurations presented with the best results highlighted. 200mm curvature mirrors formed a 4-mirror enhancement cavity and the 300mm curvature mirrors formed 6-mirror cavities.

CHAPTER 5

5. Conclusions

5.1 Summary of Thesis

The work carried out for this thesis took a proven concept for generating high powers in the visible spectrum through an efficient frequency doubling process and investigated the potential to take that power scaling ability further.

The process of generating high efficiency second harmonic generation (SHG) through the use of an internal enhancement cavity was limited in its feedback when employed in a linear resonator configuration. The work undertaken in this thesis was to develop a novel hybrid fibre and free space ring laser resonator which was designed for use with an internal enhancement cavity.

The current approached to power scaling of CW fibre lasers struggle to attain high efficiencies as they all employ an external cavity approach which also adds stability complications in terms of maintaining the resonance condition. Most ring fibre lasers tend to be single frequency and scaling their output power is difficult due to nonlinear losses mostly due to Stimulated Brillouin Scattering.

In this thesis a novel ring fibre laser geometry is presented along with its ability to generate efficient SHG through the use of an internal resonator.

5.2 Conclusions

In Chapter 3 the fibre ring laser design concept was introduced and the process in its construction was presented. The biggest challenge in its development for efficient intracavity frequency doubling was to ensure that the laser itself operated efficiently and with good stability. The key design issue was to control the feedback due to reflection at the ends of the fibre. It became apparent that even a few percent of light reflected at each end, for example the Fresnel reflection from a flat cleave, is enough to support independent lasing of the fibre gain stage and prevent ring laser operation. Two methods to eliminate this reflection were investigated, angle cleaving of the fibre ends and end capping. The angle cleaving technique was the easier of the two methods but suffered from losses on recoupling which affected the infra-red (IR) slope efficiency which would in turn limit the second harmonic power that could be generated. The bulk glass end caps performed equally as well when reducing the reflection coefficient, both were measured to be below 0.1%, but the end caps were far superior at recoupling, lifting the slope efficiency of the IR signal. Another benefit of the bulk glass end caps is their ability to be

mounted in a more robust way giving stability at higher powers as they were more immune from any thermal or mechanical vibrations. A suitable wavelength control mechanism in the form of a Volume Bragg Grating (VBG) was implemented into the system to select the lasing wavelength of the fibre gain stage and most importantly narrow the bandwidth of the signal radiation to be within the allowed phase matching bandwidth that is required for second harmonic generation (SHG).

Chapter 4 presented the results for the frequency doubling performance of the ring lasers when using both angle cleaved fibre ends and bulk end caps. As expected the angle cleaved laser struggled to generate high powers and only resulted in a maximum of 3.4W of Green output for a diode pump power of 40W. This resulted in a single pass SHG efficiency of 2% and a total conversion efficiency of 32%. This was for the large internal cavity constructed using the 300mm radius of curvature mirrors, 6-mirror cavity. The 200mm curvature mirrors, 4-mirror cavity, were not able to exceed or even match the power levels reached for the 300mm cavity.

For the bulk end capped ring laser the larger radius enhancement cavity, 300mm (6-mirror), again produced the highest output power, generating a maximum of 17.4W of green light for a diode pump power of 98W. No rollover was seen unlike the angle cleaves suggesting that further power scaling is possible.

The biggest limiting factor in all internal cavity configurations was the spatial mode matching between the IR signal beam and the beam supported inside the enhancement resonator. By design the mode sizes were not optimal due to the physical size of the system and an initial experiment at scaling down the laser proved that this would increase the output power.

Using the bulk end capped laser configuration the beam radius of the signal IR radiation was scaled down to give a beam to would be easier to couple into the 200mm (4-mirror) enhancement cavity due to it being more stable. This resulted in a larger beam waist being formed inside the crystal. Overall the green output was increased from a maximum of 11W for the larger IR beam to 15W for the reduced waist size. The recoupling efficiency into the fibre dropped and that had a negative effect on the IR slope efficiency but due to the increase in coupled light into the internal resonator the second harmonic conversion efficiency increased along with the total conversion efficiency hence yielding greater output powers. This final configuration confirmed the biggest limiting factor in the system being the spatial mode matching an indicated an easy solution to reach higher efficiencies and higher powers.

5.3 Future Work

Going forward the scaling down of the beam waist inside the ring laser will yield the biggest and easiest increase in output power. This will arise from a greater percentage of power coupled into the cavity and an increase in the IR signal slope efficiency of the fibre gain stage.

To achieve this a redesign of the system should be made to ensure the smallest possible free space path. The shorter the free space path, the shorter the limit on the Rayleigh length of the collimated free space IR beam. Divergence over the distance in the free space arms affects the recoupling efficiency and hence overall second harmonic output efficiency. The best IR slope efficiency achieved was 62%. Ytterbium fibre lasers have the potential to operate with slope efficiencies close to 80% and if it is possible to achieve this here then this would be an easy way in scaling the output powers further.

A smaller IR beam waist will allow for the design of smaller enhancement cavities in terms of the radius of curvature used for the cavity mirrors. This will allow the design of cavities that can be operated in the more stable regions than those used so far and by doing so will allow for a better control of the beam waist inside the enhancement cavity.

Looking at the VBG, although providing a narrow bandwidth and low loss it does not allow for active tuning of the wavelength of the system as it operated in reflection, any angle tuning of the VBG would misalign the system. Looking at a birefringent filter combination, as mentioned earlier in the thesis, or an alternative system that can operate in transmission will allow for tuning of the wavelength without affecting the alignment of the system.

Finally fine optimisation of the fibre gain stage to minimise losses at splice points and improvement of the polarisation extinction ratio (PER) of the system to decrease the ratio of signal power in the wrong polarisation can both improve the percentage of power coupled into the internal cavity.

Ultimately no serious limits to the output power was observed and by purely increasing the available pump power the green output power can reach the tens of watts to even hundred level. Combing this increase in pump power and optimisation of the system to increase the power coupled into the enhancement cavity can greatly improve on the frequency doubling efficiencies demonstrated.